

Title of thesis

**Modeling and Control of a Spherical Underwater Robot Vehicle
by Using a Variable Ballast Mechanism**

I, **BAMBANG SUMANTRI** hereby allow my thesis to be placed at the Information Resource Center (IRC) of Universiti Teknologi PETRONAS (UTP) with the following conditions:

1. The thesis becomes the property of UTP.
2. The IRC of UTP may make copies of the thesis for academic purposes only.
3. This thesis is classified as

Confidential

Non-confidential

If this thesis is confidential, please state the reason:

The contents of the thesis will remain confidential for _____ years.

Remarks on disclosure:

by

Endorsed

 Signature of Author

 Signature of Supervisor

Permanent : AI and Robotic Laboratory
address Electronic Engineering Polytechnic
 Institute of Surabaya, Kampus ITS
 Sukolilo, Surabaya 60111
 Indonesia.

Assoc. Prof. Dr. Mohd. Noh Karsiti

Date : _____

Date : _____

UNIVERSITI TEKNOLOGI PETRONAS

Approval by Supervisor

The undersigned certify that he has read, and recommend to the Postgraduate Studies

Programme for acceptance, a thesis entitled

**“Modeling and Control of a Spherical Underwater Robot Vehicle
by Using a Variable Ballast Mechanism ”**

submitted by

Bambang Sumantri

for the fulfillment of the requirements for the degree of

Masters of Science in Electrical and Electronic Engineering

Date: _____

Signature : _____

Main Supervisor : Assoc. Prof. Dr. Mohd. Noh Karsiti

Date : _____

UNIVERSITI TEKNOLOGI PETRONAS

**Modeling and Control of a Spherical Underwater Robot Vehicle
by Using a Variable Ballast Mechanism**

By

Bambang Sumantri

A THESIS

SUBMITTED TO THE POSTGRADUATE STUDIES PROGRAMME

AS A REQUIREMENT FOR THE

DEGREE OF MASTERS OF SCIENCE IN ELECTRICAL AND ELECTRONIC
ENGINEERING

Electrical and Electronic Engineering

BANDAR SERI ISKANDAR,

PERAK

March, 2008

DECLARATION

I hereby declare that the thesis is based on my original work except for quotations and citations which have been duly acknowledged. I also declare that it has not been previously or concurrently submitted for any other degree at Universiti Teknologi PETRONAS or other institutions.

Signature : _____

Name : Bambang Sumantri

Date : _____

DEDICATION

I dedicate this thesis to my parents, my beloved wife Catur Arik and my daughter Hana for their pouring love.

ACKNOWLEDGEMENT

First and foremost, all praise and grace goes to Allah, without whose guidance, no effort can attain success.

I am indebted to my supervisor, Assoc. Prof. Dr. Mohd Noh Karsiti, for his guidance, inspiring discussions and support throughout this research in completion of this thesis.

I am thankful to Assoc. Prof. Dr. Herman Agustiawan and Assoc. Prof. Dr. Irraivan Elemvazuthi for their enlightening discussions, comments and help at several critical points in my research work.

I am grateful to the staff of the Postgraduate Studies Office. I am also deeply grateful to my fellow postgraduate students. They have been constant sources of encouragement and friendships during the course of this research.

Finally, but most importantly, I want to thank my parents, my beloved wife and my lovely Hana from the core of my heart. They have been a source of love, support, advice and feedback for me.

ABSTRACT

A mechanism of variable ballast system which manipulates volume of water in the ballast tank is designed and modeled in this thesis. The mechanism is designed to make water always fulfill space in the variable ballast tank with varying volume. Therefore the internal dynamic that is caused by the movement of water in the tank can be avoided. The variable ballast is utilized for vertical motion actuator of a spherical URV by controlling the difference between buoyant force and gravitational force. In this thesis, the VBS can change the weight of URV body, ΔW , in range $\pm 9.96\text{ N}$ in order to make URV in positive buoyancy, neutral buoyancy or negative buoyancy. The buoyancy of URV is considered as a constant value. By using this mechanism, then the URV can move in vertical plane in the range of velocity $\pm 1.019\text{ ms}^{-1}$.

Two approaches, i.e. linearized approximation and nonlinear approach, are presented to design the controller of the dynamic model which behaves as nonlinear system. In linearized approximation, the nonlinear model is linearized about the equilibrium point by using Taylor series. Since the linearized model is controllable then a linear control strategy is applied. In order to analyze the stability of the system, Lyapunov's linearization method is used. Since the eigenvalues of the linearized model is zero, $\lambda = 0$, then the Lyapunov's linearization method cannot determine whether the nonlinear system is stable or unstable. The second method of Lyapunov stability analysis, i.e. Lyapunov direct method, is also applied. By using this method, it can be known that the equilibrium point of this depth positioning system is unstable, furthermore, nonlinear approach, i.e. state-space feedback linearization and input-output feedback linearization, are also used to stabilize this system.

These control strategies are then simulated in MATLAB/Simulink. All control strategies designed in this thesis can asymptotically stabilize the equilibrium point, for $t \rightarrow \infty$, $e \rightarrow 0$. The linearized approximation approach is the fastest to reach steady

state compare to the others, but it consumes more power. For tracking a trajectory, input-output linearization gives better performance compare to the others by resulting smallest error. If the change of trajectory is constant, then error of input-output feedback linearization converges to zero. For linearized approach and state-space feedback linearization, if change of input is 0.1ms^{-1} then absolute error converge to 2.408m and 6.082m respectively, and if change input is 0.2ms^{-1} then absolute error converge to 6.361m and 12.163m respectively.

ABSTRAK

Suatu mekanisma sistem *Variable ballast* yang memanipulasi isipadu air dalam tangki *ballast* direkabentuk dan dimodelkan dalam tesis ini. Mekanisma direkabentuk agar air sentiasa memenuhi ruang dalam tangki *variable ballast* dengan isipadu yang pelbagai. Oleh itu, dinamik dalaman yang disebabkan oleh pergerakan air dalam tangki dapat dielakkan. *Variable ballast* digunakan sebagai penggerak secara menegak *spherical URV* dengan mengawal perbezaan diantara daya mengapung dan daya graviti. Dalam tesis ini, *VBS* dapat mengubah berat badan *URV*, ΔW , dalam julat $\pm 9.96 \text{ N}$ untuk menjadikan *URV* berada dalam keadaan keapungan positif, keapungan neutral atau keapungan negatif. Keapungan *URV* dianggap sebagai suatu nilai tetap. Dengan menggunakan mekanisma ini, maka *URV* dapat bergerak dalam keadaan rata menegak dalam julat halaju $\pm 1.019 \text{ ms}^{-1}$.

Dua pendekatan, iaitu penganggaran linear dan pendekatan bukan-linear dibentangkan untuk merekabentuk pengawal model dinamik yang berfungsi sebagai sistem bukan-linear. Dalam penganggaran linear, model bukan-linear dilinearakan sebesar titik keseimbangan dengan menggunakan *Taylor series*. Supaya model linear mudah dikawal, maka strategi kawalan linear diaplikasikan. Untuk menganalisa kestabilan sistem, kaedah linear *Lyapunov* turut digunakan. Disebabkan *eigenvalues* model linear adalah kosong, $\lambda = 0$, maka kaedah linear *Lyapunov* tidak dapat menentukan sama ada sistem bukan-linear adalah stabil ataupun tidak. Kaedah kedua analisis kestabilan *Lyapunov* iaitu *Lyapunov direct method* juga turut diaplikasikan. Dengan menggunakan kaedah ini, dapat diketahui bahawa titik keseimbangan sistem pengesan kedudukan ini adalah tidak stabil, seterusnya pendekatan bukan-linear, seperti *state-space feedback linearization* dan *input-output feedback linearization* juga turut digunakan untuk menstabilkan sistem ini.

Strategi kawalan ini disimulasikan menggunakan MATLAB/Simulink. Semua strategi kawalan yang direkabentuk dalam tesis ini dapat menstabilkan titik keseimbangannya

secara asimptot, untuk $t \rightarrow \infty$, $e \rightarrow 0$. Pendekatan penganggaran linear merupakan yang tercepat untuk menjangkau keadaan tegap dibandingkan dengan yang lainnya, namun ianya menggunakan kuasa yang lebih besar. Untuk mengesan trajektori, *input-output feedback linearization* memberi persembahan yang lebih baik dibandingkan dengan yang lainnya dengan keputusan ralat yang paling kecil. Jika perubahan trajektori adalah tetap, maka ralat *input-output feedback linearization* bertumpu kepada kosong. Untuk pendekatan linear dan *state-space feedback linearization*, jika perubahan input ialah 0.1ms^{-1} maka ralat mutlak bertumpu masing-masing kepada 2.408m dan 6.082m, dan jika perubahan input ialah 0.2ms^{-1} maka ralat mutlak bertumpu masing-masing kepada 6.361m dan 12.163m.

TABLE OF CONTENTS

STATUS OF THESIS	i
APPROVAL PAGE	ii
TITLE PAGE	iii
DECLARATION	iv
DEDICATION	v
ACKNOWLEDGEMENT	vi
ABSTRACT.....	vii
ABSTRAK.....	ix
TABLE OF CONTENTS.....	xi
LIST OF TABLES	xiv
LIST OF FIGURES	xv
ABBREVIATIONS AND NOMENCLATURE.....	xix
CHAPTER 1	1
INTRODUCTION	1
1.1 Underwater Robot Vehicle (URV)	1
1.2 Variable Ballast System (VBS)	2
1.3 Problem Statement	3
1.4 Objectives of Thesis.....	4
1.5 Scope of Thesis	4
1.6 Outline of Thesis.....	5
CHAPTER 2	6
LITERATURE REVIEW	6
2.1 Introduction.....	6
2.2 Variable Ballast Mechanism.....	7
2.3 Controller Design.....	11
2.4 Summary	13

CHAPTER 3	14
MODELING OF A SPHERICAL UNDERWATER ROBOT VEHICLE.....	14
3.1 Background Theory	14
3.1.1 Coordinate System of URV	15
3.1.2 Factors Affecting Submerged Body.....	16
3.1.2.1 Gravitational Force and Buoyancy	16
3.1.2.2 Hydrodynamic damping.....	17
3.1.2.3 Added Mass	19
3.1.2.4 Hydrostatic Pressure	20
3.1.2.5 Stability	20
3.2 Design of URV	23
3.3 Vertical Motion Equations	24
3.4 Variable Ballast System.....	28
3.4.1 Variable Ballast Design	29
3.4.2 Kinematics Analysis	30
3.4.3 Dynamics Analysis	31
3.4.3.1 Power Screw	31
3.4.3.2 Worm-Gear Set	36
3.4.3.3 External Forces Analysis	41
3.5 Parameters of Spherical URV System and VBS.....	46
3.6 Summary	47
CHAPTER 4	48
CONTROL DESIGN	48
4.1 Linearized Approach.....	48
4.1.1 Properties of Control System.....	48
4.1.1.1 Controllability and Stability of Linearized Model.....	49
4.1.1.2 Observability of Linearized Model.....	52
4.1.2 Feedback Control Design.....	53
4.2 Nonlinear Approach.....	57
4.2.1 Properties of Control System.....	57
4.2.1.1 Controllability and Stability of Nonlinear Model.....	57
4.2.1.2 Observability of Nonlinear Model.....	64

4.2.2 Feedback Linearization Control Design	66
4.2.2.1 State-Space Linearization	67
4.2.2.2 Input-Output Linearization	73
4.3 Summary	76
CHAPTER 5	77
RESULTS AND DISCUSSION	77
5.1 Simulation of Open Loop System.....	77
5.1.1 Simulink Model	77
5.1.2 Simulation Result.....	80
5.2 Simulation of Linearized Approach.....	84
5.3 Simulation of Nonlinear approach.....	93
5.3.1 State-Space Linearization	93
5.3.2 Input-Output Linearization	103
5.4 Performances of The Controllers	113
5.5 Summary	116
CHAPTER 6	117
CONCLUSION AND FUTURE WORKS	117
6.1 Conclusion	117
6.2 Thesis Contribution.....	119
6.3 Future Work.....	120
PUBLICATIONS.....	121
REFERENCES	122
APPENDIX 1: M file in linearized approximation analysis.....	127
APPENDIX 2: M file in feedback linearization analysis.	128
APPENDIX 3: Simulation result for different input reference models.	130

LIST OF TABLES

Table 3.1 Parameters of URV and the ambient	47
Table 5.1 Performances of linearized control system in different range of depth operation.	85
Table 5.2 Performances of linearized controller design in different initial and final depth position.....	88
Table 5.3 Some Parameters and performances of state-space feedback linearization strategy in different range of depth operation.....	96
Table 5.4 Performances of state-space feedback linearization strategy in multi step input reference of depth position.	99
Table 5.5 Some Parameters and performances of input-output feedback linearization strategy in different range of depth operation.....	106
Table 5.6 Performances of input-output feedback linearization strategy in multi step input reference of depth position.	108
Table 5.7 Rise time (T_r), steady time (T_s) and overshoot (OS) of the controllers...	114
Table 5.8 Steady state error (RMSE) and power usage for step input.....	115
Table 5.9 Steady state error (RMSE) and power usage for trajectory input.....	115

LIST OF FIGURES

Figure 2.1 VBS design by mimicking phenomenon of sperm whales [10].	7
Figure 2.2 VBS mechanism by exploiting difference of density between oil and water [16].	8
Figure 2.3 Structure of VBS operated by high pressure air compressor [12].	9
Figure 2.4 VBS mechanism by utilizing hydraulic system [14].	10
Figure 3.1 Coordinate system of URV and DOFs.	15
Figure 3.2 Relation of gravitational force and buoyant force.	17
Figure 3.3 Position of C_B and C_M in stable condition.	21
Figure 3.4 Righting moment due to changing of angle position.	22
Figure 3.5 Unstable condition.	22
Figure 3.6 Shape of spherical URV and its parts.	23
Figure 3.7 Forces acting at URV's body.	25
Figure 3.8(a) Surface of water in ballast tank when the URV's body is shaking; (b) Position of C_M and C_B of water in the tank when tilt is change.	28
Figure 3.9 Mechanism of variable ballast system.	29
Figure 3.10 (a) Power Screw; (b) Worm gear.	30
Figure 3.11 (a) Screw and nut coupling; (b) Detail of forces working in the power screw [36].	32
Figure 3.12 Worm gear [37]	36
Figure 3.13 Detail of forces on worm gear	36
Figure 3.14 External forces working on variable ballast system.	41
Figure 5.1 Model for rate change of weight in the ballast tank.	78
Figure 5.2 Model for the change of weight in the ballast tank.	78
Figure 5.3 Model for vertical motion acceleration of URV.	79
Figure 5.4 Model for velocity and depth position of URV.	79
Figure 5.5 Model for depth positioning of a spherical URV.	80
Figure 5.6 Response of the system for positive and negative pulse input.	81
Figure 5.7 Response of the system for pulse input in different amplitude.	82

Figure 5.8 Response of the system for ramp input.	83
Figure 5.9 Schematic diagram of linearized approximation control design.	84
Figure 5.10 Simulink model of linearized control system.	84
Figure 5.11 Response of linearized controller design for single step input reference.	85
Figure 5.12 Error of depth position of linearized controller design for single step input reference.	86
Figure 5.13 Response of linearized controller design for multi steps input reference.	86
Figure 5.14 Error depth position of linearized controller design for multi steps input reference.	87
Figure 5.15 Response of linearized controller design for ramp model of input reference.	88
Figure 5.16 Error depth position of linearized controller design for ramp model of input reference.	89
Figure 5.17 Response of linearized controller design for single step input reference when $\xi = 0.8$ and $a = 0.136$	89
Figure 5.18 Response of linearized controller design for sinus model of input reference.	90
Figure 5.19 Error depth position of linearized controller design for sinus model of input reference.	91
Figure 5.20 Response of linearized controller design for triangle model of input reference.	91
Figure 5.21 Error depth position of linearized controller design for triangle model of input reference.	92
Figure 5.22 Schematic diagram of state-space feedback linearization control design.	93
Figure 5.23 Simulink model of the original input in state-space feedback linearization.	94
Figure 5.24 Simulink model of $\psi(\mathbf{x})$	94
Figure 5.25 Simulink model of $\gamma(\mathbf{x})$	95
Figure 5.26 Simulink model of state transformation $\mathbf{z} = \mathbf{z}(\mathbf{x})$	95
Figure 5.27 Simulink model of linear controller $v = k_1 z_{1d} - \mathbf{Kz}$	95
Figure 5.28 Response of the state-space feedback linearization strategy for single step model of input reference.	97

Figure 5.29 Error of the state-space feedback linearization strategy for single step model of input reference.	97
Figure 5.30 Response of the state-space feedback linearization strategy for multi step model of input reference.	98
Figure 5.31 Error of the state-space feedback linearization strategy for multi step model of input reference.	98
Figure 5.32 Response of state-space feedback linearization strategy for ramp model of input reference.	99
Figure 5.33 Error of state-space feedback linearization strategy for ramp model of input reference.	100
Figure 5.34 Response of state-space feedback linearization strategy for step input reference which is bigger than range of depth operation.	101
Figure 5.35 Response of state-space feedback linearization strategy for sinus model of input reference.	101
Figure 5.36 Error of state-space feedback linearization strategy for sinus model of input reference.	102
Figure 5.37 Response of state-space feedback linearization strategy for triangle model of input reference.	102
Figure 5.38 Error of state-space feedback linearization strategy for triangle model of input reference.	103
Figure 5.39 Schematic diagram of input-output feedback linearization control design.	103
Figure 5.40 Simulink model of the synthetic input in input-output feedback linearization control design.	104
Figure 5.41 Simulink model of the original input in input-output feedback linearization control design.	104
Figure 5.42 Simulink model of $\alpha(x)$	105
Figure 5.43 Simulink model of $\beta(x)$	105
Figure 5.44 Response of input-output feedback linearization strategy for single step model of input reference.	106
Figure 5.45 Error of input-output feedback linearization strategy for single step model of input reference	107

Figure 5.46 Response of input-output feedback linearization strategy for multi step model of input reference.	107
Figure 5.47 Error of input-output feedback linearization strategy for multi step model of input reference	108
Figure 5.48 Response of input-output feedback linearization strategy for ramp model of input reference	109
Figure 5.49 Error of input-output feedback linearization strategy for ramp model of input reference.	110
Figure 5.50 Response of input-output feedback linearization strategy for single step model of input reference bigger than range of depth operation.....	111
Figure 5.51 Response of input-output feedback linearization strategy for sinus model of input reference.	111
Figure 5.52 Error of input-output feedback linearization strategy for sinus model of input reference.	112
Figure 5.53 Response of input-output feedback linearization strategy for triangle model of input reference.	112
Figure 5.54 Error of input-output feedback linearization strategy for triangle model of input reference.	113

ABBREVIATIONS AND NOMENCLATURE

- URV : Underwater Robot Vehicle.
- DOF : Degree of Freedom.
- VBS : Variable Ballast System.
- SISO : Single Input Single Output.
- C_M : Centre of Mass.
- C_B : Centre of Buoyancy.
- RMSE : Root Mean Square Error.
- $sign(\mathbf{v})$: sign of \mathbf{v} .
- \forall : for any.
- \in : in the set.
- ∞ : infinite.
- t : time.
- ρ_w : density of water.
- C_D : drag coefficient.
- V_{fb} : volume of spherical URV.
- A_{fb} : projected area of spherical URV.
- D_{fb} : diameter of spherical URV/sphere body
- μ : dynamic viscosity of water.
- Re : Reynolds number.
- m_t : total mass of URV/body.
- m_s : initial total mass of URV.
- m_a : added mass.
- Δm : change of URV mass.
- \mathbf{v} : vertical velocity
- \mathbf{a} : acceleration.
- z : depth position.

- P_{hs} : hydrostatic pressure.
 P_{ih} : pressure inside URV's hull
 P_a : atmospheric pressure at water surface.
 V_{ih} : volume of air inside URV hull.
 g : gravitational acceleration.
 A : surface area.
 F_D : drag force.
 F_B : buoyancy.
 W : weight/gravitational force.
 W_{bs} : initial weight of water in the ballast tank
 ΔW : change of weight in ballast tank
 f_a : force due to acceleration \mathbf{a} .
 l : lead of screw per revolution.
 l_w : lead of worm per revolution.
 α : lead angle.
 Δh : change of nut position.
 μ_s : friction coefficient of screw surface.
 μ_w : friction coefficient of worm surface.
 θ : power screw normal angle
 φ_n : normal pressure angle of worm gear.
 N_w : number of thread per revolution of worm.
 N_g : number of teeth of gear
 ω_m : angular velocity of motor.
 ω_2 : angular velocity of gear.
 ω_3 : angular velocity of screw.
 f_r : friction force between screw and nut.
 F : force working on nut.
 F_{ih} : force working at surface of movable plate because of P_{ih} .

- T_3 : input torque that is required to operate the screw.
- T_F : is torque required to overcome force F .
- T_{fr} : torque required to overcome friction between screw and nut.
- d_g : diameter of gear.
- d_w : diameter of worm.
- d_m : diameter of screw.
- h : height of ballast tank.
- A_{vb} : projected area of variable ballast base.
- P_m : power provided by motor.

CHAPTER 1

INTRODUCTION

1.1 Underwater Robot Vehicle (URV)

Underwater robot vehicle has been used in many tasks in underwater environment, such as for inspection and maintenance purpose of underwater cable and pipelines network [1-3] and also used for gathering bathymetry data for oceanographic research [4]. The URV is utilized to perform task in depth where it would be too hazardous or impractical for human to do. The kind of task that is performed by URV will decide what shape of URV's body/hull is suitable. For surveying where URV must travel in long distance, torpedo-like or airplane-like is suitable. By having this shape, the URV will have streamline body so that it can decrease the drag force. Hence, the URV will be able to move in high speed. If the URV is utilized for observation therefore it does not need to move in long distance with high speed, the hull in box frame or spherical shape is suitable, e.g. JHUROV [5] and ODIN [6].

In this thesis, a spherical shape of URV's hull is used. The spherical shape is chosen because it has axially symmetric and provides uniform drag in any directions of its movement, therefore it is easy to develop the algorithm to control motion of the URV. By this advantage, a *spherical underwater robot vehicle* is suitable for test-bed. In full DOF, URV has 6 degree of freedom in its motions those are surge, sway, heave, roll, yaw, and pitch. This thesis focuses on heave motion that is movement of URV in vertical plane.

Currently, some mechanisms for motion actuator are developed. C. Watts et al. [7] developed propulsion by mimicking tail of salmon fish. By using this mechanism they want to increase the propulsive efficiency and maneuverability, thus will increase duration and operation in enclosed environments. Joshua G. Graver [8] and Jui Min Tun et al. [9] developed glider. This URV glides in the water by utilizing the change

of buoyant force and the position of centre of mass of its hull. They used *variable ballast* mechanism to change the buoyant force.

The kind of the actuators used in an URV depends upon the task want to be accomplished by the URV. It also depends on the location where it is operated. The common actuator used as propulsion is thruster. If the URV uses thruster as motion actuator, the *zero buoyancy* or *neutral buoyancy* is needed. *Zero buoyancy* or *neutral buoyancy* is a condition where the gravitational force is equal to the buoyant force. With *neutral buoyancy*, if there is no propulsion, the URV will not move and keep staying at its position. The buoyant force depends on the density of the water, so that it is not easy to make URV in *neutral buoyancy* if the mass of URV is fixed because the density of the water sometime is different from one place to another place. The diversity of water density is caused by the difference of material dissolved in the water. The availability of variable buoyancy or *variable ballast* can be used for adjusting the URV's buoyant force thus the *neutral buoyancy* can be kept. Besides that function, the *variable ballast* also can be used as motion actuator in vertical plane. By using *variable ballast* as motion actuator in vertical plane, the power used to supply the propeller can be reduced, because we can replace the usage of propeller as vertical motion actuator by this variable ballast. Therefore, the usage of power supply can be more efficient. In this thesis, the development of *variable ballast* mechanism is performed. This *variable ballast* is utilized as motion actuator of a *spherical underwater robot vehicle* in vertical plane.

1.2 Variable Ballast System (VBS)

The *variable ballast* idea is adopted from *Archimedes principle*, “When a solid body is partially or completely immersed in water, the apparent loss in weight will be equal to the weight of the displaced liquid”. So, if the specific mass of URV is equal to specific mass of water, the URV will drift in the water which is called *neutral buoyancy*. If specific mass of URV is bigger than specific mass of the water, the URV will submerge which is called *negative buoyancy* and if specific mass of

URV is less than specific mass of water, the URV will emerge which is known as *positive buoyancy*. By controlling specific mass of URV, we can control motion of URV in vertical direction in order to control depth position of URV.

Some mechanisms of VBS have been developed by researchers. Koji Shibuya et al. [10] developed variable buoyancy system based on the spermaceti oil hypothesis. Sperm whales have a spermaceti organ in their head that is filled with spermaceti oil. Spermaceti oil is high quality oil and has been used as material for candles, lubricant, and so on. There is a hypothesis about spermaceti oil of sperm whales, the sperm whales melt and congeal their spermaceti oil and change the volume of the oil to control their own buoyancy. This hypothesis appears suitable for the underwater robot because no materials for the ballast, such as sea water taken in at another place and iron, are discarded in the sea. They designed a mechanism to melt the material by heating it inside a chamber (syringe) thus the volume can be increased, hence the buoyancy also increased. In this mechanism, it needs a long time to heat the material so that the change of buoyancy is slow. K. S. Wasserman et al. [11], M. Xu and S. M. Smith [12] utilized variable ballast system in their URV. They designed mechanism to fill and release water from ballast tank by using air pressure due to control URV's buoyancy. To release water from the ballast tank, the high pressure air must be pumped to the ballast tank thus the water pushed out from the tank. To fill water into the tank, the air must be released from the tank thus the water will enter the tank freely. In this mechanism, high pressure air compressor must be available. So, the duration and the area where the URV is operated will be limited by the pressure of the air in the compressor. J. S. Riedel et al. [13] and M. Worall et al. [14] designed a variable ballast system for deep-ocean. They exploit the water as ballast to control the weight of the URV. They used hydraulic pump to control amount of the water in the ballast tank in order to change the weight of the URV.

1.3 Problem Statement

From the existing variable ballast design explained at section 1.2, the dimension and volume of the ballast tank that can be filled by the water is fixed so that if the amount

of water in the tank is not maximum, there will be an empty space. The availability of empty space in the ballast tank will make water can move freely around this space. If motion of the URV is unstable, this condition will result an internal dynamic and it is not easy to control it. Therefore, in this thesis, a mechanism of variable ballast system with variable volume of ballast tank is designed. Because of the variably volume of ballast tank, there will be no empty space in the ballast tank. Hence, the internal dynamic that is caused by the motion of water in the ballast tank can be revoked.

1.4 Objectives of Thesis

In this thesis we aim to:

1. Design a mechanism of variable ballast system.
2. Derive mathematical model of variable ballast system.
3. Design the controller for depth position of the spherical underwater robot vehicle.

1.5 Scope of Thesis

In this thesis, a mechanism of variable ballast system is designed and used as motion actuator of a spherical URV in vertical plane. The mathematical model of the VBS and vertical motion equation of a spherical URV are presented in this thesis. These models are derived based on the physical laws involved in this system. The variable ballast is used to position the URV in a particular depth. The depth control system is developed based on the derived model. Since the dynamic of the spherical URV behaves as nonlinear system, then the nonlinear controller is designed.

The dynamic model of the URV and the controller design are simulated by using Simulink/MATLAB. This simulations use some ideal parameters where the density of the water, air pressure and temperature at water surface are constant.

1.6 Outline of Thesis

This thesis is organized as follow:

Chapter 2 explains some existing variable ballast mechanisms. Review of some previous controller designs are also presented in this chapter.

Chapter 3 emphasizes the modeling of a spherical underwater robot vehicle and variable ballast system which is used as vertical motion actuator. The kinematic and dynamic model of depth positioning of a spherical URV are obtained by considering the physical laws involve in this system. This chapter also presents detail mechanism of the variable ballast system and describes detail of the used parts and design of the mechanism.

Chapter 4 defines the design of the controllers by using linearized approximation approach and nonlinear approach. The nonlinear model for depth positioning of the spherical URV is linearized using Taylor series expansion at equilibrium point. Nonlinear control approach applied in this system by using feedback linearization. As SISO nonlinear system, there are two types of feedback linearization which are state-space linearization and input-output linearization. Some properties of the control system such as controllability, observability and stability are analyzed.

Chapter 5 presents the simulation of dynamic model and controller design by using Simulink/MATLAB. Performances of these controllers are discussed and compared each others in this chapter. Some input model such as step input, ramp and trajectory are tested to system in order to know the responses and performances of the controller.

Chapter 6 is conclusions. The contribution of this thesis and the future works are also presented in this chapter.

CHAPTER 2

LITERATURE REVIEW

Variable ballast system is utilized in URV system for controlling the buoyancy of the URV. This mechanism is needed because the density of the water is uncertain from one place to other place, so that the buoyancy of the URV also becomes uncertain. Some existing VBS mechanisms are presented in this chapter. This VBS also been utilized for vertical motion actuator of URV. Some control designs applied in URV system are also presented in this chapter.

2.1 Introduction

Mission in sending of an underwater robot vehicle at certain position or known as positioning system needs some motion actuators such as thruster that is used for propelling the motion of the URV, fin or rudder that is used for steering the direction of the URV or variable ballast system that is used for maintaining zero buoyancy condition. If a URV with single thruster and stern planes want to reach a certain depth, it should drive the thruster and trim the angle of stern planes. By using these actuators, the URV does not have the capability to move in vertical plane directly without making a maneuver. If others thrusters are added to the URV direct vertically, then the URV will have capability to move in vertical plane directly by using these thrusters.

If URV uses thrusters to propel its motion, then a continuous energy must be supplied to the thrusters. This condition is not efficient in terms of energy usage. Therefore, other mechanism that can conserve the usage of energy is needed, such as variable buoyancy. Since the function of variable ballast is for controlling the buoyancy, then it can be used as vertical motion actuator by making the buoyancy of the URV into negative buoyancy, positive buoyancy or neutral buoyancy. Hence the usage of thrusters as vertical motion actuator can be replaced. By using variable ballast as

vertical motion actuator, then the usage of energy will be reduced because the URV does not need to supply energy to this actuator continuously [15].

2.2 Variable Ballast Mechanism

Variable ballast mechanism which is applied in URV system can be used for controlling the difference between buoyancy and gravitational force by controlling the density of URV's body. Some mechanisms of variable ballast were proposed by researchers [10-14, 16-22]. These mechanisms change the difference between buoyancy and gravitational force by expelling and infusing water from and into the tank.

A mechanism mimicking a phenomenon of sperm whales was designed by K. Shibuya et al. [10]. In their VBS design, they used materials which have similar nature as spermaceti oil of sperm whales. They put the material in the syringes which are arranged inside heater as shown in Figure 2.1.

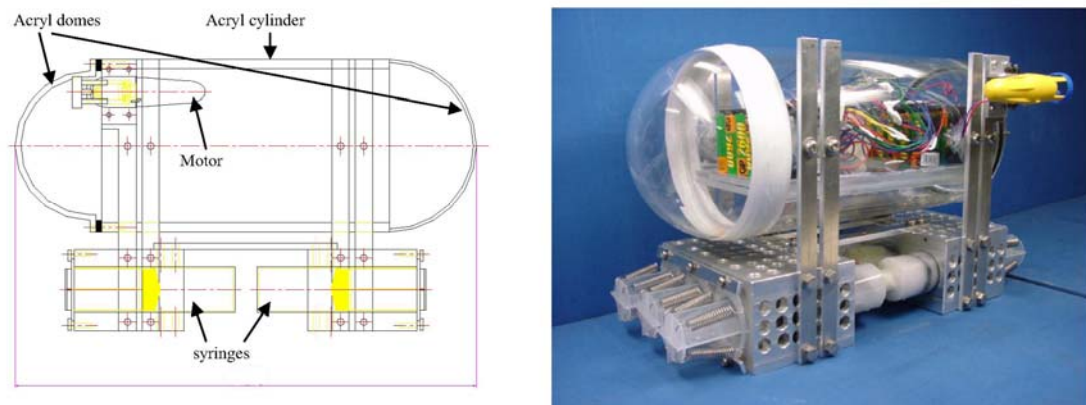


Figure 2.1 VBS design by mimicking phenomenon of sperm whales [10].

By heating the syringes, the material inside will be melt and its volume will expand so that the syringes' pistons will be pushed out. Hence, the buoyancy of URV will be increased. If URV has positive buoyancy, then it will move upward. In order to decrease the buoyancy, the temperature of the material should be lowered so that the material inside syringes will congest and the volume will be decreased. Springs which

are coupled to the syringes' pistons will attract the pistons to clog the material inside. By decreasing the volume of material inside the syringes, then the buoyancy will be decreased. If the buoyancy is negative, then the URV will move downward. By using this mechanism, there will be no material to be expelled to the environment such as iron or other material. Therefore, this mechanism will not pollute the underwater environment. In this mechanism, it needs a long duration to melt or congest the material so that it is looked impossible to change the buoyancy in fast response. If the buoyancy should be held at a particular value, then temperature must be held at certain value. It means that URV must supply power to the heater continuously. Therefore, the URV should provide more energy to this mechanism especially if the URV is operated for a long duration.

R. E. Davis et al. [16], C. C. Eriksen et al. [17], and C. Waldmann [18] developed variable ballast mechanism by exploiting the difference of density between oil and water. It is well known that density of water is bigger than density of oil. In their VBS mechanism, oil is pumped from internal reservoir into external bladder in order to increase the buoyancy or pump back the oil from external bladder into internal reservoir in order to decrease the buoyancy by using hydro pump and control valve as shown in Figure 2.2. The change of buoyancy depends upon the amount of oil pumped into bladder.

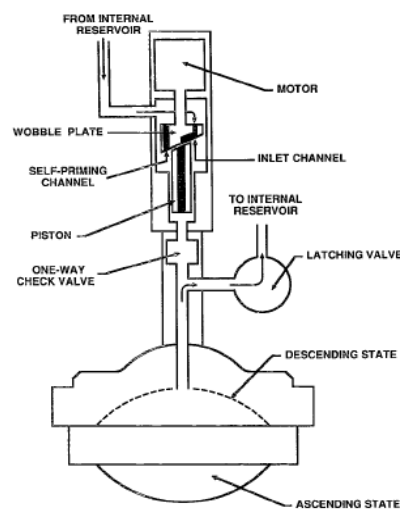


Figure 2.2 VBS mechanism by exploiting difference of density between oil and water [16].

In this VBS design, it is not easy to sense the change of buoyancy because it is done by sensing amount of oil pumped into bladed or pumped back into internal reservoir. If volume of internal reservoir is constant then if oil does not fully fill the reservoir, an empty space that is not filled by the oil will exist. This condition can make the oil move freely in the reservoir. Hence, it can raise internal dynamic of the URV system which is not easy to be controlled. It can disturb the stability of the URV.

Mechanism of variable ballast by exploiting high pressure air compressor was developed in [11, 12, 19]. In this VBS mechanism, high pressure air compressor must be provided. In order to change the buoyancy, the air must be released from compressor to increase the buoyancy or released from the ballast tank to decrease the buoyancy as illustrated in Figure 2.3.

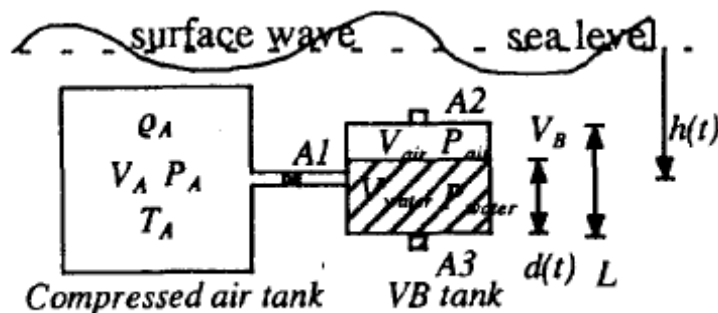


Figure 2.3 Structure of VBS operated by high pressure air compressor [12].

If the air is released from the compressor to the ballast tank then water will be pushed out from the tank. Since density of air is lower than water then the buoyancy will be increased. In order to decrease the buoyancy, the air must be released from the ballast tank by opening the control valve so that the water can enter the tank. Hence the increment of water in the ballast tank will decrease the buoyancy. In this mechanism the duration of the operation depend on the availability of high pressure air compressor. The pressure of air compressor should be higher than water pressure so that it can push the water from then in order to increase buoyancy. If at certain depth, the pressure of water is higher than air compressor, then the buoyancy cannot be

increased. Hence, if the URV does not have other vertical propeller then it will not be able to move to surface. In this mechanism also if the water does not fully fill the ballast tank, then empty space will be exist. Hence, this condition can raise internal dynamic which is not easy to be controlled.

Other mechanism of VBS system which utilized hydraulic system was designed in [13, 14, 20]. They manipulated amount of water in a fixed volume of ballast in order to control the buoyancy of the URV. Hydraulic pump was utilized to pump the water from ambient to ballast tank in order to decrease the buoyancy or pump the water from ballast tank to ambient in order to increase the buoyancy as illustrated in Figure 2.4.

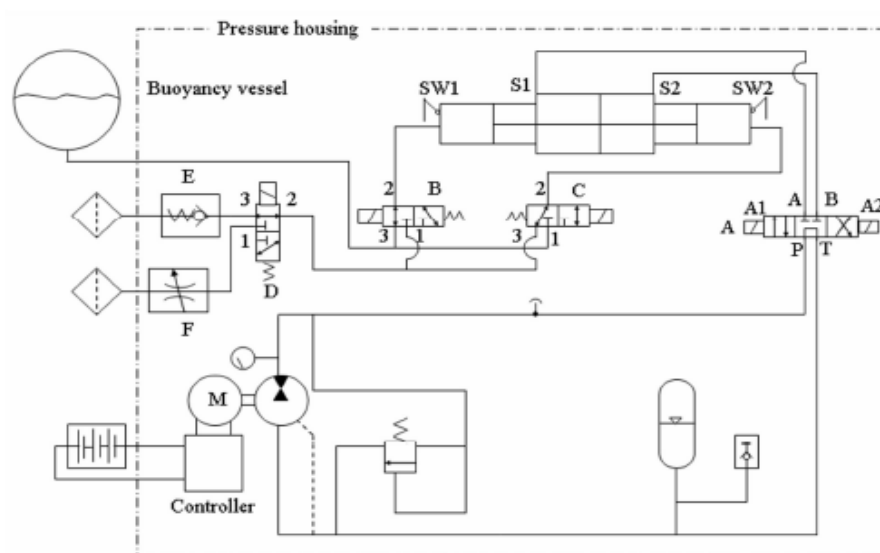


Figure 2.4 VBS mechanism by utilizing hydraulic system [14].

Since this mechanism utilized a fixed volume of ballast system, then internal dynamic can occur if the water does not fully fill the ballast tank which is uneasy to be controlled. Therefore, it is hard to design the controller in order to stabilize this system.

A variable ballast mechanism which utilized variable ballast tank was applied in [21]. This mechanism utilized a cylinder as ballast tank. Base of this cylinder is movable

and the other is opened therefore this cylinder directly contacted to the ambient. Hence, this cylinder always full with water. By moving the movable base, then the volume of cylinder can be changed, hence the volume of water in the cylinder also be changed, therefore the buoyancy also be changed. The movable base is moved by motor which is coupled through screw. In this mechanism, the water always fully fill the cylinder tank even the volume is different. Therefore, the internal dynamic that occur in VBS mechanism with fixed ballast tank can be avoided. This VBS mechanism was also applied in [22]. In these papers, mathematical model of VBS mechanism was not presented therefore it will not be easy to customize the specification of the VBS mechanism in order to apply to URV with different design. The availability of mathematical model will ease the designer to simulate the system in computer software in order to design an optimal controller.

2.3 Controller Design

Designs of the controller in URV system have been investigated by many researchers [23-33]. These controllers were designed to improve performance of the URV in order to fulfill a certain task. G. Antonelli et al. [23] proposed a controller for tracking the position and attitude of an URV with limited feedback measured by the sensor. They combined controller and observer to track desired position and attitude. The observer was used to estimate unmeasured feedback that was velocity. K. Y. Pettersen and O. Egeland [24] designed position and attitude control of an under-actuated URV. They wanted to reduce total of the actuators were used in the URV system by keep considering the performance of the system. In designing the controller, the cost that is needed to build this system must be considered. If it is possible, the usage of sensors and actuators should be reduced but still the URV can fulfill the desired task.

The nonlinearity of the URV system becomes opportunity for the researchers to develop a good controller. Many nonlinear control systems were applied in URV control design. P. A. DeBitetto [25], E. S. Ammeen and G. O. Beale [26] developed fuzzy logic controller to control depth position of an Underwater Vehicle (UV). This UV utilized variable ballast as actuator for depth positioning system. The variable

ballast mechanism was utilized in [25] used pump to control amount of water in the ballast tank. This fuzzy logic controller was used to command the pump in order to control the depth position of the UV. T. Chatchanayuenyong and M. Parnichkun [27] designed a neural network based-time sliding mode control to control a 6 DOF Autonomous Underwater Vehicle (AUV). Sliding mode control (SMC) is a type of variable structure control (VSC) that is as a combination of subsystems in which each has a fixed control structure and effective at particular region of system behavior. They used neural network to optimize the period of switching for each subsystems. Fuzzy logic controller or neural network controller was designed by neglecting the dynamic model of the system.

The existence of mathematical model of a system is important in designing the controller. By having a good mathematical model, an effective controller can be designed, and computer simulation can be built to test the performance of the controller. In [23, 28, 29], controller of the URV system was developed based upon mathematical model. In these papers, they designed an effective controller by combining controller and observer. They used observer to estimate the unmeasured variable that involved in the model.

Once mathematical model of system is obtained, some controllers can be designed and tested in computer simulation. Since the URV is a nonlinear system, a simple controller can be designed by linearizing the model of URV by using Taylor series expansion. This method linearizes the nonlinear model about steady condition or the equilibrium point [30]. Then if the linearized model is controllable, a linear feedback controller law can be design based upon this linearized model. N. E. Leonard and J. G. Graver [31] used this linearization method to design the controller of an underwater glider. They linearized the nonlinear underwater glider model about a steady glide path. Since the linearized model was controllable then the linear controller was designed. They applied LQR (Linear Quadratic Regulator) as a standard linear optimal control design method to control an underwater glider based on the linearized model.

Sometimes, the linearized model of a nonlinear system is uncontrollable so that a linear controller cannot be applied to control this system. Then a nonlinear controller must be utilized. Feedback linearization is one of nonlinear controller method. I. Schjøberg and T. I. Fossen [32], A. Chellabi and M. Nahon [33] applied this method to control motion of an underwater vehicle. They designed the controller to track a trajectory based on kinematic and dynamic model of the underwater vehicle. Therefore, the feedback linearization method is known as model-based nonlinear controller.

2.4 Summary

Variable ballast mechanism is utilized to control the difference between buoyancy and gravitational force of URV system. Therefore, it is possible to make the URV in zero buoyancy, negative buoyancy or positive buoyancy condition. Some existing variable ballast mechanisms were presented in this chapter. In these mechanisms, if the VBS utilize fixed ballast tank, then internal dynamic can occur when water does not fully fill the tank. The internal dynamic is not easy to be controlled and can disturb the stability of the URV. Therefore, VBS mechanism with variable volume of tank is needed and presented in the next chapter. In this chapter, reviews of some previous controller designs are also presented. These controllers involve non model based controller and model based controller. Model based controller can be used if the model of the system is provided. Therefore, in the next chapter, the dynamic model of a spherical underwater robot vehicle and its motion actuator is derived. Hence, the computer simulation can be built.

CHAPTER 3

MODELING OF A SPHERICAL UNDERWATER ROBOT VEHICLE

A spherical shape of a submerged body with closed frame provides uniform drag at all direction along its surface. In this chapter, the shape of a spherical URV that is used in this thesis is presented. The vertical motion equation is also derived. The forces that affect the dynamics of the system are also described. In order to control vertical motion due to control depth position of the URV, a variable ballast mechanism is used. This mechanism controls the weight of URV's body. This chapter also presents detail mechanism of the variable ballast system and describes detail of the used parts and design of the mechanism. Kinematic and dynamic model of the variable ballast system are also derived. In order to model this system some factors affecting the system should be considered. At the beginning of this chapter, some factors affecting to the URV and variable ballast system will be presented.

3.1 Background Theory

Commonly, the controller of the URV is designed to send the URV into a particular positioning or to maintain the position of the URV. In other words, it is called positioning system. The positioning system of URV involves two kinds of position those are horizontal and vertical position. In order to determine position of the URV, the coordinate system of the URV must be considered. In this sub section, the common coordinate system used in underwater vehicle system is presented. Then to maintain the position of an URV, a good control system must be designed. An effective control system can be built if the mathematical model and simulation is well established. In order to model the URV system, some factors affect this system must be considered, such as gravitational force, buoyancy, hydrodynamic damping, added mass and hydrostatic pressure.

3.1.1 Coordinate System of URV

Normally, the underwater vehicle system has six degree of freedom (DOF), including spatial coordinate x , y , and z ; and Euler angles ϕ , θ , and ψ . The illustration is shown in Figure 3.1.

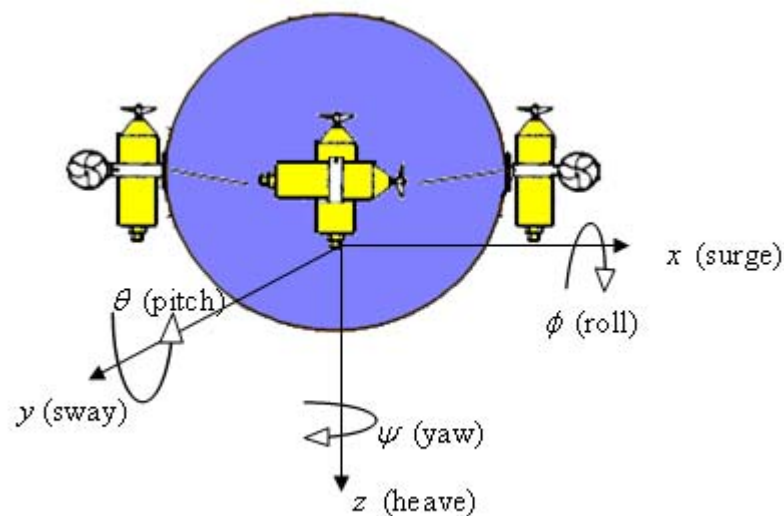


Figure 3.1 Coordinate system of URV and DOFs.

Surge, sway and heave are translation motion in x , y , and z coordinate space respectively and roll, pitch and yaw are rotation motion in x , y , and z axis respectively. In order to meet the full six degrees of freedom, the URV must be equipped with the actuators that can drive the URV in these six motions. By having six DOF, the URV will have high maneuverability. The total degree of freedom of the URV can be less than six, it depends on the application or task that want to be performed by the URV. Therefore it can save usage of the resources like power supply, sensor and also propeller and it will cause the time operation of the URV be longer.

3.1.2 Factors Affecting Submerged Body

The URV can be analogous to submerged body in the water. In order to derive the model of the URV, some factors that affect a submerged body in water must be considered, including gravitational force, buoyancy, hydrodynamic damping, added-mass and hydrostatic pressure. Gravitational force and buoyancy are two important factors that must be considered in designing an URV. These two factors influence the stability of the URV besides external force.

3.1.2.1 Gravitational Force and Buoyancy

Every object on the earth is affected by the gravitational force or weight, W . The magnitude of the gravitational force depends on the mass of the object and gravitational acceleration at the object position. Direction of the gravitational force directs to the center of the earth. This force acts at the centre of mass of the object or the body.

URV as a submerged body in the water, besides affected by gravitational force, it is also affected by buoyancy. The buoyant force, F_B , is a vertical force which acts at a submerged body in a fluid, and its magnitude is equal to the weight of the fluid displaced by the body. This is known as Archimedes' principle. The buoyant force acts at the centre of mass of the displaced fluid.

The relation between gravitational force and buoyant force of a submerged body is illustrated in Figure 3.2. If the weight of the submerged body is less than buoyant force then the body will move upward, namely positive buoyancy. If the weight is equal to the buoyant force then the body will drift in the fluid, namely neutral buoyancy or zero buoyancy. If the weight is bigger than buoyant force then the body will move downward, namely negative buoyancy.

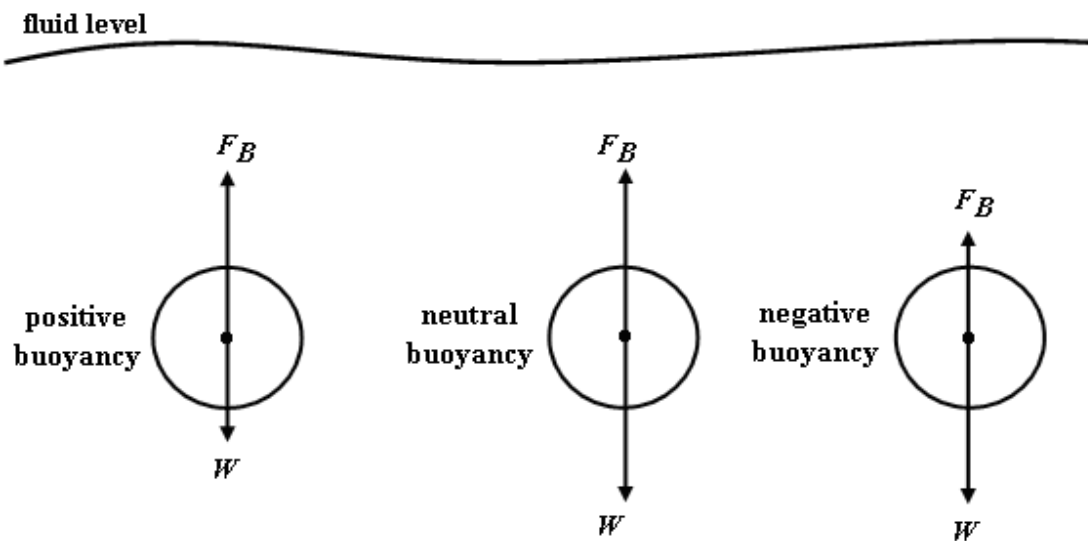


Figure 3.2 Relation of gravitational force and buoyant force.

3.1.2.2 Hydrodynamic damping

A moving body in a fluid will experience a force which is caused by the flow of fluid around the body. This force is resultant of two kinds of forces due to relative motion between the body and the fluid. These forces consist of [34]:

- The component of force in the direction of flow on a submerged body which is called the *drag force*.
- The component of force at right angles to the direction of flow which is called *lift force*.

If flow of the fluid approaches the body along the axis of symmetry then the force acting on the body is only the drag force, the lift force is equal to zero. Therefore if the fluid flows on a sphere body, which has symmetry axis along its surface, the only force exerts on the body is drag force.

If the fluid is water with density ρ_w , then for a sphere submerged body moving at a uniform velocity v , the drag force, F_D , exerts on the body can be expressed as

$$F_D = \frac{1}{2} C_D A_{fb} \rho_w \mathbf{v}^2, \quad (3.1)$$

where C_D and A_{fb} are drag coefficient and projected area of the body respectively. The drag coefficient is obtained based on the value of Reynolds number, Re , which depends on the relative velocity of the flow, shape of the body and viscosity of the fluid [34]. The Reynolds number of a sphere submerged body in the water can be obtained from

$$Re = \frac{\rho_w \mathbf{v} D_{fb}}{\mu}, \quad (3.2)$$

where D_{fb} and μ are diameter of the sphere body and dynamic viscosity of the water respectively. If the Reynolds number of the sphere body is known then the drag coefficient can be obtained based on the condition stated below [34]:

- (i) For $Re \leq 0.2$: When the velocity of flow/body is very small or fluid is very viscous such that the Reynolds number is very small as low as 0.2. In this case, Stokes analyzed theoretically the flow around a sphere under very low velocities. Stokes found that total drag coefficient can be calculated by:

$$C_D = \frac{24}{Re} \quad (3.3)$$

- (ii) For $0.2 < Re < 5$: Oseen made an improvement to the Stokes' solution by partly taking into account the effect of inertial terms. He found that

$$C_D = \frac{24}{Re} \left[1 + \frac{3}{16Re} \right]. \quad (3.4)$$

- (iii) For $5 \leq Re \leq 1000$: The value of C_D is equal to 0.4.
- (iv) For $1000 \leq Re \leq 100000$: The value of C_D in this range is more or less independent of Reynolds number, and may be taken as 0.5.
- (v) For $Re > 100000$: Value of C_D is approximately equal to 0.2.

Because of the availability of the drag force, if the body with constant dimension, shape and mass, is free fall in the water, at a certain time it will reach a constant velocity which is known as *terminal velocity*.

3.1.2.3 Added Mass

When a fix body moves in the liquid with unsteady velocity, acceleration or deceleration will be exist, and an additional effect (force) on the structure will exist. Therefore if a force F is applied to the submerged body in the water with mass m_t , the force will not just accelerate the body but also the water surrounding this body. The mass of the water which is accelerated along with the body is known as added mass, m_a . So, the total force needed to accelerate the body with the mass m_t in acceleration \mathbf{a} can be expressed as

$$F = (m_t + m_a) \mathbf{a} \quad (3.5)$$

The total added mass of an accelerated body depends on the shape of the submerged body. For a spherical submerged body in the water, the total added mass can be calculated by [34]

$$m_a = \frac{1}{12} \pi \rho_w D_{fb}^3, \quad (3.6)$$

where ρ_w and D_{fb} are density of water and diameter of the spherical body respectively.

3.1.2.4 Hydrostatic Pressure

Hydrostatic pressure is a pressure exerted by a liquid at rest condition. Every object which is immersed in the liquid will be affected by this pressure. The intensity of this pressure depends on the depth position of the object and also the specific weight of the liquid. If the object is immersed in the water, then the intensity of the hydrostatic pressure, P_{hs} , can be calculated by

$$P_{hs} = \rho_w g z, \quad (3.7)$$

where g and z are gravitational acceleration and depth position of the object respectively.

If the immersed object is horizontally flat with a surface area A , then a force on the surface of the immersed object will be produced by the hydrostatic pressure which is expressed as

$$\begin{aligned} F_{hs} &= P_{hs} A \\ &= \rho_w g z A \end{aligned} \quad (3.8)$$

3.1.2.5 Stability

The stability position of a static object in the static water is affected by the difference between the weight and buoyant force of the object. For example, if the buoyant force is bigger than the weight, the object will float at the water surface. If this object is pushed down and released, then buoyant force will against the weight and will push the object float again at surface. Therefore this vertical position is stable. But if the buoyant force is equal to the weight, when we give a certain force vertically, the body will move for awhile but cannot comeback to the original position. When the object is moving, the drag force opposes that force so that the object will be stopped. In this condition the vertical position of the object is unstable.

The position of center of mass, C_M , and center of buoyancy, C_B , is also affected by the rotational stability of the object in the water. In equilibrium condition, the position of center of mass and center of buoyancy of a static object in the water is vertically inline. If position of center of mass is below center of buoyancy (bottom heavy), then if a force is exerted to the object horizontally then it makes the angle position of the object change which is illustrated in Figure 3.3.

If C_M and C_B are not vertically inline, then this condition will produce a righting moment, RM , which is obtained from [35]

$$RM = \frac{1}{2}d(F_B + W) \sin \lambda_d, \quad (3.9)$$

where d is distance between C_M and C_B , and λ_d is angle changing which is illustrated in Figure 3.4.

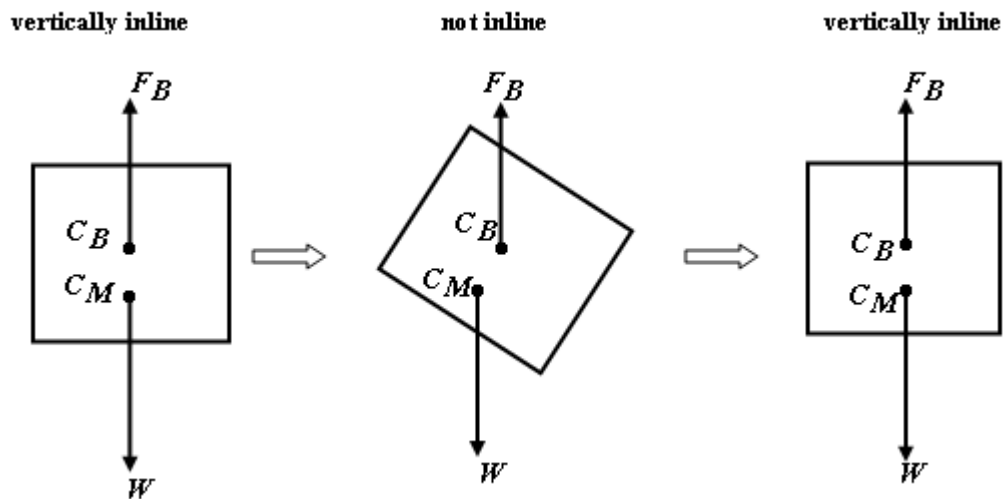


Figure 3.3 Position of C_B and C_M in stable condition.

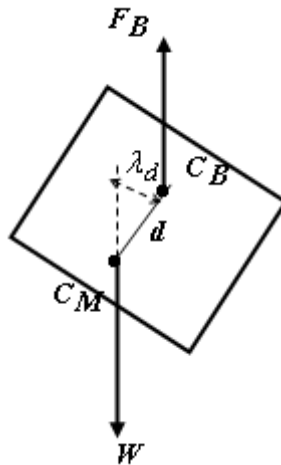


Figure 3.4 Righting moment due to changing of angle position.

This righting moment will drive the object comeback to the original angel position thus C_M and C_B are vertically inline. Therefore this configuration is stable.

If the object has internal dynamic thus can change position of center of mass, then it can make unstable condition. This condition is illustrated in Figure 3.5.

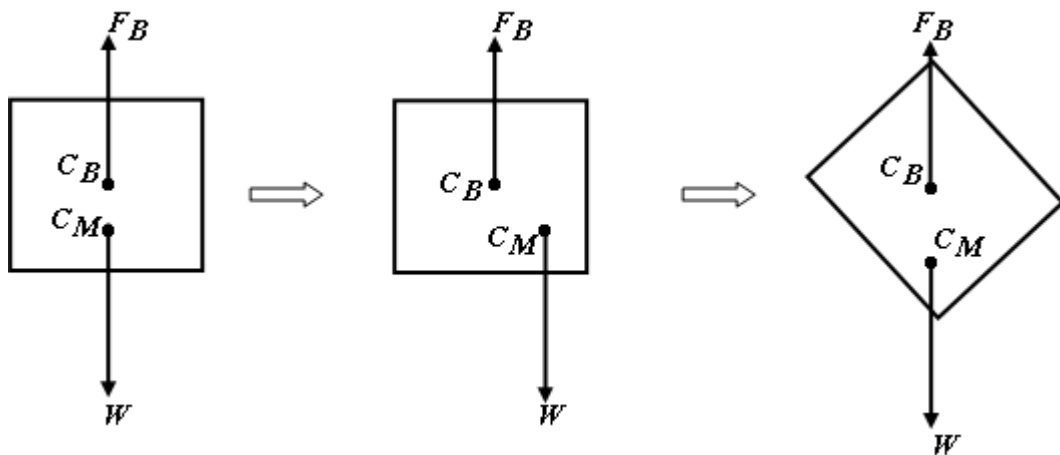


Figure 3.5 Unstable condition.

3.2 Design of URV

The shape of spherical URV used in this thesis is shown in Figure 3.6. As a sphere body, the location of center of buoyancy, C_B , of URV's body is at the center of sphere or the intersection point between vertical and horizontal diameter. The variable ballast tank is located at the top inside the hull. Location of the tank is adjusted so that the position of center of mass, C_M , is aligned vertically with C_B . Mechanism of the variable ballast and detail of its parts are explained in section 3.4. At the upper side of the hull above the tank, there are some holes as the way of water to enter into and exit from the tank. The space below the movable plate inside the hull is waterproofed so that the water cannot enter this space.

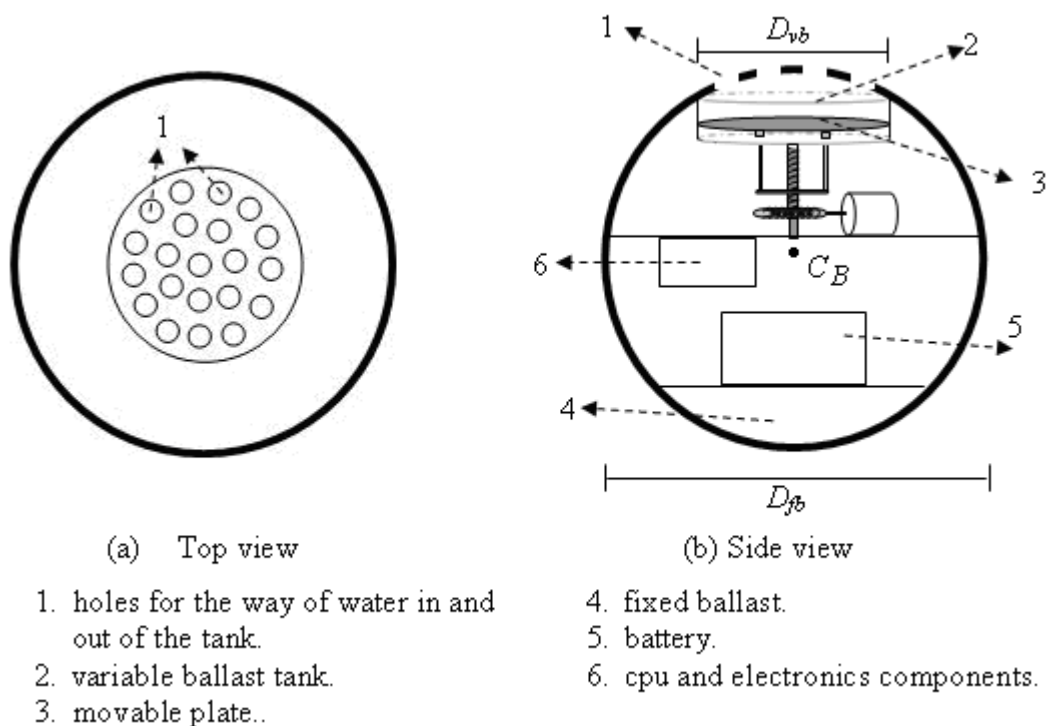


Figure 3.6 Shape of spherical URV and its parts.

In order to make the URV stable in equilibrium condition, the hull of URV must be designed with bottom heavy that is the center of mass is located at under of the equator or at underside hemisphere. To make the hull in bottom heavy, fixed ballast is

located at the bottom of the hull. The location of C_M of the hull must be aligned vertically with C_B of the hull thus in equilibrium condition, the position of the ballast tank is at the top of the URV's hull exactly. This condition is important when the URV is provided with horizontal propulsion in order to give ability to the URV to move in horizontal plane.

The diameter of URV used in this thesis is chosen as 35cm. Therefore, in order to determine the dimension of the ballast tank we have to consider the dimension of URV's hull, batteries, and other electronics devices used in the URV system. Parameters of the URV and VBS are described in section 3.5.

3.3 Vertical Motion Equations

Since the URV moves in vertical plane without any propeller, so it just depends on the gravitational force, buoyant force and other forces that appear because of its motion. By assuming there are no external forces that can disturb the motion of URV, the forces acting on the URV can be shown in Figure 3.7. Let F_B is buoyant force, W is gravitational force, F_D is drag force, f_a is force that appear because of the availability of the acceleration, m_a is added mass, and m_t is total mass of the URV's body which is constant then forces equation act at URV are given as [34]

$$W = F_B + F_D \quad (3.10)$$

and,

$$W = m_t g , \quad (3.11.a)$$

$$F_B = \rho_w V f_b g , \quad (3.11.b)$$

$$F_D = \text{sign}(\mathbf{v}) \frac{1}{2} C_D A f_b \rho_w \mathbf{v}^2 . \quad (3.11.c)$$

The direction of gravitational force and buoyant force are opposite to each other when W is downward and F_B is upward. From Eq. 3.11.c, it can be seen that the direction

of the drag force depends upon the direction of the velocity. If the URV moves downward, the velocity is positive so that the drag force is positive and its direction is upward. The drag force and velocity are negative if the URV moves upward.

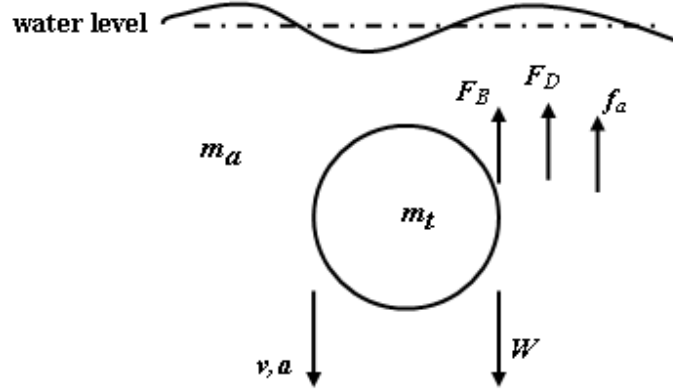


Figure 3.7 Forces acting at URV's body.

Substituting Eq. 3.11 into Eq. 3.10, then the force equation can be represented as

$$m_t g = \rho_w V_{fb} g + \text{sign}(\mathbf{v}) \frac{1}{2} C_D A_{fb} \rho_w \mathbf{v}^2. \quad (3.12)$$

Since dimension of URV, V_{fb} and A_{fb} , are constant, then the velocity \mathbf{v} , is also constant. This velocity is known as *terminal velocity*, which is expressed as

$$\mathbf{v} = \text{sign}(m_t g - \rho_w V_{fb} g) \sqrt{\frac{2(m_t g - \rho_w V_{fb} g)}{C_D A_{fb} \rho_w}}, \quad (3.13.a)$$

$$|\mathbf{v}| = \sqrt{\frac{2(m_t g - \rho_w V_{fb} g)}{C_D A_{fb} \rho_w}}. \quad (3.13.b)$$

From Eq. 3.13.a, it can be seen that the vertical motion of the URV depends on the gravitational force and the buoyant force. If $W > F_B$, then the URV moves downward and it will move upward if $W < F_B$. If $W = F_B$, the URV will stay at its position.

Since volume of URV's hull, V_{fb} , g , and ρ_w are constant, the buoyant force is also constant. So, the motion of URV depends on the total mass of URV's body, m_t . By controlling m_t , the vertical motion of the URV can be controlled.

Since equilibrium condition is occurred when $W = F_B$, then $\mathbf{v} = 0$ and $m_t = m_s$ which is initial total mass of the URV. If the total mass changes as much as Δm from the initial total mass, m_s , then the total mass of URV is expressed as

$$m_t = m_s + \Delta m. \quad (3.14)$$

By changing the total mass of URV, then the associated velocity will be change. The change of the velocity depends upon whether Δm is a variable or simply a constant. If Δm is a variable, the acceleration, \mathbf{a} , occurs. This acceleration, besides accelerates mass of URV itself, m_t , also accelerates mass of surrounding water which is known as *added mass*, m_a .

Due to this acceleration, the force f_a will occur and it is expressed as

$$f_a = (m_s + \Delta m + m_a)\mathbf{a}. \quad (3.15)$$

Considering this last force, f_a , Eq. 3.10 can be rewritten as

$$W = F_B + F_D + f_a. \quad (3.16)$$

Substituting Eq. 3.11 and Eq. 3.15 into Eq. 3.16, yields

$$m_s g + \Delta m g = F_B + \text{sign}(\mathbf{v}) \frac{1}{2} C_D A_{fb} \rho_w \mathbf{v}^2 + (m_s + \Delta m + m_a)\mathbf{a}. \quad (3.17)$$

Recalling equilibrium condition,

$$\begin{aligned} W &= F_B, \\ m_t &= m_s, \\ \mathbf{v} &= 0, \\ \mathbf{a} &= 0. \end{aligned} \quad (3.18)$$

From Eq. 3.14 obviously we have $\Delta m = 0$.

By substituting Δm and Eq. 3.18 into Eq. 3.17, yields

$$m_s g = F_B. \quad (3.19)$$

Since m_s and F_B are constant, then by the change of Δm , Eq. 3.17 becomes

$$\Delta m g = \text{sign}(\mathbf{v}) \frac{1}{2} C_D A_{fb} \rho_w \mathbf{v}^2 + (m_s + \Delta m + m_a) \mathbf{a}. \quad (3.20)$$

Since $\Delta m g = \Delta W$, then Eq. 3.20 is written as

$$\Delta W = \text{sign}(\mathbf{v}) \frac{1}{2} C_D A_{fb} \rho_w \mathbf{v}^2 + \left(m_s + \frac{\Delta W}{g} + m_a \right) \mathbf{a}. \quad (3.21)$$

By solving for the acceleration, \mathbf{a} , the dynamic equation for vertical motion is given as [12]

$$\mathbf{a} = \frac{\Delta W}{\left(m_s + m_a + \frac{\Delta W}{g} \right)} - \frac{\text{sign}(\mathbf{v}) C_D A_{fb} \rho_w \mathbf{v}^2}{2 \left(m_s + m_a + \frac{\Delta W}{g} \right)}. \quad (3.22)$$

And, if the depth position of the URV can be measured as z , then by differentiating z respect to time t , the velocity of URV in vertical plane can be expressed as

$$\mathbf{v} = \dot{\mathbf{z}}. \quad (3.23)$$

3.4 Variable Ballast System

If the design of variable ballast uses tank as chamber for controlling amount of water in URV's body in order to control buoyancy/weight of the URV. The space or volume of the used tank is fixed so that if the amount of water in the tank is not full, there will be a space which is not filled by water. This condition can make water move freely around the space of the tank if the tilt of URV is unstable such as illustrated in Figure 3.8(a). This motion can produce a moment that can disturb the stability of the URV. If tilt of URV's body is changed (as shown in Figure 3.8(b)) the center of mass, C_M , will also change. This condition sometime is undesired. Therefore, a variable-ballast with variable volume of chamber of the tank is designed in this thesis, in order to make water always fulfill the space in the tank but variably in terms of volume.

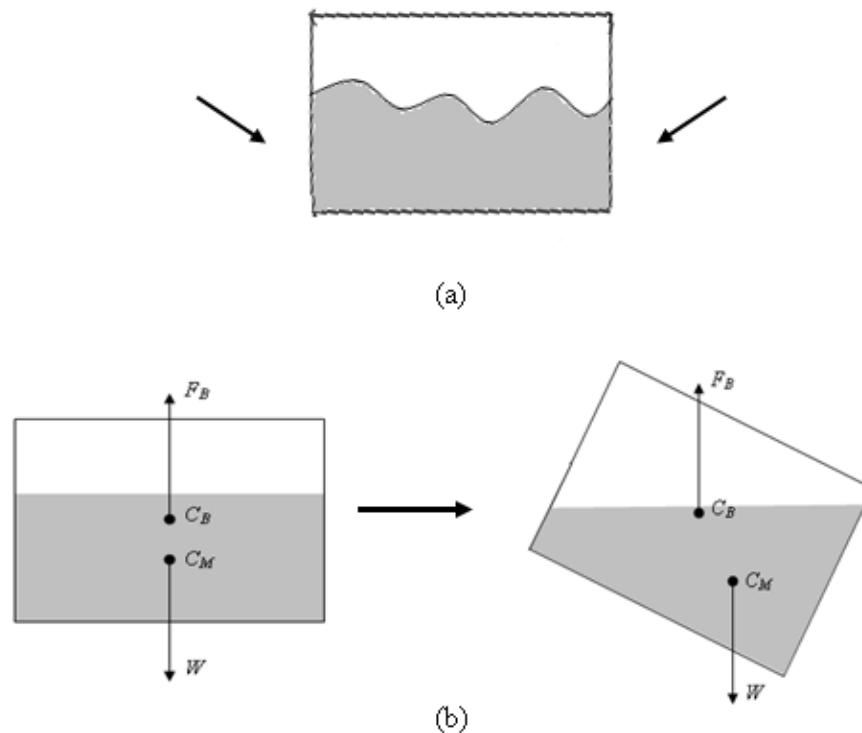


Figure 3.8(a) Surface of water in ballast tank when the URV's body is shaking;

(b) Position of C_M and C_B of water in the tank when tilt is change.

3.4.1 Variable Ballast Design

In order to make water always fill space in the ballast tank, even if the volume of water is different, then the volume of the tank itself must be adjustable which is illustrated in Figure 3.9. The shape of the variable ballast's tank is cylinder which is opened at the top side. This part is connected directly to the water environment therefore water can always fulfill the space in the tank (as shown in Figure 3.6(b)).

To make variably volume of the tank, a movable plate is located at the bottom of the tank. The space below the movable plate is waterproofed, so that water cannot enter this space. If the movable plate is moving upward, the space of the tank will be decreased as well as the volume of water in the ballast tank. If the movable plate is moving in opposite, downward, the space of the tank will be increased and also the volume of water in the ballast tank. Therefore, in any volume of water in the ballast tank there is no empty space in the ballast tank that is not filled by water.

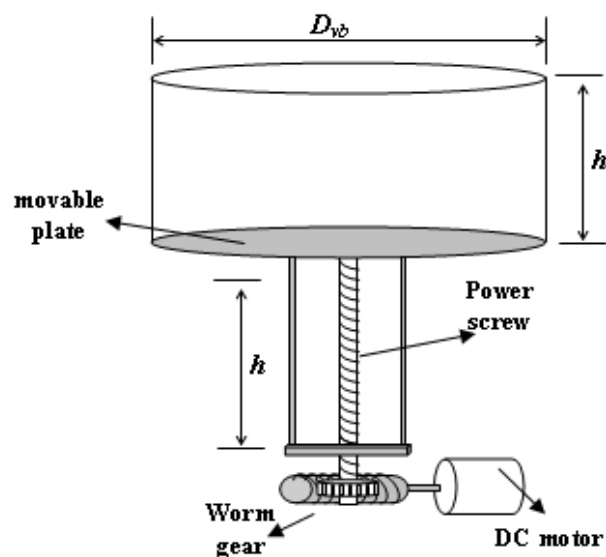


Figure 3.9 Mechanism of variable ballast system.

In order to change position of the movable plate, a DC motor is used to drive the movable plate through power screw and worm gear coupling. This variable ballast mechanism is analyzed in this chapter. It involves kinematics and dynamics analyses.

3.4.2 Kinematics Analysis

The movable plate of variable ballast system is coupled to the nut of power screw. This nut can be moved up and down by turning the screw. So, the screw converts the rotation motion into linear (vertical) motion. This coupling can be seen in Figure 3.10(a). Based on Figure 3.10(a), l is lead of screw per revolution, Δh denotes change of nut position, ω_3 is angular velocity of screw. If Δt is the time needed by screw to change nut position at Δh regarding angular velocity ω_3 , then their relation can be written as

$$\frac{\Delta h}{\Delta t} = \frac{l \omega_3}{2\pi}. \quad (3.24)$$

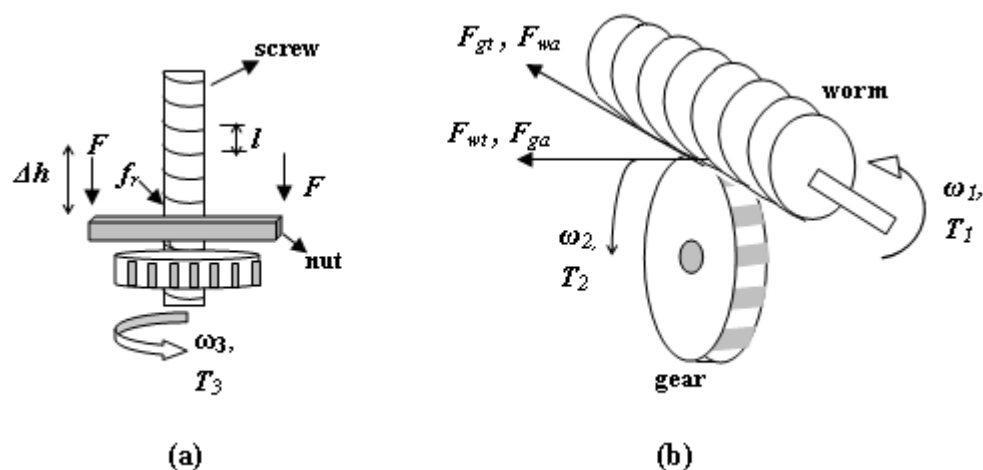


Figure 3.10 (a) Power Screw; (b) Worm gear.

To turn the power screw, a DC motor is used and coupled with worm gear as illustrated in Figure 3.10(b). The worm has number of thread per revolution equal to N_w , and the gear has number of teeth equal to N_g . If the worm is coupled directly to the motor which turns in velocity ω_m , then the gear will turn in velocity ω_2 which is expressed as

$$\omega_2 = \frac{N_w}{N_g} \cdot \omega_m. \quad (3.25)$$

As shown in Figure 3.10(a), the gear and screw is ally so that its angular velocity is the same,

$$\omega_2 = \omega_3. \quad (3.26)$$

By substituting Eq. 3.26 and Eq. 3.25 into Eq.3.24, the change of nut position can be rewritten as

$$\begin{aligned} \frac{\Delta h}{\Delta t} &= \frac{l N_w}{N_g 2\pi} \omega_m, \\ \Delta \dot{h} &= \frac{l N_w}{N_g 2\pi} \omega_m, \\ \omega_m &= \frac{N_g 2\pi \Delta \dot{h}}{l N_w}. \end{aligned} \quad (3.27)$$

3.4.3 Dynamics Analysis

The dynamic of variable ballast mechanism is analyzed by considering torques and forces acting in the system. The forces and torques involved in the mechanism come from internal mechanism those are from the DC motor and the transmission system, and also come from external that is from the surrounding as hydrostatic pressure.

3.4.3.1 Power Screw

As illustrated in Figure 3.10(a), T_3 is input torque that is required to operate the screw to move the nut which is coupled with movable plate, can be expressed as

$$T_3 = T_F + T_{fr}, \tag{3.28}$$

where T_F is torque required to overcome force F , and T_{fr} is torque required to overcome friction between screw and nut. To evaluate these terms, the equilibrium conditions are applied such as illustrated in Figure 3.11.

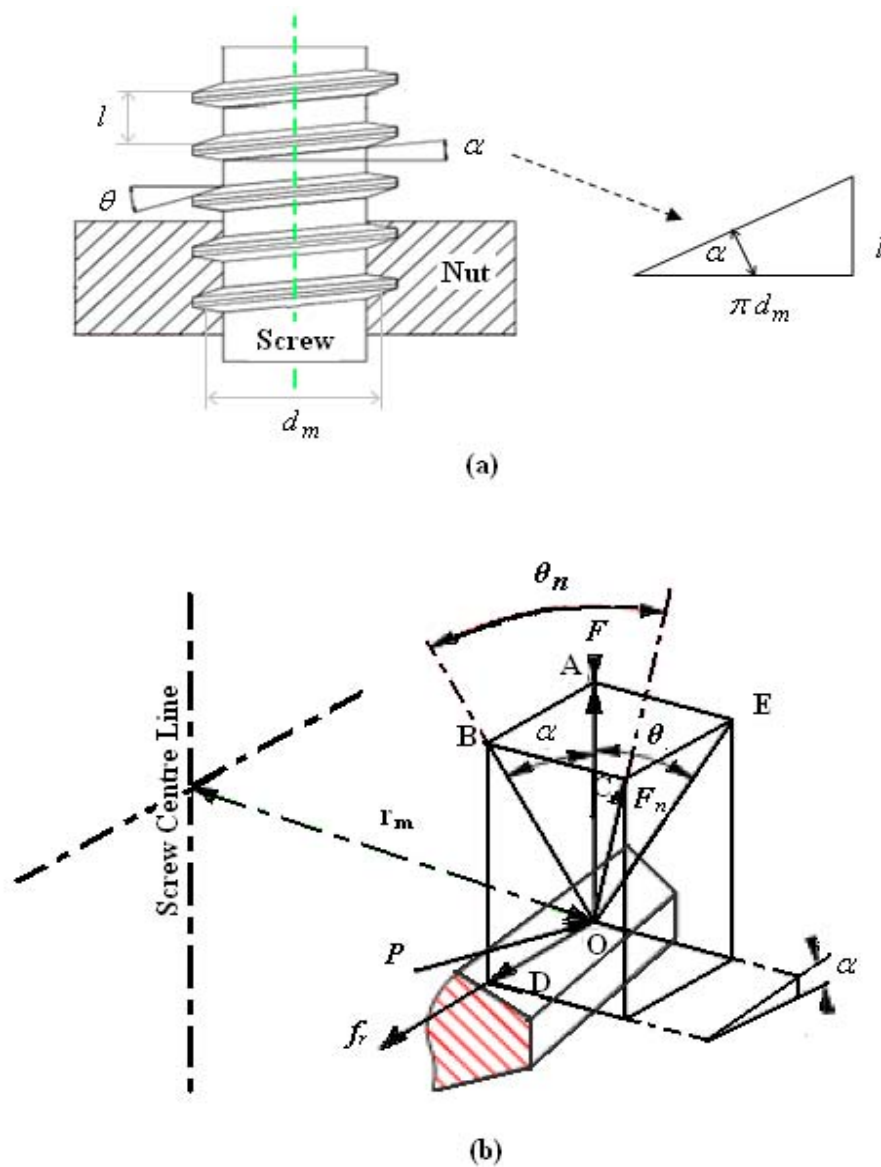


Figure 3.11 (a) Screw and nut coupling; (b) Detail of forces working in the power screw [36]

Figure 3.11(a) illustrates coupling between nut and screw and also its parameters that must be considered. There is an additional useful geometric relationship between lead angle, α , and lead, l . Suppose the triangular segment of a plane wrapped around the screw is considered in such a way that slanted edge lies along the helix and follows it for one revolution, obviously we have

$$\tan \alpha = \frac{l}{\pi d_m} . \quad (3.29)$$

Figure 3.11(b) illustrates a force P which is applied at a mean radius r_m which causes the load to be raised. The reactive forces act at point O on the screw thread surface. The reactive force F_n acting normal to the surface has the following components:

OD = f_r which is the friction force opposing movement up the thread surface

OA = is equal and opposite to the force being lifted. (F)

OB = is the vector sum of OD and OA and forms an angle θ_n with vector F_n

Summing the forces in the vertical direction results in

$$F_n \cos \theta_n \cos \alpha = F + f_r \sin \alpha . \quad (3.30)$$

If coefficient friction of screw surface is μ_s , then friction force is expressed as

$$f_r = \mu_s F_n . \quad (3.31)$$

By substituting Eq. 3.31 into Eq. 3.30, yields

$$F_n = \frac{F}{\cos \theta_n \cos \alpha - \mu_s \sin \alpha} . \quad (3.32)$$

By considering forces in horizontal direction, obviously we have

$$P = f_r \cos \alpha + F_n \cos \theta_n \sin \alpha, \quad (3.33)$$

and by substituting Eq. 3.31 into Eq. 3.33, yields

$$P = F_n (\mu_s \cos \alpha + \cos \theta_n \sin \alpha). \quad (3.34)$$

By equating F_n at Eq. 3.34 and Eq. 3.32, force P applied on screw in order to lift force F can be expressed as

$$P = F \left(\frac{\mu_s \cos \alpha + \cos \theta_n \sin \alpha}{\cos \theta_n \cos \alpha - \mu_s \sin \alpha} \right). \quad (3.35)$$

By analyzing again Figure 3.11(b), it also can be concluded that:

$$\begin{aligned} BC &= AE = OA \cdot \tan \theta = OB \cdot \cos \alpha \tan \theta, \\ \tan \theta_n &= \frac{BC}{OB} = \cos \alpha \tan \theta. \end{aligned} \quad (3.36)$$

If lead angle α is small, then $\cos \alpha \approx 1$, so we have

$$\begin{aligned} \tan \theta_n &\approx \tan \theta, \\ \theta_n &\approx \theta. \end{aligned} \quad (3.37)$$

Substituting Eq. 3.37 into Eq. 3.35, yields

$$\begin{aligned} P &= F \left(\frac{\mu_s \cos \alpha + \cos \theta \sin \alpha}{\cos \theta \cos \alpha - \mu_s \sin \alpha} \right), \\ P &= F \left(\frac{\mu_s + \cos \theta \tan \alpha}{\cos \theta - \mu_s \tan \alpha} \right). \end{aligned} \quad (3.38)$$

Again, by substituting Eq. 3.29 into Eq. 3.38, force P applied on screw to lift load F can be rewritten as

$$P = F \left(\frac{\pi \mu_s d_m + l \cos \theta}{\pi d_m \cos \theta - \mu_s l} \right). \quad (3.39)$$

In order to lift load F , a torque, T_{3U} , must be applied to the screw. If the screw has mean diameter d_m , then the torque applied to the screw can be expressed as

$$T_{3U} = P \frac{d_m}{2}. \quad (3.40)$$

Substituting Eq. 3.39 into Eq. 3.40, the applied torque required to lift load F can be expressed as

$$T_{3U} = \frac{d_m}{2} F \left(\frac{\pi \mu_s d_m + l \cos \theta}{\pi d_m \cos \theta - \mu_s l} \right). \quad (3.41)$$

In order to lower load F , a torque must be applied to the screw in reverse direction with T_{3U} and it is named as T_{3L} . Applying torque in reverse direction will also deliver force P in reverse direction. By using same procedure in deriving T_{3U} , the torque required to lower load F can be expressed as

$$T_{3L} = \frac{d_m}{2} F \left(\frac{\pi \cdot \mu_s \cdot d_m - l \cdot \cos \theta}{\pi \cdot d_m \cos \theta + \mu_s \cdot l} \right). \quad (3.42)$$

3.4.3.2 Worm-Gear Set

Conceptually in worm-gear set, the worm can be analogous to the screw power, and worm gear or gear can be analogous to the nut, see Figure 3.12. The forces resolution for power screw may therefore be directly applied to the case of a worm by observing that screw lead angle α is equivalent to worm lead angle λ_w , and power screw normal angle θ_n is equivalent to normal pressure angle φ_n for the worm gear. Illustration of these forces, based on Figure 3.11(b), can be seen in Figure 3.13.

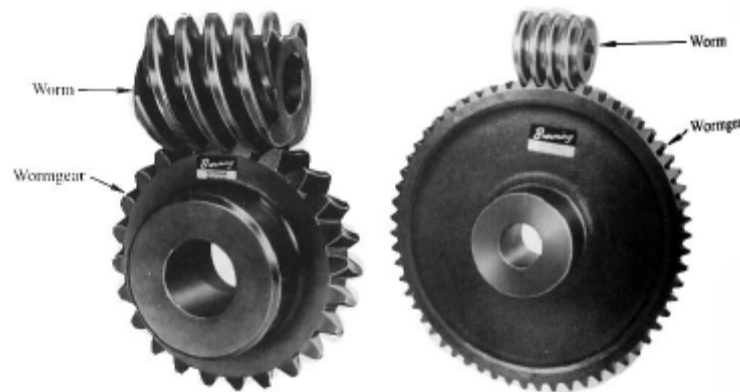


Figure 3.12 Worm gear [37]

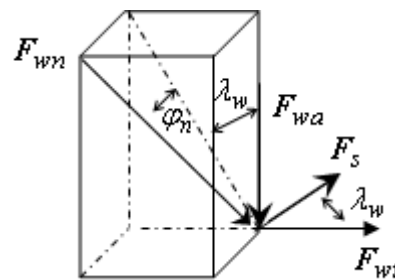


Figure 3.13 Detail of forces on worm gear

If worm has lead l_w per revolution and diameter d_w , then worm lead angle λ_w can be determined by

$$\tan \lambda_w = \frac{l_w}{\pi d_w}. \quad (3.43)$$

Based on Figure 3.13, by summing the forces in vertical direction obviously results in

$$F_{wa} = F_{wn} \cos \varphi_n \cos \lambda_w - F_s \sin \lambda_w, \quad (3.44)$$

where F_{wa} is axial force of worm, F_{wn} is reactive force on worm, and F_s friction force of worm. If coefficient friction of worm surface is μ_w , then the friction force F_s is expressed as

$$F_s = \mu_w F_{wn}. \quad (3.45)$$

If Eq. 3.45 is substituted into Eq. 3.44, then the reactive force F_{wn} is written as

$$F_{wn} = \frac{F_{wa}}{\cos \varphi_n \cos \lambda_w - \mu_w \sin \lambda_w}. \quad (3.46)$$

If forces in horizontal direction are considered, then by summing of these forces will result

$$F_{wt} = F_{wn} \cos \varphi_n \sin \lambda_w + F_s \cos \lambda_w, \quad (3.47)$$

where F_{wt} is tangential force of worm.

By substituting Eq. 3.46 into Eq. 3.47, the tangential force of worm can be expressed as [38]

$$F_{wt} = F_{wa} \left(\frac{\cos \varphi_n \sin \lambda_w + \mu_w \cos \lambda_w}{\cos \varphi_n \cos \lambda_w - \mu_w \sin \lambda_w} \right),$$

$$F_{wt} = F_{wa} \left(\frac{\cos \varphi_n \tan \lambda_w + \mu_w}{\cos \varphi_n - \mu_w \tan \lambda_w} \right). \quad (3.48)$$

Then, by substituting Eq. 3.43 into Eq. 3.48, yields

$$F_{wt} = F_{wa} \left(\frac{l_w \cos \varphi_n + \pi \mu_w d_w}{\pi d_w \cos \varphi_n - \mu_w l_w} \right),$$

$$F_{wa} = F_{wt} \left(\frac{\pi d_w \cos \varphi_n - \mu_w l_w}{l_w \cos \varphi_n + \pi \mu_w d_w} \right). \quad (3.49)$$

From Figure 3.10(b), it is shown the relation of forces working at gear and worm. Forces on gear are related by equilibrium to forces on the worm as

$$F_{gt} = F_{wa}, \quad (3.50.a)$$

$$F_{ga} = F_{wt}, \quad (3.50.b)$$

where F_{gt} and F_{ga} are tangential and axial force working at gear respectively. If T_2 is torque applied on gear with diameter d_g , then this torque T_2 is expressed as

$$T_2 = \frac{d_g}{2} F_{gt}. \quad (3.51)$$

By equating Eq. 3.49 and Eq. 3.50.a and substitute into Eq. 3.51, yields

$$T_2 = \frac{d_g F_{wt}}{2} \left(\frac{\pi d_w \cos \varphi_n - \mu_w l_w}{l_w \cos \varphi_n + \pi \mu_w d_w} \right). \quad (3.52)$$

To actuate this mechanism, the worm is coupled directly to the shaft of a DC motor. If T_m is motor torque applied on worm to result tangential force F_{wt} which is expressed as

$$F_{wt} = \frac{2}{d_w} T_m, \quad (3.53)$$

then by substituting Eq. 3.53 into Eq. 3.52, torque applied on gear is expressed as

$$T_2 = \frac{d_g T_m}{d_w} \left(\frac{\pi d_w \cos \varphi_n - \mu_w l_w}{l_w \cos \varphi_n + \pi \mu_w d_w} \right). \quad (3.54)$$

Reviewing Figure 3.10 again, obviously can be seen that the gear and power screw are allied in same shaft so that torque required to actuate the gear, T_2 , will be equal to the torque required to turn power screw, T_3 . Since $T_3 = T_2$, then $T_{3U} = T_{2U}$ and T_{3U} is torque needed by screw to lift up the load F . In order to produce torque T_{3U} on the screw or T_{2U} on the gear, the DC motor must produce torque T_{mU} . If $T_3 = T_{3U}$, $T_2 = T_{2U}$, and $T_m = T_{mU}$ then by equating Eq. 3.41 and Eq. 3.44 yields

$$\frac{d_g T_{mU}}{d_w} \left(\frac{\pi d_w \cos \varphi_n - \mu_w l_w}{l_w \cos \varphi_n + \pi \mu_w d_w} \right) = \frac{d_m}{2} F \left(\frac{\pi \mu_s d_m + l \cos \theta}{\pi d_m \cos \theta - \mu_s l} \right),$$

$$T_{mU} = \frac{d_m d_w F}{2 d_g} \left(\frac{\pi \mu_s d_m + l \cos \theta}{\pi d_m \cos \theta - \mu_s l} \right) \left(\frac{l_w \cos \varphi_n + \pi \mu_w d_w}{\pi d_w \cos \varphi_n - \mu_w l_w} \right). \quad (3.55)$$

By using the same analogy for calculating T_{mU} , then the torque of the motor required to lower the load F which is known as T_{mL} , can be expressed as

$$T_{mL} = \frac{d_m d_w F}{2 d_g} \left(\frac{\pi \mu_s d_m - l \cos \theta}{\pi d_m \cos \theta + \mu_s l} \right) \left(\frac{l_w \cos \varphi_n + \pi \mu_w d_w}{\pi d_w \cos \varphi_n - \mu_w l_w} \right). \quad (3.56)$$

From Eq. 3.55 and Eq. 3.56, it can be shown that many coefficients, which are constant, are involved in the equation, so that if the constants are simplified then we have

$$\begin{aligned}
\frac{d_m d_w}{2 d_g} &= k_{pr}, \\
\left(\frac{\pi \mu_s d_m + l \cos \theta}{\pi d_m \cos \theta - \mu_s l} \right) &= k_{TU}, \\
\left(\frac{\pi \mu_s d_m - l \cos \theta}{\pi d_m \cos \theta + \mu_s l} \right) &= k_{TL}, \\
\left(\frac{l_w \cos \varphi_n + \pi \mu_w d_w}{\pi d_w \cos \varphi_n - \mu_w l_w} \right) &= k_{wg},
\end{aligned} \tag{3.57}$$

where k_{pr} is coefficient of power transmission ratio between worm gear set and power screw, k_{TU} and k_{TL} are coefficient of power screw in lifting and lowering load mechanism respectively, and k_{wg} is coefficient of worm gear set. Hence, Eq. 3.55 and Eq. 3.56 can be simplified into

$$\begin{aligned}
T_{mU} &= k_{pr} k_{TU} k_{wg} F \\
T_{mL} &= k_{pr} k_{TL} k_{wg} F
\end{aligned} \tag{3.58}$$

or it can be written as

$$T_m = k_m F, \tag{3.59}$$

where

$$\begin{aligned}
k_m = k_{mU} &= k_{pr} k_{TU} k_{wg} \Rightarrow T_m = T_{mU}, \text{ and} \\
k_m = k_{mL} &= k_{pr} k_{TL} k_{wg} \Rightarrow T_m = T_{mL}.
\end{aligned}$$

From Eq. 3.59, it can be seen that torque T_m is the input, and F is the output. Although not explicitly stated, it does not mean that if $T_m = 0$ then F must be zero. Because of friction, a certain value of F must be reached to make it *self-locking*,

before power screw start rotating and allow the load lift or lower, and it is called *overhauling*. To guarantee the screw will be self-locking, a condition based on the geometric parameter and coefficient of friction must be fulfilled [38].

3.4.3.3 External Forces Analysis

Torque and force which are provided by the motor and its mechanics system are used to overcome the load F in order to control amount of water in the ballast tank. Load F itself is total force working on the movable plate of variable ballast system which is coming from inside and outside of URV's hull. The illustration of forces working on the movable plate is shown in Figure 3.14.

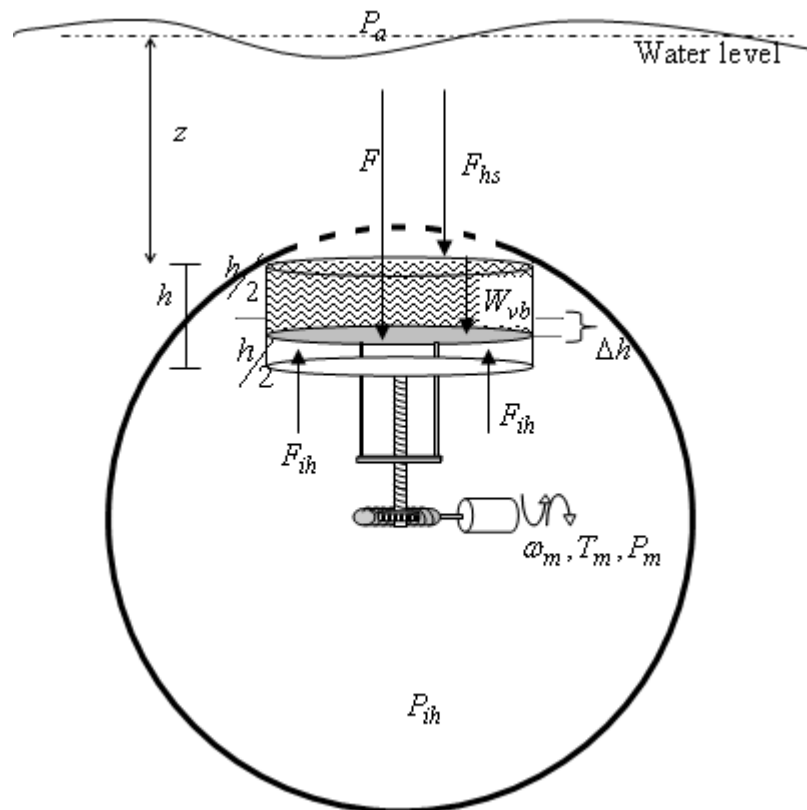


Figure 3.14 External forces working on variable ballast system.

If Figure 3.14 is analyzed, the force coming from inside hull, F_{ih} , is caused by the change of air pressure inside the hull, P_{ih} , due to the change of space inside the hull. As explained before, the variable ballast mechanism is used to control weight of URV by controlling volume of water in ballast tank. To control volume of the water, a mechanism like piston is designed. In this mechanism, a movable plate which is base of space in the tank that can be filled by water is used. By controlling position of the movable plate which is height of the tank, the volume of water in the tank can be controlled. Since space under movable plate is impermeable, by the change of position of movable plate, the volume of space inside URV's hull is also change. This change impacts to the air pressure inside the hull.

As known that relation between pressure and volume, V_{ih} , in closed space is expressed as [39]

$$P_{ih} V_{ih} = \text{constant} . \quad (3.60)$$

So, if the volume of air inside URV's hull is changed, then its pressure is also changed. In initial condition or in equilibrium condition, the pressure inside the hull is equal to the pressure of the air at water surface, P_a . By assuming the air pressure at water surface and temperature inside URV's hull are constant then since the volume of space inside the hull is constant, the pressure inside the hull is also constant. If volume of the space inside the hull is changed because of the change of position of movable plate, the pressure P_{ih} is also change and will cause a force act at movable plate surface, known as F_{ih} . The relation of P_a , P_{ih} , and F_{ih} is expressed as

$$F_{ih} = (P_{ih} - P_a) A_{vb} , \quad (3.61)$$

where A_{vb} is projected area of movable plate which is base of variable ballast tank.

In initial condition, where $P_{ih} = P_a$, volume of the air or empty space inside URV's hull is V_{ih} , and the position of movable plate is at the middle of full height of the tank, so if the maximum height of the tank is h then the position of movable plate is at $0.5h$ from the top of the tank, which is known as initial position. At this position, Δh , which is the change of movable plate position, is equal to zero ($\Delta h = 0$). So that if position of movable plate is upper than initial position ($< 0.5h$) then $\Delta h < 0$ and if lower than initial position then $\Delta h > 0$. By the change of Δh , the volume of the air or space inside the hull will change as ΔV . The relation is expressed as

$$\Delta V = \Delta h A_{vb}. \quad (3.62)$$

From Eq. 3.62, it is seen that the change of volume of the air inside the hull is equal to the change of volume of water in the ballast tank.

By changing the volume of the air, the pressure is also changed from its initial condition and expressed as

$$P_a V_{ih} = P_{ih} (V_{ih} - \Delta V),$$

$$P_{ih} = \frac{P_a V_{ih}}{V_{ih} - \Delta V}. \quad (3.63)$$

By substituting Eq. 3.62 into Eq. 3.63 and substitute the result into Eq. 3.61, then force acts on movable plate's surface due to change of volume of the air inside hull is expressed as

$$F_{ih} = \frac{\Delta h (A_{vb})^2 P_a}{V_{ih} - \Delta h A_{vb}}. \quad (3.64)$$

From Figure 3.14, it can be shown that load F is resultant of F_{hs} , ΔW , and F_{ih} , and the relation is expressed as

$$F = W_{vb} + F_{hs} - F_{ih}, \quad (3.65)$$

where W_{vb} is weight of the water in the ballast tank and F_{hs} is hydrostatic force on surface of movable plate. Weight of water in the ballast tank depends on volume of the water in this tank. In equilibrium or initial condition, the volume of water is half of maximum volume of the tank, $W_{vb} = W_{bs}$. By the change of position of movable plate in Δh , the weight of water in ballast is also will change in ΔW from initial weight. So that at any condition, W_{vb} can be expressed as

$$W_{vb} = W_{bs} + \Delta W. \quad (3.66)$$

Hydrostatic force, F_{hs} , is force acting on surface of immersed body caused by the height of liquid (water) above of it, or in other word it can be said that hydrostatic force is weight of the liquid above immersed surface. In this system, the height of liquid above is equal to the depth position of the URV. If depth position of URV is measured form water surface to top part of URV's body known as z , then F_{hs} acting on surface of movable plate is expressed as [34]

$$F_{hs} = \rho_w g A_{vb} z, \quad (3.67)$$

where ρ_w and g are density of water and gravitational acceleration respectively.

Substituting Eq. 3.64, Eq. 3.66, and Eq. 3.67 into Eq. 3.65, load F can be expressed as

$$F = W_{bs} + \Delta W + \rho_w g A_{vb} z - \frac{\Delta h (A_{vb})^2 P_a}{V_{ih} - \Delta h A_{vb}}, \quad (3.68)$$

and the change of water in the ballast tank is expressed as

$$\begin{aligned}\Delta W &= \Delta h A_{vb} \rho_w g, \\ \Delta h A_{vb} &= \frac{\Delta W}{\rho_w g}.\end{aligned}\quad (3.69)$$

Substituting Eq. 3.69 into Eq. 3.68, then the load F can be rewritten as

$$F = W_{bs} + \Delta W + \rho_w g A_{vb} z - \frac{\Delta W A_{vb} P_a}{\rho_w g V_{ih} - \Delta W}.\quad (3.70)$$

Recalling Eq. 3.59 and substitutes Eq. 3.70 into this equation, then torque of the motor that is required to change position of movable plate in order to control amount of water in ballast tank is expressed as

$$T_m = k_m \left(W_{bs} + \Delta W + \rho_w g A_{vb} z - \frac{\Delta W A_{vb} P_a}{\rho_w g V_{ih} - \Delta W} \right).\quad (3.71)$$

In order to change position of the movable plate, the DC motor must provide power P_m and rotates at angular velocity ω_m in order to produce torque at T_m , and can be expressed as

$$P_m = T_m \omega_m.\quad (3.72)$$

By substituting Eq. 3.27 and Eq. 3.71 into Eq. 3.72, obviously yields

$$P_m = k_m \left(W_{bs} + \Delta W + \rho_w g A_{vb} z - \frac{\Delta W A_{vb} P_a}{\rho_w g V_{ih} - \Delta W} \right) \frac{N_g 2\pi \dot{h}}{l N_w}.\quad (3.73)$$

If $\frac{N_g 2\pi}{l N_w} = k_{gc}$ is known as coefficient of velocity reduction of power screw and

worm gear couple, then Eq. 3.73 can be rewritten as

$$P_m = k_m k_{gc} \Delta \dot{h} \left(W_{bs} + \Delta W + \rho_w g A_{vb} z - \frac{\Delta W A_{vb} P_a}{\rho_w g V_{ih} - \Delta W} \right). \quad (3.74)$$

From Eq. 3.69, if A_{vb} , ρ_w , and g are simply constant, then by differentiating this equation results

$$\Delta \dot{h} = \frac{\Delta \dot{W}}{\rho_w g A_{vb}}, \quad (3.75)$$

where $\Delta \dot{h}$ is rate change of position of movable plate and $\Delta \dot{W}$ is rate change of weight of water in the ballast tank.

By substituting Eq. 3.75 into Eq. 3.74 and solving $\Delta \dot{W}$, then the rate change of weight of water in the ballast tank is obviously expressed as

$$\Delta \dot{W} = \frac{\rho_w g A_{vb} P_m}{k_m k_{gc} \left(W_{bs} + \Delta W + \rho_w g A_{vb} z - \frac{\Delta W A_{vb} P_a}{\rho_w g V_{ih} - \Delta W} \right)}. \quad (3.76)$$

3.5 Parameters of Spherical URV System and VBS

As mentioned in section 3.2, the diameter of the spherical URV used in the thesis is 35 cm. By considering the ambient parameters as ideal and constant condition, then in order to give ability to the URV moves downward in velocity about 1 ms^{-1} , parameters of URV's hull, variable ballast system and ambient are chosen as given in Table 3.1.

For the VBS mechanism, some constants value are chosen as standard value [38], those are $d_m = 0.01 \text{ m}$; $d_w = 0.01 \text{ m}$; $d_g = 0.026 \text{ m}$; $\mu_s = 0.15$; $\mu_w = 0.15$;

$l = 0.002 \text{ m}$; $l_w = 0.00314 \text{ m}$; $\theta = 15^\circ$; $\varphi_n = 20^\circ$; $N_w = 1$; and $N_g = 26$.

Table 3.1 Parameters of URV and the ambient

Parameters	Symbols	Values
Ambient parameters:		
Atmospheric pressure at water surface	P_a	1 atm
Density of water	ρ_w	998 kg/m ³
Dynamic viscosity of water	μ	10 ⁻³ Ns/m ²
Gravitational acceleration	g	9.81 m/s ²
URV's hull:		
Initial mass of URV	m_s	22.39 kg
Added mass of URV	m_a	11.2 kg
Diameter of URV	D_{fb}	0.35 m
Projected area of URV	A_{fb}	0.09616 m ²
Initial volume of empty space inside URV's hull	V_{ih}	50 % of V_{fb}
Variable ballast system:		
Diameter of variable ballast tank	D_{vb}	0.18 m
Projected area of base of variable ballast tank	A_{vb}	0.0254 m ²
Maximum height of variable ballast tank	h	0.08 m
Initial weight of water in ballast tank	W_{bs}	9.96 N
Transmission ratio of worm gear and power screw	k_{gc}	8.164x10 ⁴ rad/m
Coefficient of worm gear and power screw couple for downward moving	k_{mL}	4.601x10 ⁻⁵
Coefficient of worm gear and power screw couple for upward moving	k_{mU}	1.122x10 ⁻⁴
Power saturation resulted by DC motor	$\pm P_m \text{ max}$	±100 Watt
Angular velocity saturation of DC motor	$\pm \omega_m \text{ max}$	±157 rad/s

3.6 Summary

The dynamic model of depth positioning of a spherical URV is obtained by considering the physical laws involved in this system. Since the dimension of VBS is bounded therefore the change of weight is also bounded, then the dynamic model obtained in this chapter behave as nonlinear system. Therefore, in order to control this system, this nonlinearity must be considered. In the next chapter, the control systems will be designed in order to control the depth position of this spherical URV.

CHAPTER 4

CONTROL DESIGN

In order to position the spherical URV by using variable ballast mechanism, a proper controller must be designed. Since the dynamic model of this system is nonlinear, then linearized and nonlinear approaches are presented in this chapter. In nonlinear approach, feedback linearization which consist of state-space feedback linearization and input-output feedback linearization are presented. Analysis of control properties involving stability, controllability and observability are also presented in this chapter based on linearized model and original nonlinear model.

4.1 Linearized Approach

In the linearized approach, the original nonlinear model is linearized then a linear controller will be designed based on the linearized model. Before design of the controller is presented, some properties of control design based on linearized model will be analyzed in this section.

4.1.1 Properties of Control System

Knowing the properties of control system such as stability, controllability, and observability, is important in designing the controller. By analyzing the controllability of the system, it can be known whether the system is controllable or uncontrollable. Therefore, if the system is controllable then the controller can be designed. The controller is designed in order to stabilize the system. The stability of the system can be analyzed in Lyapunov sense.

4.1.1.1 Controllability and Stability of Linearized Model

Revisit a linear system, the linear system is to be controllable if a given control input \mathbf{u} can steer the system from $\mathbf{x}(0)$, as origin, into $\mathbf{x}(T)$, as a given target, in finite time [40]. A linear system which is expressed in state space as

$$\begin{aligned}\dot{\mathbf{x}} &= \mathbf{A}\mathbf{x} + \mathbf{B}\mathbf{u} \\ \mathbf{y} &= \mathbf{C}\mathbf{x}\end{aligned}\tag{4.1}$$

with $\mathbf{x} \in \mathbf{R}^n$ is completely controllable if and only if the controllable matrix \mathbf{C}_M has full rank, n which is order of the system. The controllability matrix \mathbf{C}_M is expressed as

$$\mathbf{C}_M = [\mathbf{B} \quad \mathbf{A}\mathbf{B} \quad \mathbf{A}^2\mathbf{B} \quad \dots \quad \mathbf{A}^{n-1}\mathbf{B}]\tag{4.2}$$

If a linear system is controllable, then control law $\mathbf{u} = \mathbf{K}(\mathbf{x} - \mathbf{x}_e)$ makes the closed loop system asymptotic stable about equilibrium point \mathbf{x}_e , where \mathbf{K} is feedback gain. A nonlinear system can be approximated with linear system using Taylor series expansion about a particular point. If the linearized model is controllable, then a linear control law can be implemented. Recalling the dynamic model of depth positioning of a spherical URV which is derived in chapter 3, can be expressed as

$$\begin{aligned}\dot{x}_1 &= x_2 \\ \dot{x}_2 &= \frac{x_3}{(m_s + m_a + \frac{x_3}{g})} - \frac{\text{sign}(x_2)C_D A_{fb} \rho_w x_2^2}{2(m_s + m_a + \frac{x_3}{g})} \\ \dot{x}_3 &= \frac{\rho_w g A_{vb}}{k_m k_{gc} \left(W_{bs} + x_3 + \rho_w g A_{vb} x_1 - \frac{A_{vb} P_a x_3}{\rho_w g V_{ih} - x_3} \right)} u \\ y &= x_1\end{aligned}\tag{4.3}$$

where $x_1 = z$, $x_2 = \mathbf{v}$, and $x_3 = \Delta W$ are state variables and $u = P_m$ is the input. If the equilibrium point occurs at any depth position, when power input, velocity and change of weight is zero, then $x_1 = x_{1e} = z_e$, $x_2 = x_{2e} = 0$, $x_3 = x_{3e} = 0$ and $u = u_e = 0$. Then by considering the linearization of Eq. 4.3 about equilibrium point, the linearized model of the system by using Taylor expansion is given as

$$\dot{\bar{\mathbf{x}}} = \left(\frac{\partial \mathbf{f}}{\partial \mathbf{x}} \right)_{\mathbf{x}=\mathbf{x}_e} \bar{\mathbf{x}} + \left(\frac{\partial \mathbf{f}}{\partial \mathbf{u}} \right)_{\mathbf{u}=\mathbf{u}_e} \bar{\mathbf{u}} \quad (4.4)$$

By solving Eq. 4.4, the linearized model is written in state space as

$$\begin{bmatrix} \dot{\bar{x}}_1 \\ \dot{\bar{x}}_2 \\ \dot{\bar{x}}_3 \end{bmatrix} = \begin{bmatrix} 0 & 1 & 0 \\ 0 & 0 & \frac{1}{m_s + m_a} \\ 0 & 0 & 0 \end{bmatrix} \begin{bmatrix} \bar{x}_1 \\ \bar{x}_2 \\ \bar{x}_3 \end{bmatrix} + \begin{bmatrix} 0 \\ 0 \\ \frac{\rho_w g A_{vb}}{k_m k_{gc}(W_{bs} + \rho_w g A_{vb} z_e)} \end{bmatrix} \bar{u} \quad (4.5)$$

$$y = x_1$$

By using method in Eq. 4.2, the controllability matrix \mathbf{C}_m of linearized model can be obtained as

$$\mathbf{C}_m = \begin{bmatrix} 0 & 0 \\ 0 & \frac{\rho_w g A_{vb}}{k_m k_{gc}(W_{bs} + \rho_w g A_{vb} z_e)(m_s + m_a)} \\ \frac{\rho_w g A_{vb}}{k_m k_{gc}(W_{bs} + \rho_w g A_{vb} z_e)} & 0 \end{bmatrix} \begin{bmatrix} \frac{\rho_w g A_{vb}}{k_m k_{gc}(W_{bs} + \rho_w g A_{vb} z_e)(m_s + m_a)} \\ 0 \\ 0 \end{bmatrix} \quad (4.6)$$

From Eq. 4.6, the rank of controllable matrix \mathbf{C}_m is 3 which is equal to the order of the system, $n = 3$. Then according to the Kalman rank condition [40], this linearized model is completely controllable, therefore the linear control law can be implemented.

Considering the stability of the system about the equilibrium point based on the linearized model, Lyapunov provides a method that is called Lyapunov's linearization method [41]. This method is concerned with the local stability of a nonlinear system. It is a formalization of intuition that a nonlinear system should behave similarly to its linearized approximation for small range motion. The relationship between the stability of linear system, Eq. 4.5, and that of the original nonlinear system, Eq. 4.3, is described as:

- If the linearized system is strictly stable which positions of all eigenvalues are at the left-half of complex plane, then the equilibrium point is asymptotically stable for the actual nonlinear system.
- If the linearized system is strictly unstable which at least position of one eigenvalue is at the right-half of complex plane, then the equilibrium point is unstable for the actual nonlinear system.
- If the linearized system is marginally stable which positions of all eigenvalues are at the left-half of complex plane, but at least one of them is on the $j\omega$ axis, then it cannot conclude anything from the linear approximation, the equilibrium point may be stable, asymptotically stable, or unstable for the actual nonlinear system.

Recalling the linearized model of depth positioning of the spherical URV in Eq. 4.5, the eigenvalues of the open loop system can be obtained from the characteristic equation as

$$|\lambda \mathbf{I} - \mathbf{A}| = 0 \quad (4.7)$$

By substituting \mathbf{A} matrix of linearized model in Eq. 4.5 into Eq. 4.7, then the characteristic equation of the system can be written as

$$\lambda^3 = 0 \quad (4.8)$$

Since the eigenvalues are on the $j\omega$ axis, then the Lyapunov's linearization method cannot conclude whether the equilibrium point of the actual nonlinear system in open loop condition is stable or unstable.

4.1.1.2 Observability of Linearized Model

A system to be completely observable if the state of the system or plan can be determined from a finite number of its most recent inputs and outputs [42]. Determining the state of the system from its inputs and outputs is important capability in control system design because in some situations it is necessary to know the actual states to control that states effectively. The observability of a system can be analyzed from the observability matrix.

The linear model at Eq. 4.1 is completely observable if the observability matrix, \mathbf{O}_m , has full rank. The observability matrix \mathbf{O}_m , can be obtained from

$$\mathbf{O}_m = \begin{bmatrix} \mathbf{C} \\ \mathbf{CA} \\ \mathbf{CA}^2 \\ \vdots \\ \mathbf{CA}^{n-1} \end{bmatrix} \quad (4.9)$$

where \mathbf{C} and \mathbf{A} are output matrix and coefficient matrix of the linear model respectively and n is order of the system. Then, if rank of matrix \mathbf{O}_m , is equal to n then the linear system is completely observable.

Recalling the linearized model from Eq. 4.5, the observability matrix can be obtained as

$$\mathbf{O}_m = \begin{bmatrix} 1 & 0 & 0 \\ 0 & 1 & 0 \\ 0 & 0 & \frac{1}{m_s + m_a} \end{bmatrix} \quad (4.10)$$

Since $\frac{1}{m_s + m_a}$ is constant and $\frac{1}{m_s + m_a} \neq 0$, then it is obvious that rank of the observability matrix \mathbf{O}_m , is 3 which is equal to the order of the system. Therefore the linearized model for depth positioning of the spherical URV is completely observable.

4.1.2 Feedback Control Design

The existence of feedback in automatic control system can improve performance of the control system even external disturbance is present. Therefore the availability of feedback control can stabilize the system.

Consider to an unstable linear or linearized system, in order to stabilize it, the poles placement method can be used. By designing the gain feedback, the poles of the closed loop linear system can be located at left-half of complex plane.

The closed loop system with gain feedback, \mathbf{K} , for linear system at Eq. 4.1 can be written as

$$\begin{aligned} \dot{\mathbf{x}}(t) &= [\mathbf{A} - \mathbf{B}\mathbf{K}]\mathbf{x}(t) + \mathbf{B}\mathbf{F}\mathbf{r}(t) \\ \mathbf{y} &= \mathbf{C}\mathbf{x}(t) \end{aligned} \quad (4.11)$$

where \mathbf{F} and $\mathbf{r}(t)$ are scaling factor and command input or input reference respectively. The control law of this closed loop system is

$$\mathbf{u}(t) = \mathbf{F} \mathbf{r}(t) - \mathbf{K} \mathbf{x}(t) \quad (4.12)$$

If $[\mathbf{A} - \mathbf{B}\mathbf{K}] = \mathbf{A}_{cl}$, then Eq. 4.11 can be written as

$$\dot{\mathbf{x}}(t) = \mathbf{A}_{cl} \mathbf{x}(t) + \mathbf{B}\mathbf{F} \mathbf{r}(t) \quad (4.13)$$

$$\mathbf{y} = \mathbf{C}\mathbf{x}(t)$$

By choosing a proper value of \mathbf{K} then the system will be asymptotically stable, therefore for $t \rightarrow \infty$, yields

$$\dot{\mathbf{x}}(\infty) = \dot{\mathbf{x}}_{\infty} = 0 \quad (4.14)$$

if \mathbf{r}_d is desired command input then yields

$$0 = \mathbf{A}_{cl} \mathbf{x}_{\infty} + \mathbf{B}\mathbf{F} \mathbf{r}_d$$

By solving \mathbf{x}_{∞} , yields

$$\mathbf{x}_{\infty} = -\mathbf{A}_{cl}^{-1} \mathbf{B}\mathbf{F} \mathbf{r}_d \quad (4.15)$$

In steady state condition,

$$\mathbf{y}_{\infty} = \mathbf{C}\mathbf{x}_{\infty} = \mathbf{r}_d \quad (4.16)$$

By solving \mathbf{x}_{∞} , yields

$$\mathbf{x}_{\infty} = \mathbf{C}^{-1} \mathbf{r}_d \quad (4.17)$$

By equating Eq. 4.17 and Eq. 4.15, yields

$$\mathbf{C}^{-1} \mathbf{r}_d = -\mathbf{A}_{cl}^{-1} \mathbf{B} \mathbf{F} \mathbf{r}_d$$

By solving \mathbf{F} , yields

$$\mathbf{F} = [\mathbf{C} [-\mathbf{A}_{cl}^{-1}] \mathbf{B}]^{-1} \quad (4.18)$$

Recalling the linearized model for depth positioning of a spherical URV as modeled by Eq. 4.5, if $\mathbf{K} = [k_1 \ k_2 \ k_3]$ and the command input $\mathbf{r} = z_d$ which is the desired depth position and also be the equilibrium point, $z_e = z_d$, then the closed loop system can be written as

$$\begin{bmatrix} \dot{\bar{x}}_1 \\ \dot{\bar{x}}_2 \\ \dot{\bar{x}}_3 \end{bmatrix} = \begin{bmatrix} 0 & 1 \\ 0 & 0 \\ -k_1 \frac{\rho_w g A_{vb}}{k_m k_{gc}(W_{bs} + \rho_w g A_{vb} z_d)} & -k_2 \frac{\rho_w g A_{vb}}{k_m k_{gc}(W_{bs} + \rho_w g A_{vb} z_d)} \end{bmatrix} \begin{bmatrix} \bar{x}_1 \\ \bar{x}_2 \\ \bar{x}_3 \end{bmatrix} + \begin{bmatrix} 0 \\ 0 \\ \frac{\rho_w g A_{vb}}{k_m k_{gc}(W_{bs} + \rho_w g A_{vb} z_d)} \end{bmatrix} \mathbf{F} z_d - k_3 \frac{1}{m_s + m_a} \begin{bmatrix} \bar{x}_1 \\ \bar{x}_2 \\ \bar{x}_3 \end{bmatrix} \quad (4.19)$$

Then by using MATLAB, \mathbf{F} can be solved as, (see Appendix 1)

$$\mathbf{F} = [k_1]$$

So, the control input for depth positioning of a spherical URV is presented as

$$u(t) = k_1 z_d - [k_1 \quad k_2 \quad k_3] \mathbf{x}(t) \quad (4.20)$$

From Eq. 4.19, if

$$\frac{1}{m_s + m_a} = C_1$$

and

$$\frac{\rho_w g A_{vb}}{k_m k_{gc} (W_{bs} + \rho_w g A_{vb} z_d)} = C_2$$

are time invariant, then Eq. 4.19 can be rewritten as

$$\begin{bmatrix} \dot{\bar{x}}_1 \\ \dot{\bar{x}}_2 \\ \dot{\bar{x}}_3 \end{bmatrix} = \begin{bmatrix} 0 & 1 & 0 \\ 0 & 0 & C_1 \\ -k_1 C_2 & -k_2 C_2 & -k_3 C_2 \end{bmatrix} \begin{bmatrix} \bar{x}_1 \\ \bar{x}_2 \\ \bar{x}_3 \end{bmatrix} + \begin{bmatrix} 0 \\ 0 \\ C_2 \end{bmatrix} k_1 z_d \quad (4.21)$$

Then the characteristic equation of the closed loop system is

$$\lambda^3 + k_3 C_2 \lambda^2 + k_2 C_1 C_2 \lambda + k_1 C_1 C_2 \quad (4.22)$$

The desired characteristic equation of the closed loop system for depth positioning of the spherical URV is

$$(\lambda + 2\xi a)(\lambda^2 + 2\xi a \lambda + a^2), \quad \xi, a > 0 \quad (4.23)$$

Therefore, the closed loop system is asymptotically stable. By matching coefficient of Eq. 4.22 and Eq. 4.23, then the gains is obtained as

$$\begin{aligned}
 k_1 &= \frac{2\xi a^3}{C_1 C_2} \\
 k_2 &= \frac{a^2(4\xi^2 + 1)}{C_1 C_2} \\
 k_3 &= \frac{4\xi a}{C_2}
 \end{aligned} \tag{4.24}$$

4.2 Nonlinear Approach

In nonlinear approach, the controller is designed based upon the original nonlinear model. Before design the controller, some properties of the control design are analyzed based upon the original nonlinear model and presented in this section.

4.2.1 Properties of Control System

Some nonlinear systems could not be approximated through linearized model in order to know the properties of the control system. In this sub section, the properties of the control system are analyzed from the original nonlinear model involving controllability, stability and observability.

4.2.1.1 Controllability and Stability of Nonlinear Model

An affine nonlinear system with single input and single output (SISO) can be expressed as

$$\begin{aligned}
 \dot{\mathbf{x}} &= \mathbf{f}(\mathbf{x}) + \mathbf{g}(\mathbf{x})u \\
 y &= h(\mathbf{x})
 \end{aligned} \tag{4.25}$$

In order to simplify checking controllability of nonlinear system at Eq. 4.25, local analysis is done, i.e. the results are valid only in neighborhood of operating point, but

global results are available elsewhere [43]. Local controllability can be determined by examining the rank of the controllability matrix which is analogous to the linear controllability matrix. The controllability matrix of nonlinear system can be obtained by using Lie brackets which is expressed as [43]

$$\mathbf{C}(\mathbf{x}) = \begin{bmatrix} ad_{\mathbf{f}}^{k-1} \mathbf{g}(\mathbf{x}) & ad_{\mathbf{f}}^k \mathbf{g}(\mathbf{x}) & \dots & ad_{\mathbf{f}}^{n-1} \mathbf{g}(\mathbf{x}) \end{bmatrix} \quad (4.26)$$

where $1 \leq k \leq n$, n is order of the system, and

$$\begin{aligned} ad_{\mathbf{f}}^0 \mathbf{g}(\mathbf{x}) &= \mathbf{g}(\mathbf{x}) \\ ad_{\mathbf{f}}^1 \mathbf{g}(\mathbf{x}) &= [\mathbf{f}, \mathbf{g}] = \nabla \mathbf{g} \mathbf{f} - \nabla \mathbf{f} \mathbf{g} \\ ad_{\mathbf{f}}^i \mathbf{g}(\mathbf{x}) &= [\mathbf{f}, ad_{\mathbf{f}}^{i-1} \mathbf{g}(\mathbf{x})] \quad \text{for } i = 1, 2, \dots \end{aligned}$$

Revisit nonlinear model at Eq. 4.3, then vector $\mathbf{f}(\mathbf{x})$ and $\mathbf{g}(\mathbf{x})$ can be express as

$$\mathbf{f}(\mathbf{x}) = \begin{pmatrix} x_2, & \frac{x_3 - \text{sign}(x_2) B_2 x_2^2}{(B_1 + \frac{x_3}{g})}, & 0 \end{pmatrix}^T \quad (4.27)$$

$$\mathbf{g}(\mathbf{x}) = \begin{pmatrix} 0, 0, & \frac{B_3}{\left(W_{bs} + x_3 + B_4 x_1 - \frac{B_5 x_3}{B_6 - x_3} \right)} \end{pmatrix}^T \quad (4.28)$$

where

$$B_1 = m_s + m_a ;$$

$$B_2 = \frac{C_D A_f b \rho_w}{2} ;$$

$$B_3 = \frac{\rho_w g A_{vb}}{k_m k_{gc}} ;$$

$$B_4 = \rho_w g A_{vb};$$

$$B_5 = A_{vb} P_a; \text{ and}$$

$$B_6 = \rho_w g V_{ih}.$$

The controllability matrix $\mathbf{C}(\mathbf{x})$ is obtained by using Lie brackets and solved in MATLAB (see Appendix 2). This controllability matrix has full rank, 3, which is equal to the order of the system. Thus, the nonlinear model at Eq. 4.3 holds the condition to be controllable.

Considering the stability of nonlinear model, Lyapunov provides a method that is known as Lyapunov direct method. Lyapunov's stability analyzes stability of the system at equilibrium state. The first step in analyzing stability using Lyapunov direct method is constructing possible Lyapunov function, $V(\mathbf{x})$. Once Lyapunov function is obtained, the Lyapunov stability can be analyzed. The Lyapunov theorems [44] say:

1. If it is possible to find a continuous scalar function $V(\mathbf{x})$ which has continuous first derivatives and which satisfies:

- | | |
|---|--|
| a. $V(\mathbf{x}) > 0, \quad \forall \mathbf{x} \neq 0$ | $V(\mathbf{x})$ is positive definite |
| b. $\dot{V}(\mathbf{x}) \leq 0$ | $\dot{V}(\mathbf{x})$ is negative semidefinite |
| c. $V(\mathbf{x}) \rightarrow \infty$ as $\ x\ \rightarrow \infty$ | $V(\mathbf{x})$ is radially unbounded |

then the condition state \mathbf{x}_e which is satisfies $\mathbf{f}(\mathbf{x}_e, \mathbf{0}) = \mathbf{0}$ is globally stable in the Lyapunov sense. If only condition a and b are satisfied, then the equilibrium state is local stable in the vicinity of the origin.

2. If it is possible to find a continuous scalar function $V(\mathbf{x})$ which has continuous first derivatives and which satisfies:

- | | |
|---|--|
| a. $V(\mathbf{x}) > 0, \quad \forall \mathbf{x} \neq 0$ | $V(\mathbf{x})$ is positive definite |
| b. $\dot{V}(\mathbf{x}) < 0$ | $\dot{V}(\mathbf{x})$ is negative definite |
| c. $V(\mathbf{x}) \rightarrow \infty$ as $\ x\ \rightarrow \infty$ | $V(\mathbf{x})$ is radially unbounded |

then the condition state \mathbf{x}_e which is satisfies $\mathbf{f}(\mathbf{x}_e, \mathbf{0}) = \mathbf{0}$ is globally asymptotically stable in the Lyapunov sense.

One of the methods used for constructing Lyapunov function is the variable gradient method [41, 44] . The variable gradient method is a formal approach to construct Lyapunov function. An assumption of a certain form for the gradient of an unknown Lyapunov function is involved, and the Lyapunov function is obtained by integrating this assumed gradient.

If we consider the unforced nonlinear model of Eq. 4.25, then $\dot{\mathbf{x}} = \mathbf{f}(\mathbf{x})$, $\mathbf{x} \in \mathbf{R}^n$, for which $\mathbf{f}(\mathbf{0}) = \mathbf{0}$, and $V(\mathbf{x})$ is the possible Lyapunov function for this system. If $\mathbf{x}(t) : \mathbf{R}^+ \rightarrow \mathbf{R}^n$ is any differentiable function with $\mathbf{x}(0) = \mathbf{0}$, then for any possible Lyapunov function:

$$\dot{V}(\mathbf{x}) = \nabla V^T \dot{\mathbf{x}} = \nabla V^T \mathbf{f}(\mathbf{x}) \quad (4.29)$$

The possible Lyapunov function is obtained by integration, respectively

$$V(\mathbf{x}) = \int_{\mathbf{0}}^{\mathbf{x}} \nabla V^T d\mathbf{x} \quad (4.30)$$

where $\nabla V = \{\partial V / \partial x_1, \dots, \partial V / \partial x_n\}^T$ is the gradient function which is assumed as the form

$$\nabla V_i = \sum_{j=1}^n a_{ij} x_j \quad (4.31)$$

where a_{ij} is coefficients to be determined. The gradient function must satisfy the condition of symmetry, therefore

$$\frac{\partial \nabla V_i}{\partial x_j} = \frac{\partial \nabla V_j}{\partial x_i} \quad (\text{for } i, j = 1, 2, \dots, n) \quad (4.32)$$

Revisit the nonlinear model from Eq. 4.3, since this model is unforced, $u = 0$, then

$$\dot{\mathbf{x}} = \begin{pmatrix} x_2, & \frac{x_3 - \text{sign}(x_2)B_2x_2^2}{(B_1 + \frac{x_3}{g})}, & 0 \end{pmatrix}^T \quad (4.33)$$

Since the order of the system $n = 3$, then we assume the gradient of Lyapunov function candidate has the following form

$$\begin{aligned} \nabla V_1 &= a_{11}x_1 + a_{12}x_2 + a_{13}x_3 \\ \nabla V_2 &= a_{21}x_1 + a_{22}x_2 + a_{23}x_3 \\ \nabla V_3 &= a_{31}x_1 + a_{32}x_2 + a_{33}x_3 \end{aligned} \quad (4.34)$$

To satisfy symmetry condition, then

$$\frac{\partial \nabla V_1}{\partial x_2} = \frac{\partial \nabla V_2}{\partial x_1}; \quad \frac{\partial \nabla V_1}{\partial x_3} = \frac{\partial \nabla V_3}{\partial x_1}; \quad \text{and} \quad \frac{\partial \nabla V_2}{\partial x_3} = \frac{\partial \nabla V_3}{\partial x_2}$$

or:

$$\begin{aligned} x_1 \frac{\partial a_{11}}{\partial x_2} + a_{12} + x_2 \frac{\partial a_{12}}{\partial x_2} + x_3 \frac{\partial a_{13}}{\partial x_2} &= a_{21} + x_1 \frac{\partial a_{21}}{\partial x_1} + x_2 \frac{\partial a_{22}}{\partial x_1} + x_3 \frac{\partial a_{23}}{\partial x_1} \\ x_1 \frac{\partial a_{11}}{\partial x_3} + x_2 \frac{\partial a_{12}}{\partial x_3} + a_{13} + x_3 \frac{\partial a_{13}}{\partial x_3} &= a_{31} + x_1 \frac{\partial a_{31}}{\partial x_1} + x_2 \frac{\partial a_{32}}{\partial x_1} + x_3 \frac{\partial a_{33}}{\partial x_1} \\ x_1 \frac{\partial a_{21}}{\partial x_3} + x_2 \frac{\partial a_{22}}{\partial x_3} + a_{23} + x_3 \frac{\partial a_{23}}{\partial x_3} &= x_1 \frac{\partial a_{31}}{\partial x_2} + a_{32} + x_2 \frac{\partial a_{32}}{\partial x_2} + x_3 \frac{\partial a_{33}}{\partial x_2} \end{aligned} \quad (4.35)$$

Using assumed gradient at Eq. 5.34 as well as the dynamic model from Eq. 4.33 and substitute to Eq. 4.29 then we have

$$\dot{V}(\mathbf{x}) = \begin{bmatrix} a_{11}x_1 + a_{12}x_2 + a_{13}x_3 \\ a_{21}x_1 + a_{22}x_2 + a_{23}x_3 \\ a_{31}x_1 + a_{32}x_2 + a_{33}x_3 \end{bmatrix}^T \begin{pmatrix} x_2, & \frac{x_3 - \text{sign}(x_2)B_2x_2^2}{(B_1 + \frac{x_3}{g})}, & 0 \end{pmatrix}^T$$

$$\dot{V}(\mathbf{x}) = a_{11}x_1x_2 + a_{12}x_2^2 + a_{13}x_3x_2 + \frac{a_{21}x_1x_3 + a_{22}x_2x_3 + a_{23}x_3^2}{(B_1 + \frac{x_3}{g})} - \frac{(a_{21}x_1 + a_{22}x_2 + a_{23}x_3)\text{sign}(x_2)B_2x_2^2}{(B_1 + \frac{x_3}{g})} \quad (4.36)$$

In order to fulfill symmetry condition, a proper a_{ij} for $(i, j = 1, 2, 3)$ must be chosen. If we chose $a_{11} = a_{12} = a_{21} = a_{13} = a_{31} = 0$, $a_{22} = 1$, and $a_{23} = a_{32} = -1$, then Eq. 4.36 can be written as

$$\dot{V}(\mathbf{x}) = \frac{x_2x_3 - x_3^2}{(B_1 + \frac{x_3}{g})} - \frac{(x_2 - x_3)\text{sign}(x_2)B_2x_2^2}{(B_1 + \frac{x_3}{g})} \quad (4.37)$$

Then by simplifying Eq. 4.37 obviously we have

$$\dot{V}(\mathbf{x}) = \frac{(x_3 - \text{sign}(x_2)B_2x_2^2)(x_2 - x_3)}{(B_1 + \frac{x_3}{g})} \quad (4.38)$$

If $a_{33} = 1$, then gradient from Eq. 4.34 can be expressed in vector as

$$\nabla V = \begin{bmatrix} 0 \\ x_2 - x_3 \\ x_3 - x_2 \end{bmatrix} \quad (4.39)$$

The possible Lyapunov function can be obtained as

$$\begin{aligned} V(\mathbf{x}) &= \int_0^{x_1} 0 \, dx_1 + \int_0^{x_2} x_2 \, dx_2 + \int_0^{x_3} (x_3 - x_2) \, dx_3 \\ &= \frac{x_2^2}{2} - x_2 x_3 + \frac{x_3^2}{2} \end{aligned} \quad (4.40)$$

From some parameters and specification (see table 3.1) used in the system, it is known that:

1. x_2 and x_3 are upper and lower bounded.
2. $m_s + m_a > \frac{x_3}{g}$

Therefore, from the above conditions of the system, and if condition

$$\text{sign}(x_2)B_2x_2^2 < x_3 \text{ and } x_2 < x_3$$

or if

$$\text{sign}(x_2)B_2x_2^2 > x_3 \text{ and } x_2 > x_3$$

are satisfied then the gradient $\dot{V}(\mathbf{x})$ at Eq. 4.38 is negative definite, otherwise it is positive definite. Therefore, $\dot{V}(\mathbf{x})$ satisfy the condition to be first derivative of Lyapunov function because it is locally negative definite.

By considering the possible Lyapunov function at Eq. 4.40, if $x_2 = x_3$, then $V(\mathbf{x}) = 0$, otherwise $V(\mathbf{x}) > 0$; $\forall \mathbf{x} \neq 0$. Therefore, it can be concluded that $\forall \mathbf{x} \neq 0$, the Lyapunov function $V(\mathbf{x})$ is positive semidefinite. From characteristic of $\dot{V}(\mathbf{x})$ and $V(\mathbf{x})$, it can be concluded that the origin as one of the equilibrium point is unstable in Lyapunov sense. In order to stabilize this nonlinear system, state feedback will be used and explained in this chapter.

4.2.1.2 Observability of Nonlinear Model

As mentioned before, determining the state of the system from its inputs and outputs is an important capability because in some situation it is necessary to know the actual state to control that state effectively. For the linear time invariant control system, the observability can be known from observability matrix which is obtained directly from \mathbf{A} and \mathbf{C} matrix. It is so different in nonlinear control system. To analyze the observability of the nonlinear control system, we will need to work with a Lie algebra formed of operators rather than vector fields [45].

Revisit the nonlinear system from Eq. 4.25, let \mathbf{x} denotes the state vector and $y = h(\mathbf{x})$ denotes the output, then the observability map, $\Phi(\mathbf{x})$, for the system can be determined from Lie derivative of vector \mathbf{f} along h at point \mathbf{x} which is expressed as

$$\Phi(\mathbf{x}) = \begin{bmatrix} L_f^i h(\mathbf{x}) \\ L_f^{i+1} h(\mathbf{x}) \\ \vdots \\ L_f^{n-1} h(\mathbf{x}) \end{bmatrix} \quad \text{for } i = 0, 1, \dots, n-1, n \text{ is order of the system}$$

$$= \begin{bmatrix} h(\mathbf{x}) \\ \frac{\partial h}{\partial \mathbf{x}} \mathbf{f}(\mathbf{x}) \\ \frac{\partial}{\partial \mathbf{x}} \left(\frac{\partial h}{\partial \mathbf{x}} \mathbf{f}(\mathbf{x}) \right) \mathbf{f}(\mathbf{x}) \\ \vdots \\ \frac{\partial}{\partial \mathbf{x}} \left(\frac{\partial h}{\partial \mathbf{x}} (\dots) \right) \mathbf{f}(\mathbf{x}) \end{bmatrix} \quad (4.41)$$

The Jacobian of observability map is called observability matrix which is expressed as

$$\frac{\partial}{\partial \mathbf{x}} \Phi(\mathbf{x}) = \begin{bmatrix} dh(\mathbf{x}) \\ dL_f h(\mathbf{x}) \\ dL_f^2 h(\mathbf{x}) \\ \vdots \\ dL_f^{n-1} h(\mathbf{x}) \end{bmatrix} \quad (4.42)$$

The nonlinear system is to be observable if the Jacobian or observability matrix,

$\frac{\partial}{\partial \mathbf{x}} \Phi(\mathbf{x})$, has full rank [46].

For the dynamic system from Eq. 4.3, the output is chosen as $y = x_1$. Then the observability map can be expressed as

$$\Phi(\mathbf{x}) = \begin{bmatrix} x_1 \\ x_2 \\ \frac{x_3 - \text{sign}(x_2)B_2x_2^2}{(B_1 + \frac{x_3}{g})} \end{bmatrix} \quad (4.43)$$

The observability matrix can be obtained by solving the Jacobian of the observability map which is expressed as

$$\frac{\partial}{\partial \mathbf{x}} \Phi(\mathbf{x}) = \begin{bmatrix} 1 & 0 & 0 \\ 0 & 1 & 0 \\ 0 & -\frac{2\text{sign}(x_2)B_2x_2}{B_1 + \frac{x_3}{g}} & \frac{gB_1 + \text{sign}(x_2)B_2x_2^2}{g(B_1 + \frac{x_3}{g})^2} \end{bmatrix} \quad (4.44)$$

The observability matrix of the dynamic system has full rank for all possible values of \mathbf{x} . Therefore the dynamic model of depth positioning of spherical URV given at Eq. 4.3 is observable.

4.2.2 Feedback Linearization Control Design

Feedback linearization is one of the methods in designing feedback controller for nonlinear control system. The main idea of this method is to algebraically transform nonlinear systems dynamics into (fully or partly) linear ones, therefore linear control techniques can be applied. This differs entirely from conventional linearization method because feedback linearization is achieved by exact state transformation and feedback, rather than by linear approximations of the dynamics. The feedback linearization can be viewed as ways of transforming original system models into equivalent models of a simple form. The transforming model is in the form of linear model, therefore in order to design the controller, the linear control designed can be considered.

The depth positioning system of a spherical URV modeled by Eq. 4.3 has single input and single output, therefore single input single output (SISO) feedback linearization strategies are considered. There are two approaches in SISO feedback linearization which are as follow [41, 46, 47]:

- **Input-state linearization or state-space linearization**

In the state-space linearization approach, the goal is to linearize the map between the transformed input and the entire vector of transformed state variable. It means that the whole states of the system are linearized. The linear control strategy is then designed for the linearized state-space model. In the application, not all models are state-space linearizable. There are some condition must be satisfied.

▪ **Input-output linearization**

In the input-output linearization approach, the objective is to linearize the map between transformed input and the actual output. A linear controller strategy is then synthesized for the linearized input-output model.

4.2.2.1 State-Space Linearization

A single input single output of nonlinear model given as Eq. 4.25 is to be state-space linearizable if and only if it satisfies the below conditions [41, 48]:

- Controllable, the matrix $\begin{bmatrix} \mathbf{g}(\mathbf{x}) & ad_{\mathbf{f}}\mathbf{g}(\mathbf{x}) & \cdots & ad_{\mathbf{f}}^{n-1}\mathbf{g}(\mathbf{x}) \end{bmatrix}$ has rank n or it has full rank.
- The vector fields $(\mathbf{g}(\mathbf{x}), ad_{\mathbf{f}}\mathbf{g}(\mathbf{x}), \dots, ad_{\mathbf{f}}^{n-2}\mathbf{g}(\mathbf{x}))$ are involutive.

A set of vector field $\{X_1(x), \dots, X_p(x)\}$ is involutive if there is scalar function $\delta_{ijk}(x)$ such that Eq. 4.45 is satisfied.

$$ad_{X_i} X_j(x) = \sum_{k=1}^p \delta_{ijk}(x) X_k(x), \quad 1 \leq i, j \leq p, i \neq j \quad (4.45)$$

Therefore when Lie bracket is taken with in this vector field, a new vector will not be generated. Hence the rank of $\{X_1(x), \dots, X_p(x), [X_i, X_j], \dots\}; 1 \leq i, j \leq p, i \neq j$ is equal to p .

If both condition are satisfied, then new state variable $\mathbf{z} = \phi(\mathbf{x})$ and new input v are determined in such that satisfy a linear time-invariant relation

$$\dot{\mathbf{z}} = \mathbf{A}\mathbf{z} + \mathbf{b}v \quad (4.46)$$

where

$$\mathbf{A} = \begin{bmatrix} 0 & 1 & \cdots & 0 & 0 \\ 0 & 0 & \cdots & 0 & 0 \\ \vdots & \vdots & \vdots & \vdots & \vdots \\ 0 & 0 & \cdots & 0 & 1 \\ 0 & 0 & \cdots & 0 & 0 \end{bmatrix}; \quad \mathbf{b} = \begin{bmatrix} 0 \\ 0 \\ \vdots \\ 0 \\ 1 \end{bmatrix}.$$

The feedback control law can be designed as

$$u = \psi(\mathbf{x}) + \gamma(\mathbf{x})v \quad (4.47)$$

where

$$\psi(\mathbf{x}) = -\frac{L_{\mathbf{f}}^n z_1}{L_{\mathbf{g}} L_{\mathbf{f}}^{n-1} z_1}; \quad \gamma(\mathbf{x}) = \frac{1}{L_{\mathbf{g}} L_{\mathbf{f}}^{n-1} z_1};$$

and n is order of the system. The new state \mathbf{z} is called the linearizing state, and the control law at Eq. 4.47 is called linearizing control law. The $\phi(\mathbf{x})$ is diffeomorphism in such that $\mathbf{x} = \phi^{-1}(\mathbf{z})$ is satisfied.

In order to determine the linearizing state \mathbf{z} , the first state z_1 must be determined by considering the following conditions [41]:

$$\begin{aligned} \nabla_{z_1} ad_{\mathbf{f}}^i \mathbf{g} &= 0 & i = 0, \dots, n-2 \\ \nabla_{z_1} ad_{\mathbf{f}}^{n-1} \mathbf{g} &\neq 0 & n \text{ is order of the system} \end{aligned} \quad (4.48)$$

Then the state transformation $\mathbf{z}(\mathbf{x}) = [z_1 \quad L_{\mathbf{f}}z_1 \quad \cdots \quad L_{\mathbf{f}}^{n-1}z_1]^T$ is used as a new set of state variables, and the state equation verify

$$\begin{aligned} \dot{z}_k &= z_{k+1} & k &= 1, \dots, n-1 \\ \dot{z}_n &= L_{\mathbf{f}}^n z_1 + L_{\mathbf{g}} L_{\mathbf{f}}^{n-1} z_1 u \end{aligned} \quad (4.49)$$

Consider to designing the state-space feedback linearization for dynamic model given at Eq. 4.3, it must satisfy the conditions to be state-space linearizable before continuing the controller designing. As mentioned in sub section 4.2.1.1, this dynamic model is controllable thus it holds first condition to be state-space linearizable.

In view of the second condition of nonlinear system to be state-space linearizable, since the dynamic model at Eq. 4.3 is 3rd order system then the set of the vector fields be examined for its involutivity are $\{\mathbf{g}(\mathbf{x}), ad_{\mathbf{f}}\mathbf{g}(\mathbf{x})\}$. By using Lie bracket, the vector $ad_{\mathbf{f}}\mathbf{g}(\mathbf{x})$ is obtained as

$$ad_{\mathbf{f}}\mathbf{g}(\mathbf{x}) = \begin{bmatrix} 0 \\ -\frac{B_1 B_3 g + \text{sign}(x_2) B_2 B_3 x_2^2}{g \left(B_1 + \frac{x_3}{g} \right)^2 \left(W_{bs} + B_4 x_1 + x_3 - \frac{B_5 x_3}{B_6 - x_3} \right)} \\ -\frac{B_3 B_4 x_2}{\left(W_{bs} + B_4 x_1 + x_3 - \frac{B_5 x_3}{B_6 - x_3} \right)^2} \end{bmatrix} \quad (4.50)$$

Then by using m file in MATLAB (Appendix 2), the involutivity of these vector fields are analyzed. Since the rank of set of vector $\{\mathbf{g}(\mathbf{x}), ad_{\mathbf{f}}\mathbf{g}(\mathbf{x}), [\mathbf{g}(\mathbf{x}), ad_{\mathbf{f}}\mathbf{g}(\mathbf{x})]\}$ is equal to 2, then these vector fields are involutive. Therefore the dynamic model for

depth positioning of the spherical URV given at Eq. 4.3 is state-space linearizable then state-space feedback linearization controller can be designed.

By considering the conditions given in Eq. 4.48, the first component z_1 of the new state vector \mathbf{z} should satisfy

$$\frac{\partial z_1}{\partial x_3} = 0 \quad \frac{\partial z_1}{\partial x_2} = 0 \quad \frac{\partial z_1}{\partial x_1} \neq 0 \quad (4.51)$$

Thus z_1 must be a function of x_1 only. The simplest solution to this equation is

$$z_1 = x_1 \quad (4.52)$$

The other states can be obtained by considering function $\mathbf{f}(\mathbf{x})$ given in Eq. 4.27.

$$\begin{aligned} z_2 &= \nabla_{z_1} \mathbf{f} = x_2 \\ z_3 &= \nabla_{z_2} \mathbf{f} = \frac{x_3 - \text{sign}(x_2) B_2 x_2^2}{(B_1 + \frac{x_3}{g})} = \dot{x}_2 \end{aligned} \quad (4.53)$$

Then by considering Eq. 4.51, the state space of state transformation is written as

$$\dot{\mathbf{z}} = \begin{bmatrix} 0 & 1 & 0 \\ 0 & 0 & 1 \\ 0 & 0 & 0 \end{bmatrix} \mathbf{z} + \begin{bmatrix} 0 \\ 0 \\ 1 \end{bmatrix} v \quad (4.54)$$

where v is new input of state transformation which is determined as

$$v = \dot{z}_3 = \nabla_{z_3} \mathbf{f} + \nabla_{z_3} \mathbf{g} u$$

$$= \frac{2B_2^2 x_2^3 - 2\text{sign}(x_2)B_2 x_2 x_3}{\left(B_1 + \frac{x_3}{g}\right)^2} + \frac{gB_1 B_3 + \text{sign}(x_2)B_2 B_3 x_2^2}{g\left(B_1 + \frac{x_3}{g}\right)^2 \left(W_{bs} + B_4 x_1 + x_3 - \frac{B_5 x_3}{B_6 - x_3}\right)} u \quad (4.55)$$

Then, if the original input u in Eq. 4.55 is solved, obviously we have

$$u = \frac{g\left(2\text{sign}(x_2)B_2 x_2 x_3 - 2B_2^2 x_2^3\right) \left(W_{bs} + B_4 x_1 + x_3 - \frac{B_5 x_3}{B_6 - x_3}\right)}{\left(gB_1 B_3 + \text{sign}(x_2)B_2 B_3 x_2^2\right)} \quad (4.56)$$

$$+ \frac{g\left(B_1 + \frac{x_3}{g}\right)^2 \left(W_{bs} + B_4 x_1 + x_3 - \frac{B_5 x_3}{B_6 - x_3}\right)}{\left(gB_1 B_3 + \text{sign}(x_2)B_2 B_3 x_2^2\right)} v$$

where,

$$\frac{g\left(2\text{sign}(x_2)B_2 x_2 x_3 - 2B_2^2 x_2^3\right) \left(W_{bs} + B_4 x_1 + x_3 - \frac{B_5 x_3}{B_6 - x_3}\right)}{\left(gB_1 B_3 + \text{sign}(x_2)B_2 B_3 x_2^2\right)} = \psi(x); \text{ and}$$

$$\frac{g\left(B_1 + \frac{x_3}{g}\right)^2 \left(W_{bs} + B_4 x_1 + x_3 - \frac{B_5 x_3}{B_6 - x_3}\right)}{\left(gB_1 B_3 + \text{sign}(x_2)B_2 B_3 x_2^2\right)} = \gamma(x).$$

Therefore Eq. 4.47 is hold and a linear control strategy can be designed based on transformed model given in Eq. 4.54.

If we compare the transformed state variables to the original state variables, it is clearly seen that the transformed state variables have physical meaning that are depth position, velocity, and acceleration for z_1 , z_2 and z_3 respectively.

By considering system in Eq. 4.54 as linear system, then linear feedback control strategy can be applied in order to stabilize the depth positioning system of the spherical URV. If feedback gain $\mathbf{K} = [k_1 \ k_2 \ k_3]$ is applied to the closed loop system of model in Eq.4.54, and the desired depth position is given as z_{1d} , then the new input v can be obtained as

$$v = k_1 z_{1d} - \mathbf{Kz} \quad (4.57)$$

By locating the eigenvalues, λ , of this closed loop system in left of half-complex plane, this feedback gain will asymptotically stabilize the system. The eigenvalues of the closed loop system of Eq. 4.54 can be obtained from the characteristic equation that is

$$\lambda^3 + k_3 \lambda^2 + k_2 \lambda + k_1 = 0 \quad (4.58)$$

and if the desired characteristic equation of the closed loop system for depth positioning of the spherical URV is

$$(\lambda + 2\xi a)(\lambda^2 + 2\xi a \lambda + a^2) = 0, \quad \xi, a > 0 \quad (4.59)$$

Thus the system is asymptotically stabilized, then by matching the coefficient of Eq. 4.58 and Eq. 4.59, the gain of the feedback can be expressed as

$$\begin{aligned}
 k_1 &= 2\xi a^3 \\
 k_2 &= 4\xi^2 a^2 + a^2 \\
 k_3 &= 4\xi a
 \end{aligned} \tag{4.60}$$

Since this controller asymptotically stabilizes the system then for $t \rightarrow \infty$, the output $y = z_1 = x_1 \rightarrow z_{1d}$.

4.2.2.2 Input-Output Linearization

The main idea of the input-output feedback linearization is to transform m equations via feedback into simple decoupled integrators, where m represents the number of inputs. This control technique is designed by differentiating the output, y , until the physical input, u , appears in the r^{th} derivative of the output. Then the input is chosen to cancel the nonlinearities and rising a synthetic input v . The simple relation between synthetic input v and the output y is obtained as (multiple integrator form)

$$y^{(r)} = v \tag{4.61}$$

where r is the relative degree obtained from differentiation. For the depth positioning model of the spherical URV given at Eq. 4.3, the output is chosen as $y = z = x_1$, which is the depth position. Then by differentiating this output until physical input u appears, obviously we have

$$\begin{aligned}
\dot{y} &= \dot{x}_1 = x_2 \\
\ddot{y} &= \dot{x}_2 = \frac{x_3 - \text{sign}(x_2)B_2x_2^2}{\left(B_1 + \frac{x_3}{g}\right)} \\
\ddot{y} &= \frac{\left(B_1g + \text{sign}(x_2)B_2x_2^2\right)\dot{x}_3 - (B_1g + x_3)2\text{sign}(x_2)B_2x_2\dot{x}_2}{g\left(B_1 + \frac{x_3}{g}\right)^2} \\
\ddot{y} &= \left(\frac{\left(B_1g + \text{sign}(x_2)B_2x_2^2\right)}{g\left(B_1 + \frac{x_3}{g}\right)^2} \right) \left(\frac{B_3}{\left(W_{bs} + B_4x_1 + x_3 - \frac{B_5x_3}{B_6 - x_3}\right)} u \right) \\
&\quad - \left(\frac{(B_1g + x_3)2\text{sign}(x_2)B_2x_2}{g\left(B_1 + \frac{x_3}{g}\right)^2} \right) \left(\frac{x_3 - \text{sign}(x_2)B_2x_2^2}{\left(B_1 + \frac{x_3}{g}\right)} \right) \\
&= \frac{B_1B_3g + \text{sign}(x_2)B_2B_3x_2^2}{g\left(B_1 + \frac{x_3}{g}\right)^2\left(W_{bs} + B_4x_1 + x_3 - \frac{B_5x_3}{B_6 - x_3}\right)} u + \frac{2B_2^2x_2^3 - 2\text{sign}(x_2)B_2x_2x_3}{\left(B_1 + \frac{x_3}{g}\right)^2}
\end{aligned} \tag{4.62}$$

From Eq. 4.62, it is seen clearly the relation between y and u , that is u appear at third differentiating of y . If the control input is chosen as

$$u = \frac{1}{\beta(\mathbf{x})}(v - \alpha(\mathbf{x})) \tag{4.63}$$

where

$$\beta(\mathbf{x}) = \frac{B_1B_3g + \text{sign}(x_2)B_2B_3x_2^2}{g\left(B_1 + \frac{x_3}{g}\right)^2\left(W_{bs} + B_4x_1 + x_3 - \frac{B_5x_3}{B_6 - x_3}\right)}; \text{ and}$$

$$\alpha(\mathbf{x}) = \frac{2B_2^2x_2^3 - 2\text{sign}(x_2)B_2x_2x_3}{\left(B_1 + \frac{x_3}{g}\right)^2}.$$

Since \mathbf{x} is bounded therefore $\beta(\mathbf{x}) \neq 0$ then the nonlinearities at Eq. 4.62 can be canceled and obtain simple input-output relation as

$$\ddot{y} = v \quad (4.64)$$

By considering Eq. 4.64 as linear system, then by applying feedback gain \mathbf{K} for the closed loop system yields the control law as

$$v = -k_1y - k_2\dot{y} - k_3\ddot{y} \quad (4.65)$$

where $[k_1 \quad k_2 \quad k_3] = \mathbf{K}$.

For stabilizing the system, poles placement method is used. A proper value of \mathbf{K} must be chosen in order to locate the poles at the left-half of complex plane. The characteristic equation of this closed loop system is given as

$$\lambda^3 + k_3\lambda^2 + k_2\lambda + k_1 = 0 \quad (4.66)$$

If desired characteristic equation of the closed loop system for depth positioning of the spherical URV is

$$(\lambda + 2\xi a)(\lambda^2 + 2\xi a\lambda + a^2) = 0, \quad \xi, a > 0 \quad (4.67)$$

thus the closed loop system is asymptotically stable, then by matching coefficient of Eq. 4.66 and Eq. 4.61, the feedback gains is obtained as

$$\begin{aligned}k_1 &= 2\xi a^3 \\k_2 &= 4\xi^2 a^2 + a^2 \\k_3 &= 4\xi a\end{aligned}\tag{4.68}$$

If y_d is a desired output then by applying tracking error $e(t) = y(t) - y_d(t)$, the control law is obtained as

$$v = \ddot{y}_d - k_1 e - k_2 \dot{e} - k_3 \ddot{e}\tag{4.69}$$

As an asymptotically stable system, this control law leads to exponential convergent tracking where for $t \rightarrow \infty$, $e(t) \rightarrow 0$.

4.3 Summary

The control design of a nonlinear system can be approximated through linearization of the nonlinear model. Since the linearized model of the system is controllable, then the linear control system can be applied. In this chapter, the nonlinear model for depth positioning of the spherical URV is linearized using Taylor series expansion at equilibrium point. Nonlinear control approach also applied in this system by using feedback linearization. As SISO nonlinear system, there are two kinds of feedback linearization which are state-space linearization and input-output linearization. Both approaches of feedback linearization are applied and presented in this chapter, in order to control the depth position of a spherical URV. Some properties of the control system such as controllability, observability and stability are analyzed based on linearized model and the original nonlinear model.

CHAPTER 5

RESULTS AND DISCUSSION

Dynamic model obtained in chapter 3 and control design derived in chapter 4 are simulated in Simulink/MATLAB. Simulink model of the dynamic model and control design are presented in this chapter. Some results are analyzed and discussed in this chapter.

5.1 Simulation of Open Loop System

In order to study the responses of the system resulted from the modeling process, the simulation using Simulink/MATLAB is built based on the mathematical models. Each model is simulated in separate Simulink block. Some input models are tested in order to analyze responses of the model.

5.1.1 Simulink Model

From Eq. 3.76, Simulink model of rate change of weight in the ballast tank, $\Delta\dot{W}$, is shown in Figure 5.1. From Figure 5.1, it can be seen that value of k_m depends on power input, P_m , which results torque T_m to change amount of water in the ballast tank. If $P_m > 0$ then $T_m = T_{mL}$ therefore $k_m = k_{mL}$, otherwise $k_m = k_{mU}$.

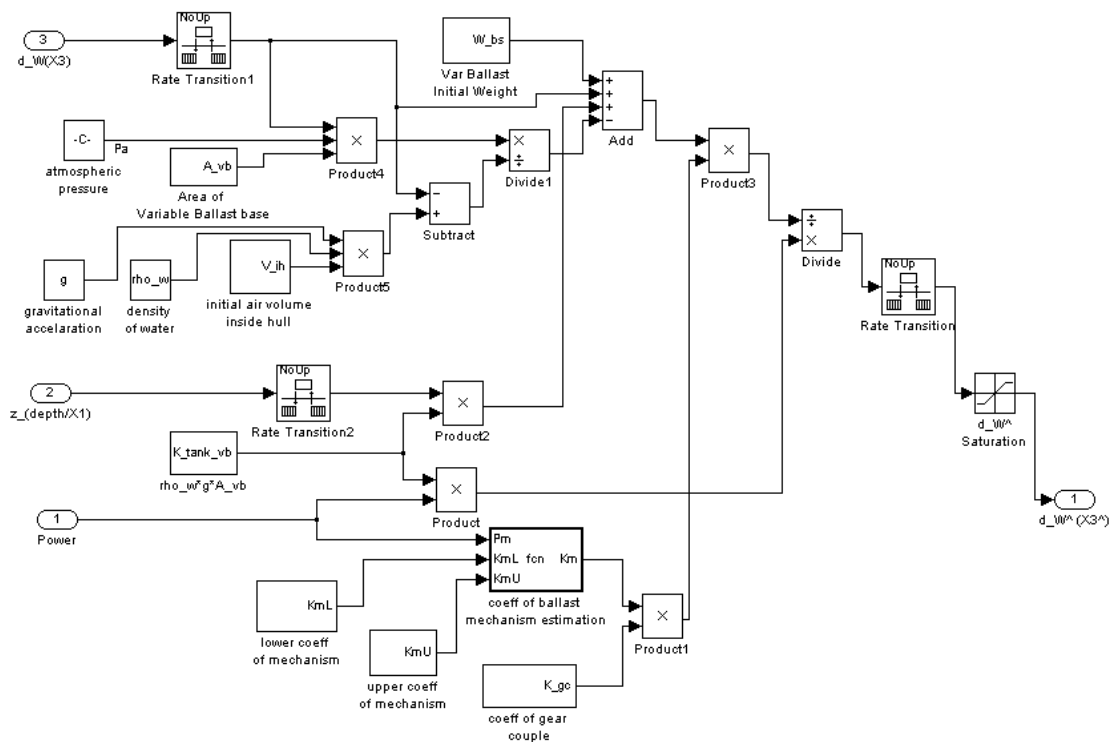


Figure 5.1 Model for rate change of weight in the ballast tank.

The rate change of weight in the ballast tank, $\Delta \dot{W}$, has saturation values ($\pm \Delta \dot{W}_{sat}$). This saturation value depends on the maximum angular velocity of the DC motor that drives this mechanism both in counterclockwise and clockwise direction. Then, the change of weight in the ballast tank, ΔW , can be obtained by integrating $\Delta \dot{W}$ which is shown in Figure 5.2. ΔW also has saturation values ($\pm \Delta W_{sat}$) which depends upon the maximum volume of the ballast tank.

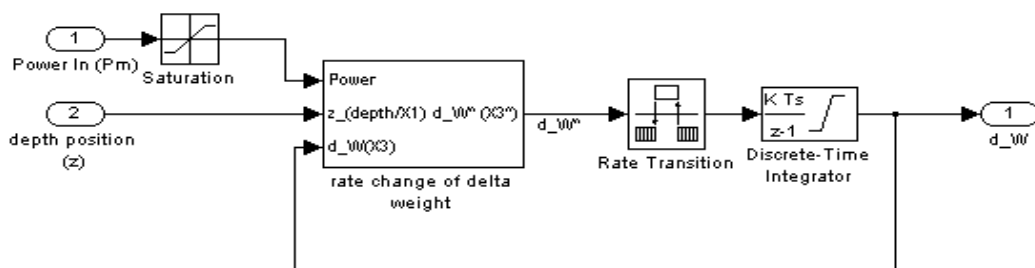


Figure 5.2 Model for the change of weight in the ballast tank.

The Simulink model of URV motion in vertical plane which is taken from Eq. 3.22, is shown in Figure 5.3.

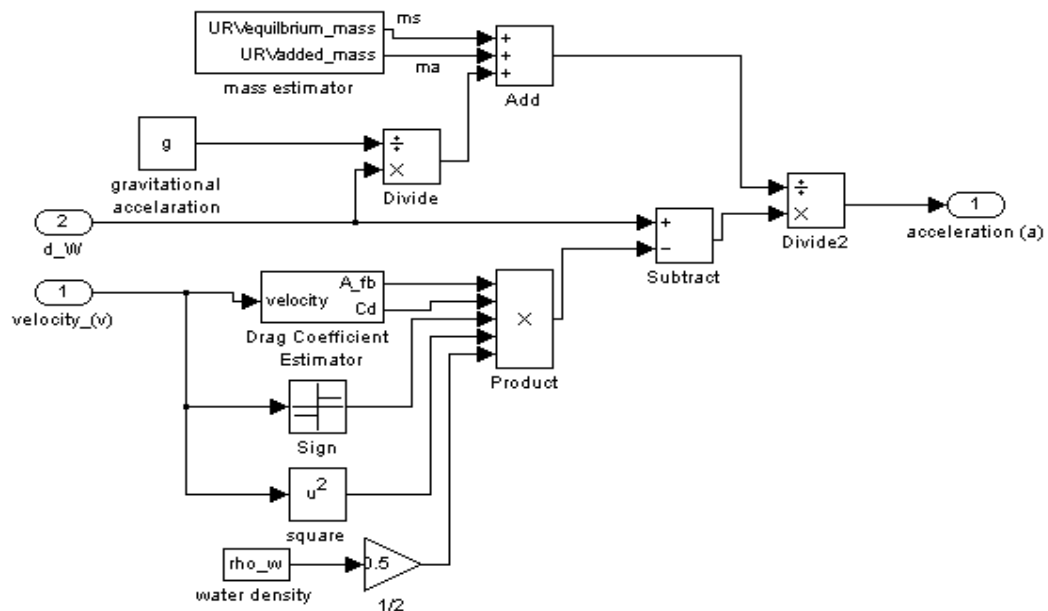


Figure 5.3 Model for vertical motion acceleration of URV.

Output of this model is acceleration of the URV. In order to obtain velocity of URV's vertical motion, \mathbf{v} , an integration block diagram is used. In order to get the depth position of the URV, this velocity is integrated. The Simulink model is shown in Figure 5.4. The condition of depth position and velocity are depth position always be positive ($z \geq 0$) and for $z = 0 \Rightarrow \mathbf{v} \geq 0$.

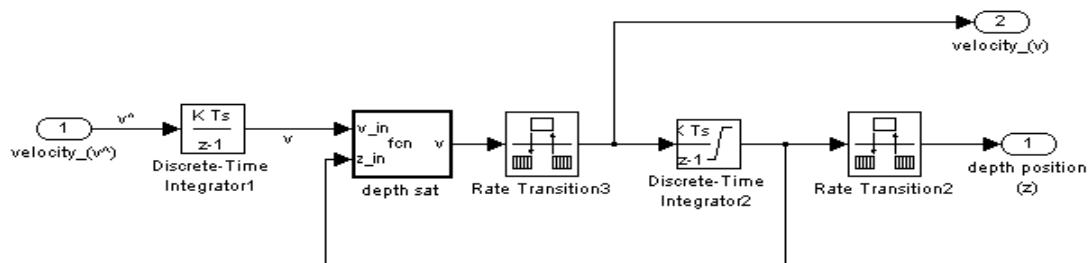


Figure 5.4 Model for velocity and depth position of URV.

By combining all models, obviously Simulink model for depth positioning of the spherical URV is shown in Figure 5.5.

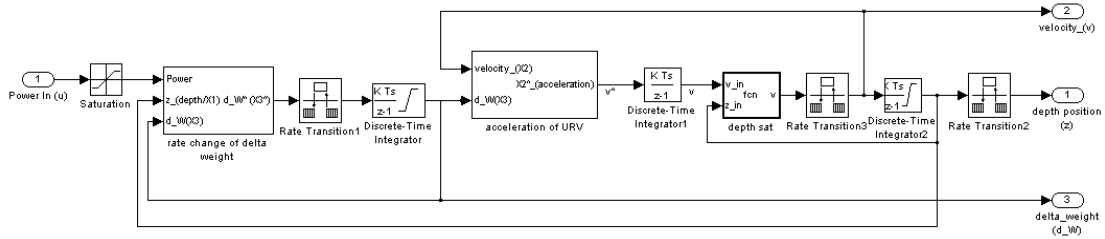


Figure 5.5 Model for depth positioning of a spherical URV.

From Figure 5.5, it can be shown that the power input, P_m , has saturation values that is $\pm P_m \text{ max}$. This power depends upon the power provided by the DC motor.

5.1.2 Simulation Result

The dynamic model for depth positioning of the spherical URV involves many constants and parameters both for URV and its ambient. The assumption of these constants and parameters used in the simulation are presented in Table 3.1. Some types of input are tested to analyze the response of the model. The first input tested in the open loop simulation is a single pulse input. The responses of the model are shown in Figure 5.6. The given power input from the DC motor, P_m , is a single pulse with an amplitude of 50 Watt. The origin position of URV is at 0 meter from the surface. Then by applying this input, the URV will descend from the surface.

From Figure 5.6, it is also seen when the power is applied to the motor as a positive value, the weight change, ΔW , is increased and reaches saturation around 9.96 N, as the maximum value of ΔW , and velocity \mathbf{v} reaches saturation at 1.019 ms^{-1} . When the power is reset to zero, ΔW still remains at the last value, and the URV still moves with velocity \mathbf{v} , which is proportional to ΔW . If power is given as negative, then ΔW will be decreased but velocity \mathbf{v} will still be positive since ΔW is positive. The depth position of URV, z , will increase since the velocity is available as positive.

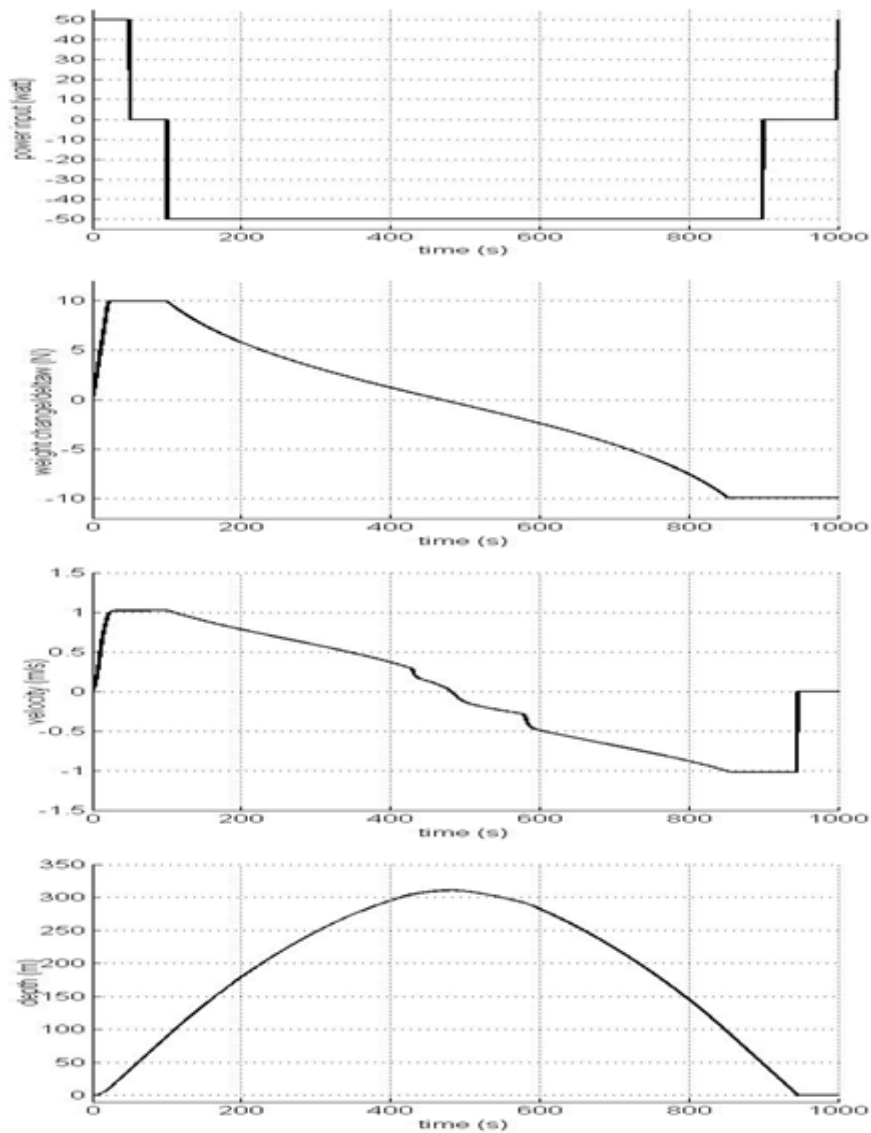


Figure 5.6 Response of the system for positive and negative pulse input.

If the velocity is negative, the URV is ascending as shown in Figure 5.7. The increment of ΔW depends on the total power given by the motor to actuate the variable ballast and also depends on the depth position of the URV. If the power given is small then the increment of ΔW is also small, and since the power is available, ΔW will keep increasing till reach saturation. If same power is given to the system but in different depth positions, the increment of ΔW at deeper position is lower than shallower position. This is caused by the availability of hydrostatic force which is become higher at deeper position. If power is keep applied as negative value, then

ΔW will reach negative saturation at -9.96 N and velocity \mathbf{v} also reach negative saturation at -1.019 ms^{-1} as shown in Figure 5.6.

When the power is zero, ΔW remains at its last value as well as velocity \mathbf{v} . The velocity will remain constant until ΔW change and velocity in this condition is known as *terminal velocity*. This is the advantage of using variable ballast as vertical motion actuator, even the zero power is given to the actuator, the URV still moves therefore it will save the power usage. If $\Delta W = 0$, then the zero velocity occurs and the URV is in zero buoyancy condition. The depth position of URV, z , will remain at its last position, and this condition is called *equilibrium point*. The equilibrium point occurs at any depth position since \mathbf{v} and ΔW is equal to zero.

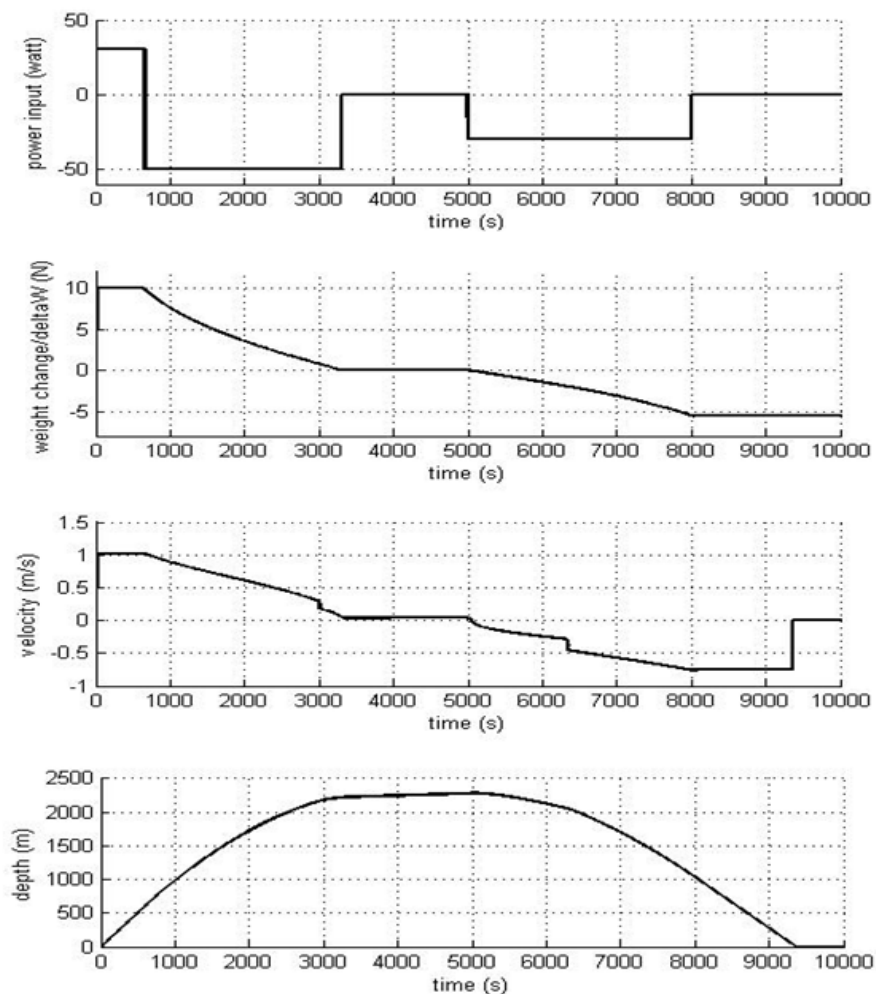


Figure 5.7 Response of the system for pulse input in different amplitude.

If ramp input is applied, then the response of the system is shown in Figure 5.8. By looking to the response, obviously the nonlinearity of the weight change of the URV's body and the velocity in vertical motion are shown. By the increment of P_m , \mathbf{v} and ΔW also increase until both of these reach saturation. Depth position, z , keeps increasing since $\mathbf{v} > 0$.

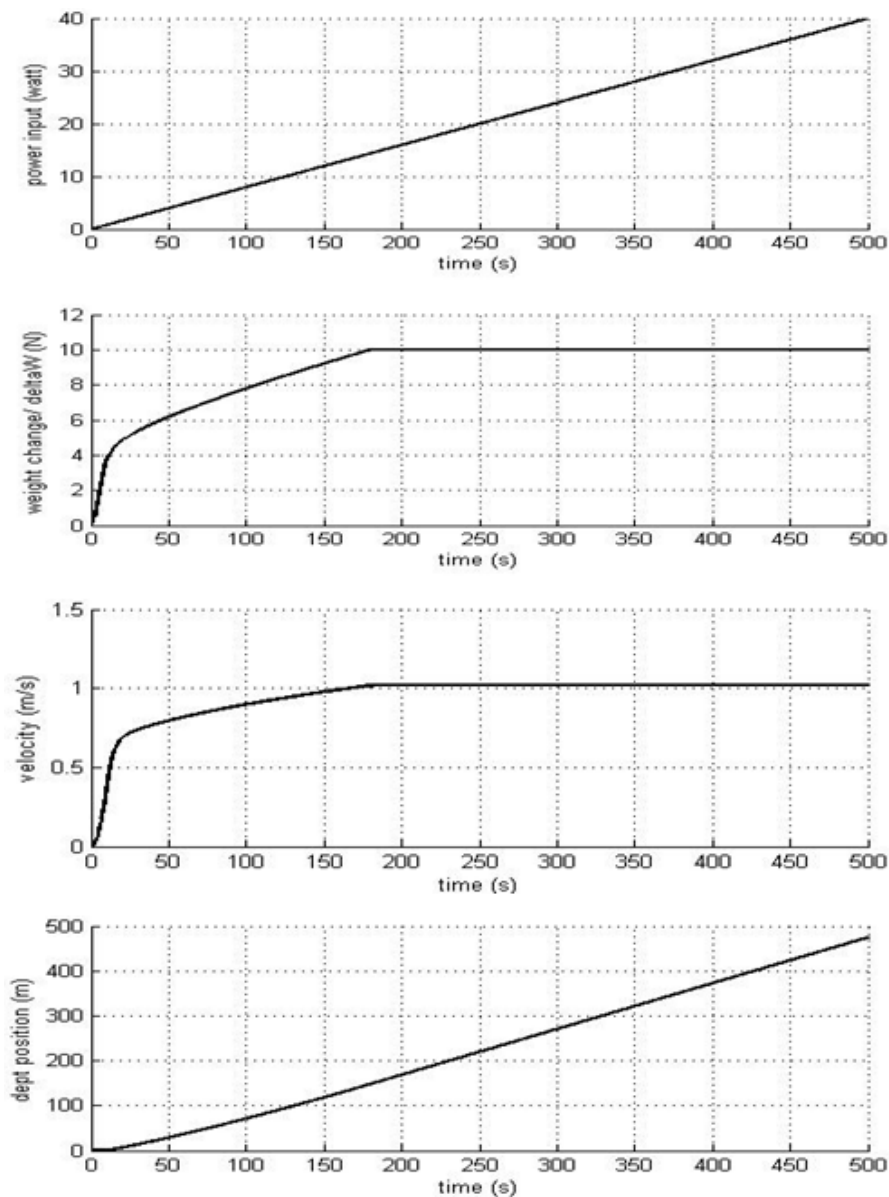


Figure 5.8 Response of the system for ramp input.

5.2 Simulation of Linearized Approach

By using MATLAB/Simulink, the linearized approximation strategy is simulated. This controller is applied to control the original nonlinear model for depth positioning of a spherical URV which the block diagram is shown in Figure 5.9. The control law from Eq. 4.20 can be constructed in Simulink model as shown in Figure 5.10.

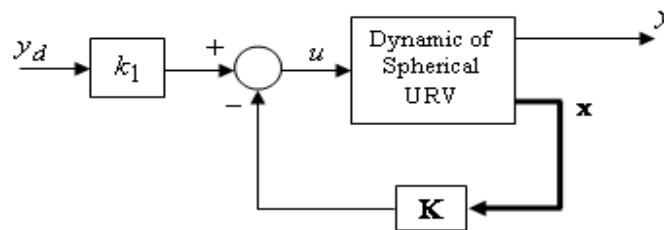


Figure 5.9 Schematic diagram of linearized approximation control design.

The feedback gains k_1 , k_2 , and k_3 are obtained by tuning ξ and a . The value of ξ and a are obtained intuitively by tuning in the maximum range operation of the system that is depth position. By choosing proper value of ξ and a , the closed loop system will be asymptotically stable. Some parameters of the control system obtained from simulation with different depth operation are shown in the Table 5.1. The simulation is performed in 1000 second and the time sampling is 0.1 second.

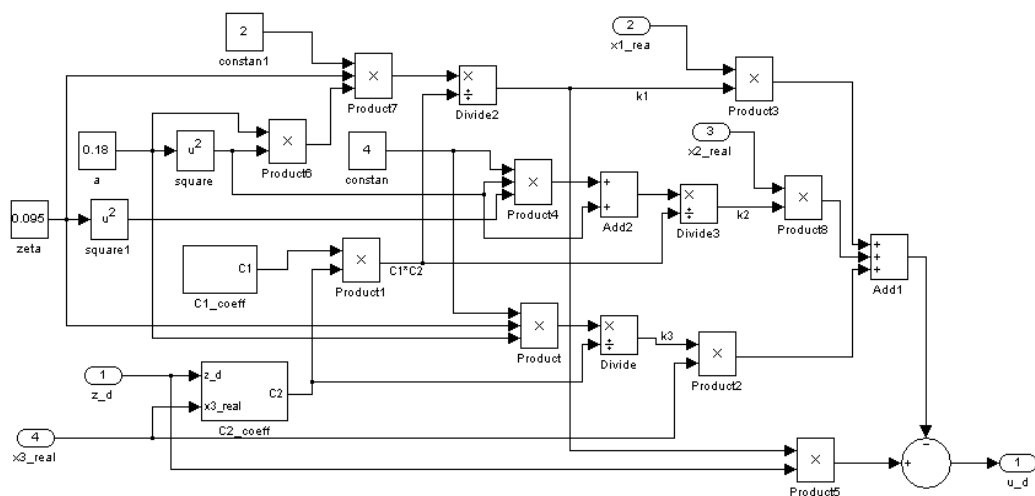


Figure 5.10 Simulink model of linearized control system.

Table 5.1 Performances of linearized control system in different range of depth operation.

Range operation(m)	ξ	a	T_r (s)	T_s (s)	Overshoot (%)	e_{ss} /RMSE (m)	% error	Energy usage (Watt second)
0-50	1	0.212	45.8	73.4	0.079	0.019	0.038	7676
0-100	0.8	0.136	89.4	133.1	0.06	0.05	0.05	13740
0-150	0.85	0.109	132.8	189.6	0.656	0.168	0.112	20450
0-200	0.76	0.092	176.3	247.3	0.867	0.336	0.168	26900

Some models of desired depth position as input references are tested in order to know the response of this control design. By choosing $\xi = 0.8$ and $a = 0.136$ which are obtained from simulation in the depth operation from 0–100 meter, the response of the control system for some different model of desired depth position are shown in Figure 5.11, Figure 5.13, Figure 5.15, Figure 5.17 and the error of the depth position for corresponding input model are shown in Figure 5.12, Figure 5.14, Figure 5.16.

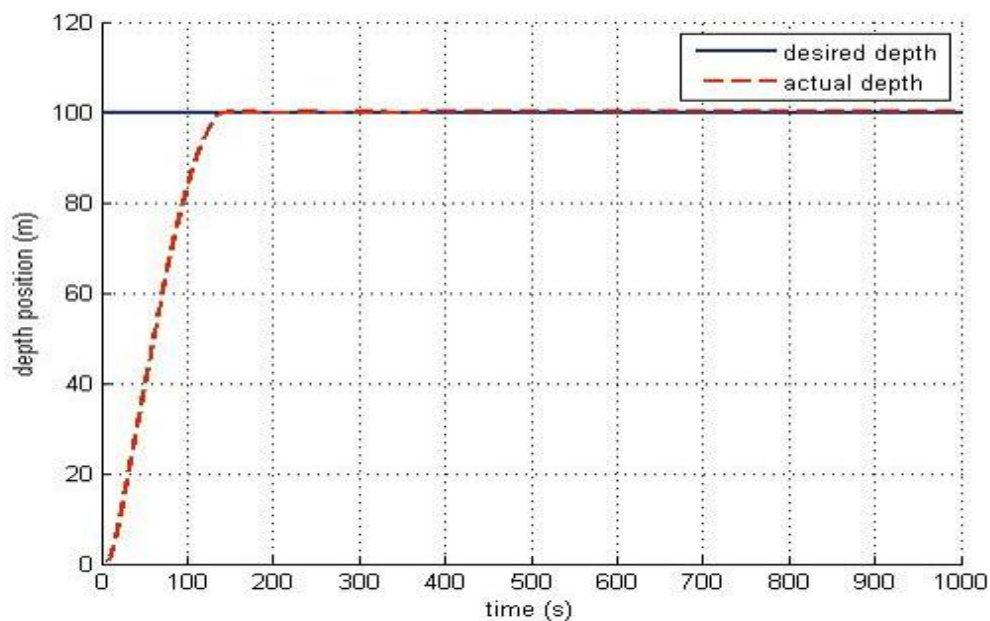


Figure 5.11 Response of linearized controller design for single step input reference.

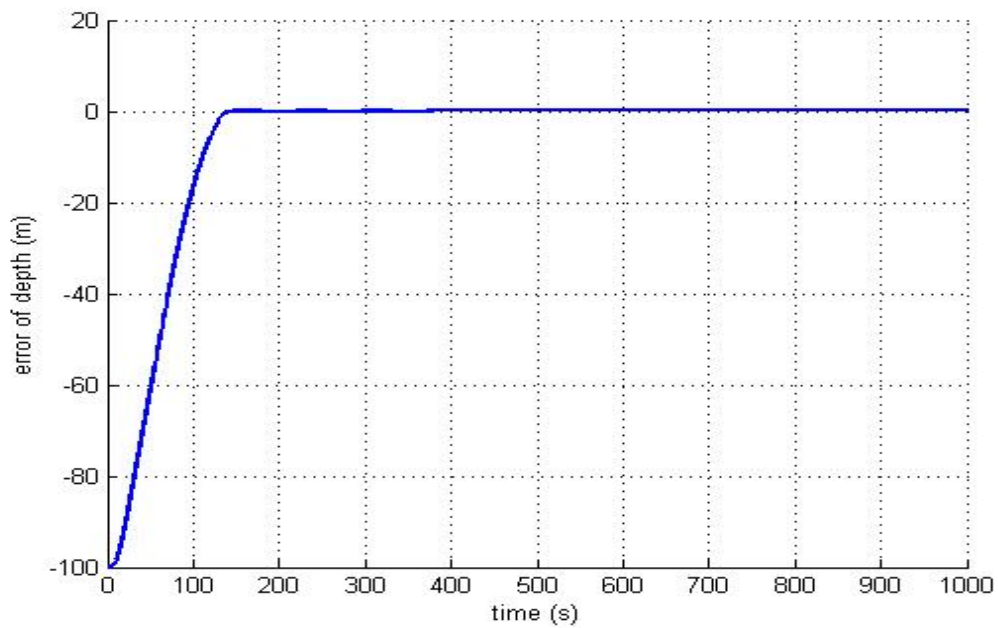


Figure 5.12 Error of depth position of linearized controller design for single step input reference.

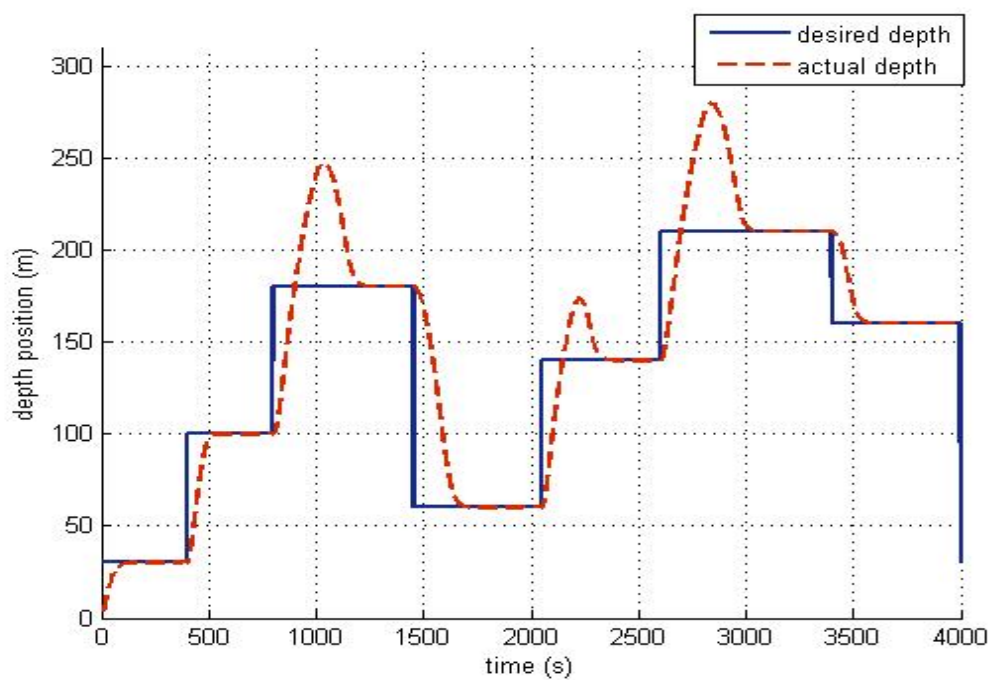


Figure 5.13 Response of linearized controller design for multi steps input reference.

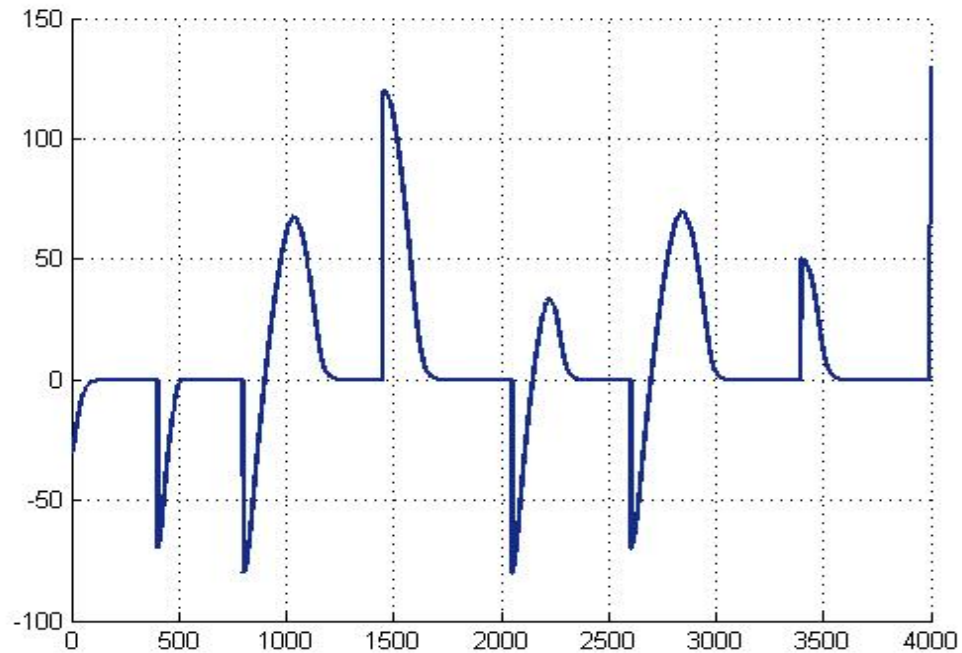


Figure 5.14 Error depth position of linearized controller design for multi steps input reference.

From Figure 5.13, it is seen that the gain of the feedback \mathbf{K} , which depends upon ζ and a , is effective for certain range of depth operation. By giving multi steps input reference, the response of the control system for some different initial and final depth positions are presented. Some of index performances of this system are presented in Table 5.2.

As mentioned before, that the feedback gain \mathbf{K} is obtained as the optimum gain for depth operation from 0 to 100 meter. If the desired depth position is deeper than this range, then the response is not optimal, the overshoot occurs and becomes bigger for the deeper desired depth position. The settling time is increased also.

If the input reference is changed from step input into ramp input with saturation value which is desired depth position, the response of the system is shown in Figure 5.15.

Table 5.2 Performances of linearized controller design in different initial and final depth position.

Step change (Depth position) (m)	T_r (s)	T_s (s)	Overshoot (%)	$e_{ss}/RMSE$ (m)	% error	Energy usage (Watt second)
0-30	59.2	108.8	0.005	0.04	0.133	1859.034
30-100	68.9	102.7	0.061	0.088	0.088	10642.417
100-30	84.2	170.7	0.005	0.044	0.147	7741.709
30-160	105.2	387.1	31.601	0.253	0.158	34967.527
160-30	128.4	248.1	0.005	0.032	0.107	15154.273
110-160	52.9	227.4	14.221	0.273	0.171	19204.848
160-110	77.8	141.6	0.001	0.155	0.141	8914.826

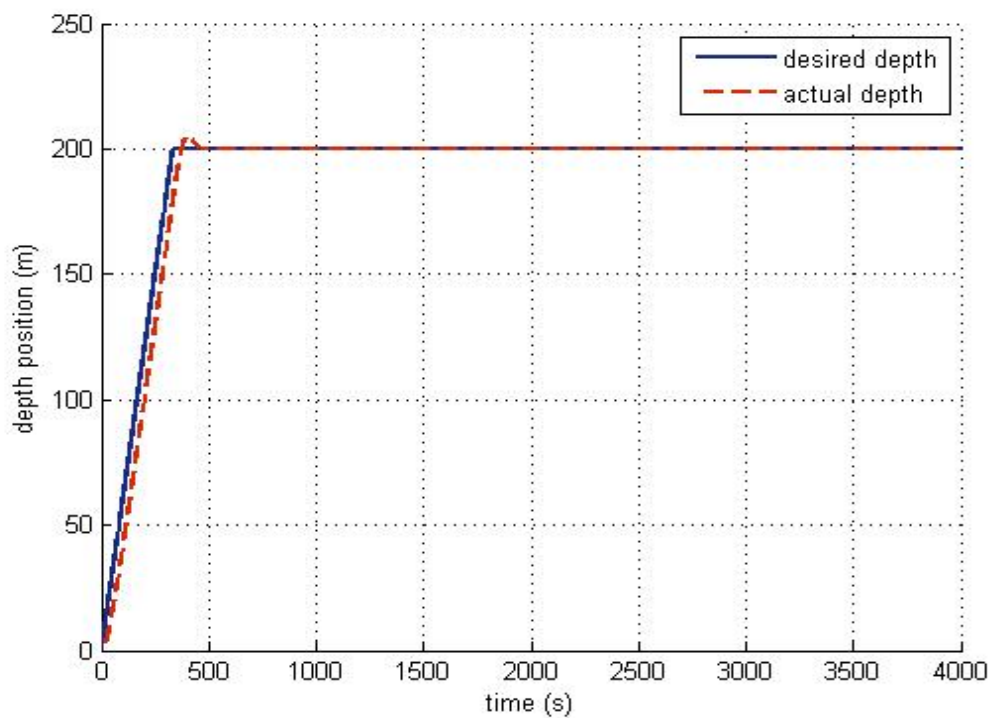


Figure 5.15 Response of linearized controller design for ramp model of input reference.

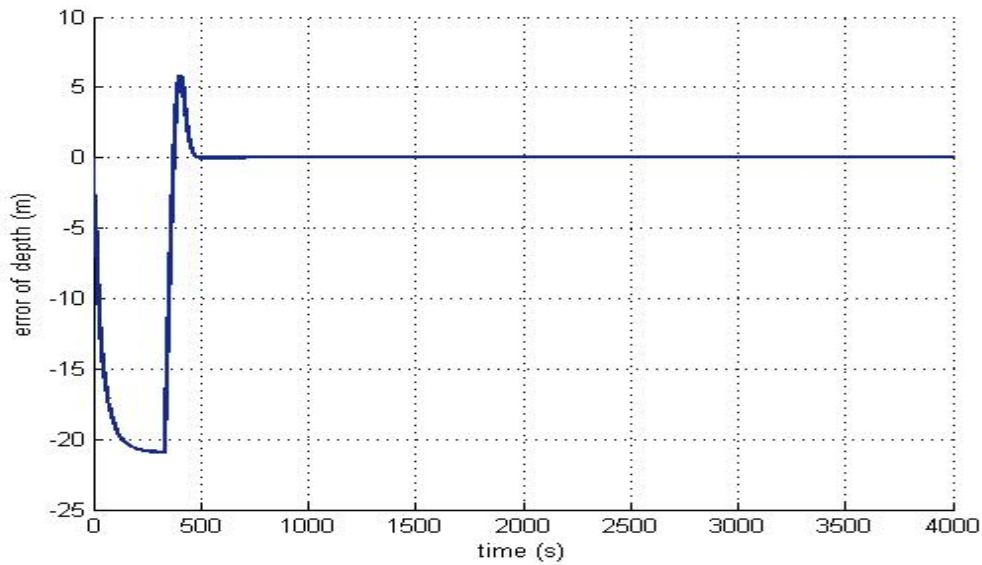


Figure 5.16 Error depth position of linearized controller design for ramp model of input reference.

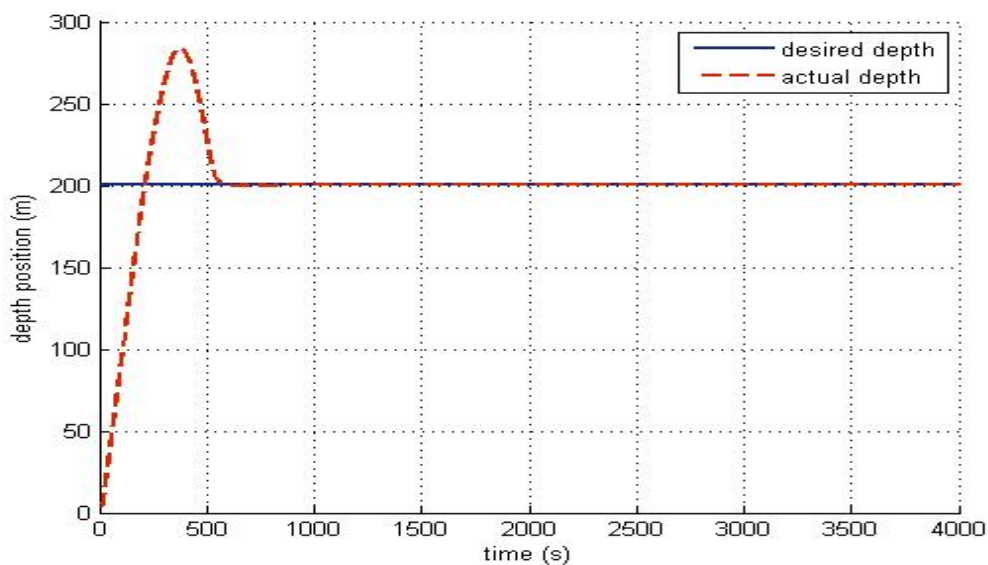


Figure 5.17 Response of linearized controller design for single step input reference when $\xi = 0.8$ and $a = 0.136$.

From Figure 5.15, it is shown that by the same gain of feedback \mathbf{K} but desired depth position is deeper than maximum range of depth operation, the ramp model input reference gives better response as compared to step input model in Figure 5.17. In other words, by changing step input model into a trajectory input model, the response

of the control system can be improved, the settling time $T_s = 436.3$ s and steady state error $e_{ss} = 0.097$ m. In Figure 5.17, the desired depth position $z_d = 200$ m is applied as step input model and the value of the gain \mathbf{K} is obtained from tuning at $z_d = 100$ m. The steady time and error steady state are obtained as $T_s = 560.7$ s and $e_{ss} = 0.099$ m respectively. If we consider to the energy usage, single step input model consumes 54600 Watt second and ramp input model consumes 8943 Watt second. Therefore by manipulating this input reference, the energy usage also can be saved.

Since the controller based on the linearized model can stabilize the system by tracking the error converge to zero than it can be expected that this control strategy can track a given trajectory input reference. If the input reference is dynamic or given as a trajectory, then the responses of the control system are shown in Figure 5.18 and Figure 5.20. The models of input reference are given as sinus and triangle. The error can be seen in Figure 5.19 and Figure 5.21 for each input model respectively.

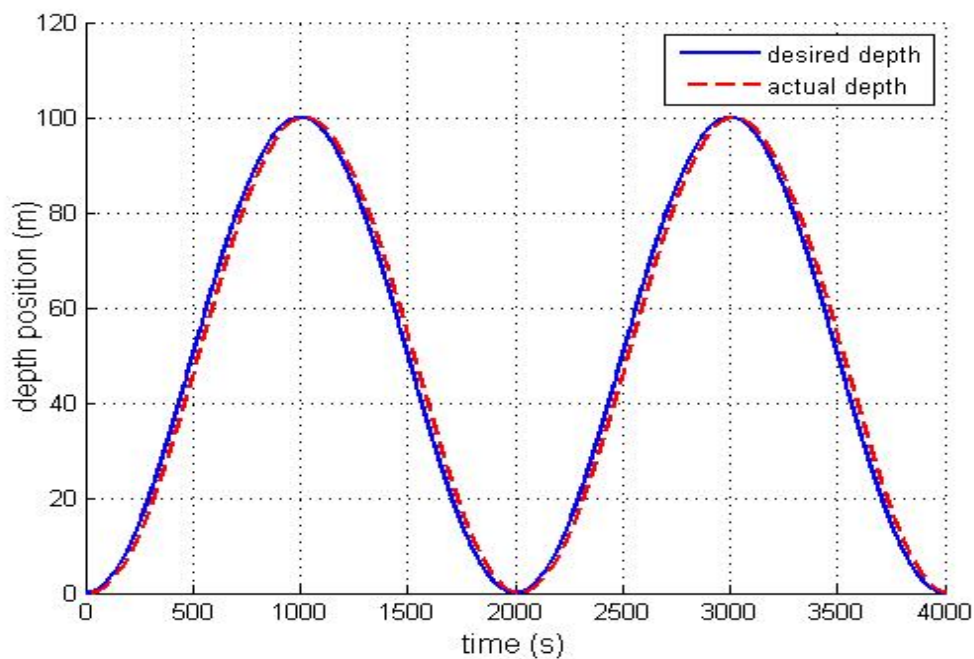


Figure 5.18 Response of linearized controller design for sinus model of input reference.

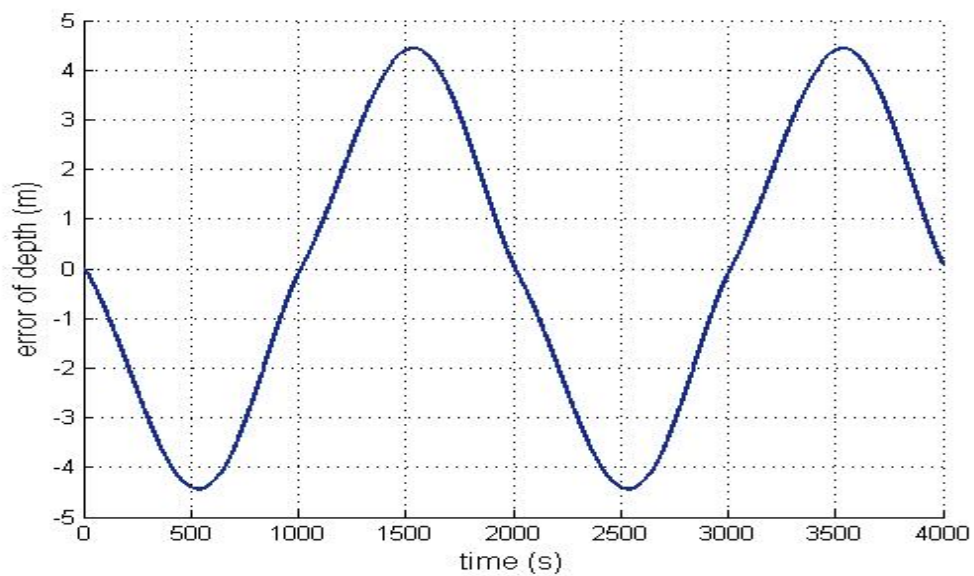


Figure 5.19 Error depth position of linearized controller design for sinus model of input reference.

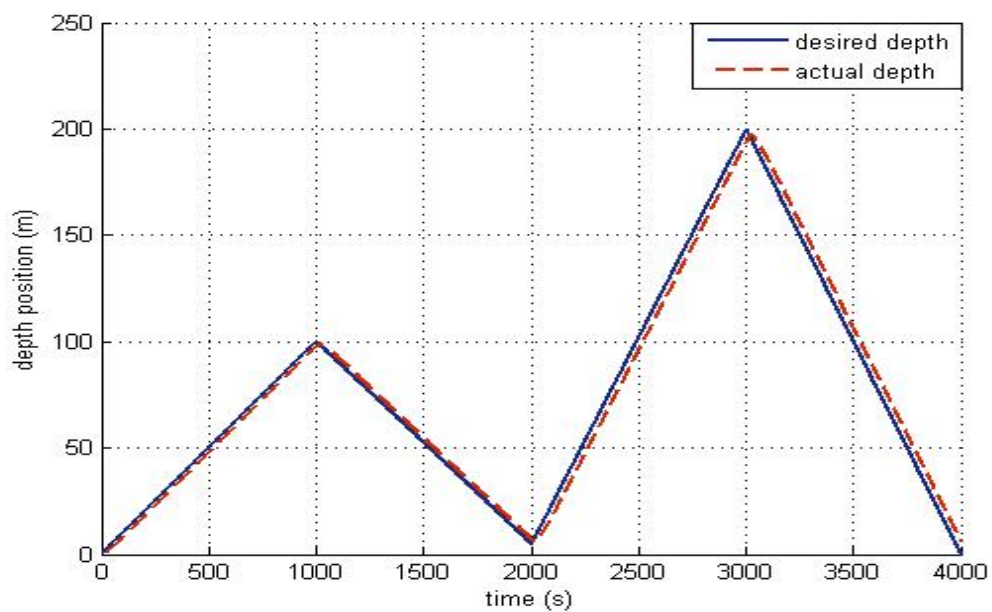


Figure 5.20 Response of linearized controller design for triangle model of input reference.

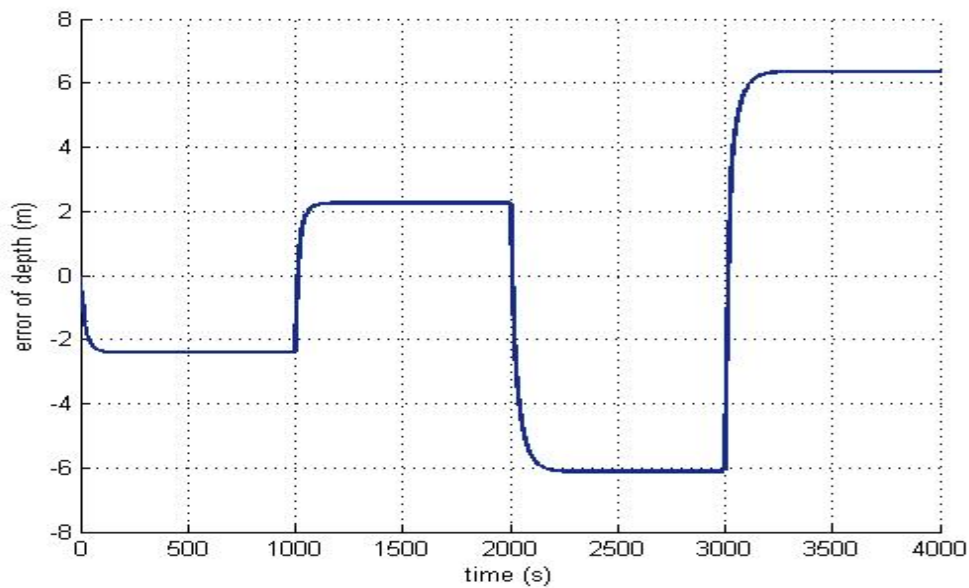


Figure 5.21 Error depth position of linearized controller design for triangle model of input reference.

By giving a trajectory input reference, from the simulation can be seen that the output is lagging from the reference. If the change of the input reference is constant, the error is almost constant as shown in Figure 5.20 and Figure 5.21. From simulation if the change of input is 0.1ms^{-1} then absolute error converge to 2.408m and if change input is 0.2ms^{-1} then absolute error converge to 6.361m. For sinus model, the error (RMSE) is 2.956 m, energy needed in the operation is 1935.541 Watt second. For the triangle model, as shown in Figure 5.20, the error (RMSE) is 4.58 m and energy needed in the operation is 4215 Watt second.

If URV is sent to a particular depth position and let it stays at this position, it is seen that the controller can asymptotically stabilize the system, because for $t \rightarrow \infty$, $e \rightarrow 0$. But, if the desired depth position is dynamic (given as trajectory), then the error is not convergent to zero, but still the controller can track the trajectory.

5.3 Simulation of Nonlinear approach

The mathematical equations of the controller strategy derived in the previous chapter will be simulated in this subsection in order to know the performances of each control strategies. The simulation will be performed in MATLAB/Simulink.

5.3.1 State-Space Linearization

The simulation for state-space feedback linearization strategy is built based on schematic diagram given in Figure 5.22. The Simulink model is built based upon mathematical model obtained at previous sub section. The original input for the nonlinear system is shown in Figure 5.23. The functions $\psi(\mathbf{x})$ and $\gamma(\mathbf{x})$ are shown in Figure 5.24 and Figure 5.25 respectively. The states transformation and linear controller for the transformed states are shown in Figure 5.26 and Figure 5.27 respectively. In order to know the performances of this control strategy, some input model are tested.

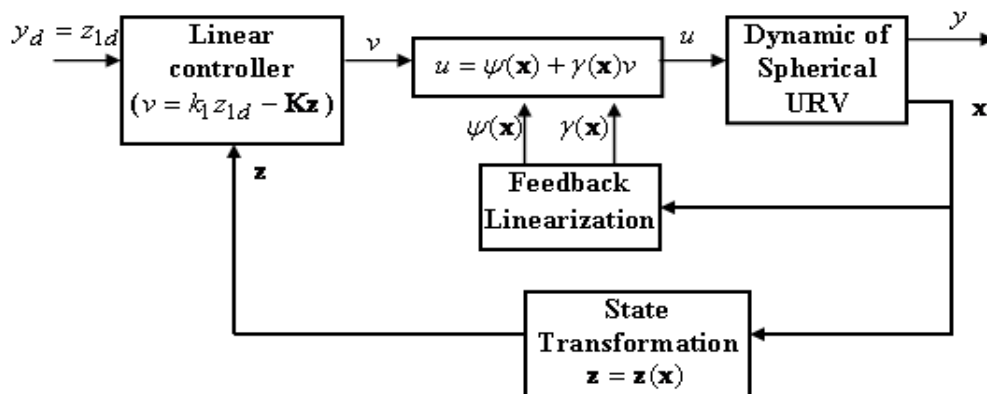


Figure 5.22 Schematic diagram of state-space feedback linearization control design.

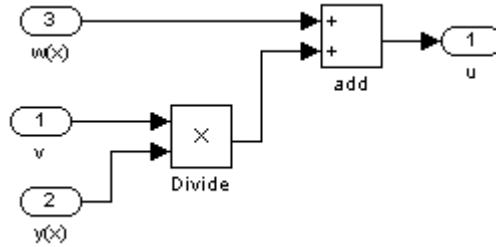


Figure 5.23 Simulink model of the original input in state-space feedback linearization.

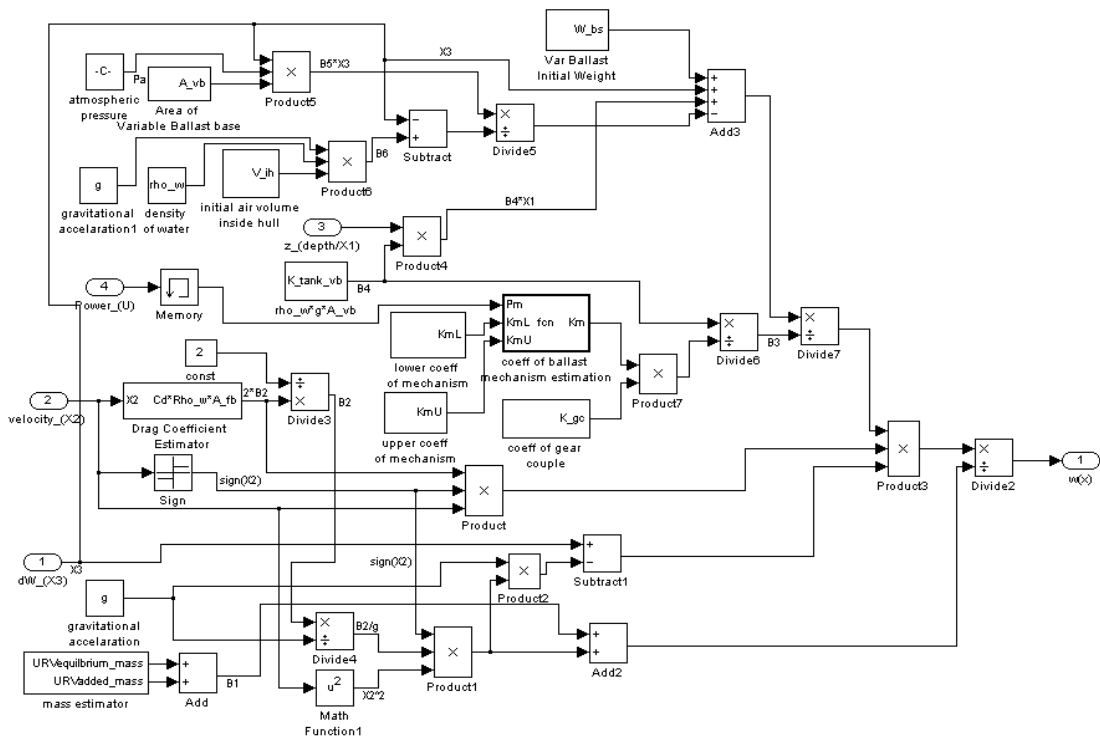


Figure 5.24 Simulink model of $\psi(\mathbf{x})$.

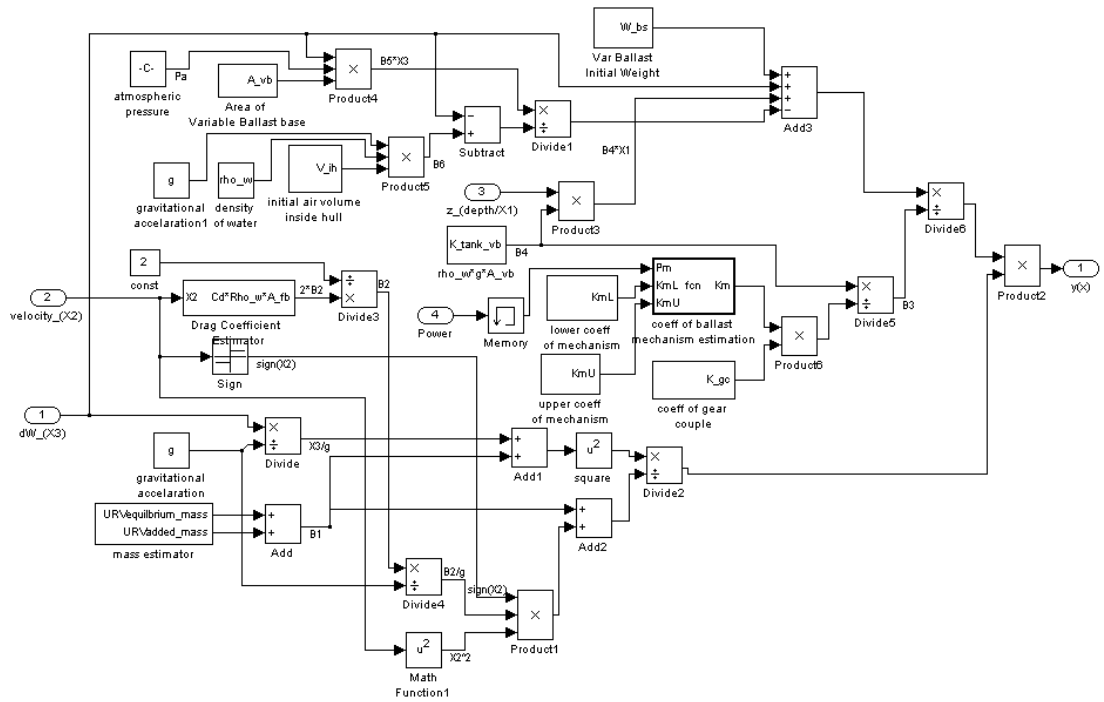


Figure 5.25 Simulink model of $\gamma(\mathbf{x})$.

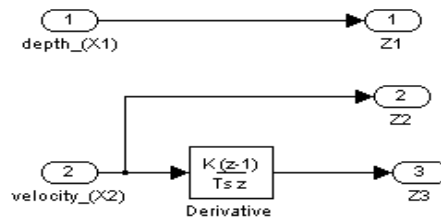


Figure 5.26 Simulink model of state transformation $\mathbf{z} = \mathbf{z}(\mathbf{x})$.

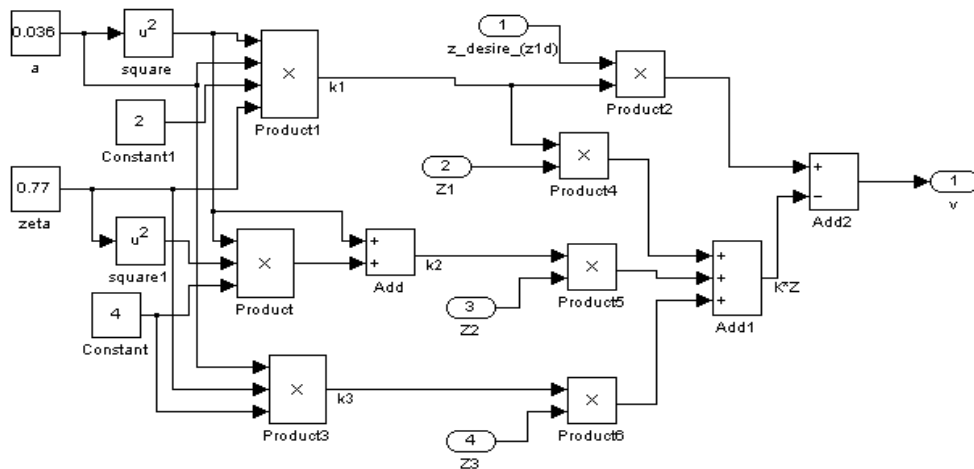


Figure 5.27 Simulink model of linear controller $v = k_1 z_{1d} - \mathbf{Kz}$.

In order to stabilize the system, we just consent in linear controller that is by tuning the feedback gain. A proper value of ξ and a must be chosen in order to obtain a good performance of the controller. The feedback gain is tuned at a particular range of depth, because it only optimum in a certain range but not for out of the range. If a step input reference is applied with different magnitude, the controller will result performances those are shown in Table 5.3.

Table 5.3 Some Parameters and performances of state-space feedback linearization strategy in different range of depth operation

Range operation (Depth) (m)	ξ	a	T_r (s)	T_s (s)	Overshoot (%)	$e_{ss}/RMSE$ (m)	% error	Energy usage (Watt second)
0-50	0.764	0.068	46.3	73.7	0.162	0.066	0.132	3900.315
0-100	0.77	0.036	89.1	159.7	1.194	0.204	0.204	7742.287
0-150	0.85	0.026	133.8	197.8	0.369	0.300	0.200	11320.82
0-200	0.82	0.019	177.9	262.3	0.561	0.567	0.284	14962.127

Furthermore, the control strategy will be tested with different model of input reference in the same feedback gain that was tuned in the range of depth position from 0-100 m, $\xi = 0.77$ and $a = 0.036$. If a step input is applied in magnitude 100 m, the response of the system is shown in Figure 5.28, and the error is shown in Figure 5.29. If a multi step input is applied with different magnitude of the step, the system will response that is shown in Figure 5.30 and the error is shown in Figure 5.31.

By giving the multi step model of input reference, the response of the system when it is operated in different origin and final depth position, can be known. The performances of the controller are given in Table 5.4. From Table 5.4, it is seen when the input is start from 30 m and end at 100 m, results different response when it start from 0 m and end at 100 m, see Table 5.3, the overshoot is bigger. If the power usage is considered, even its distance is shorter, Table 5.4 consumes bigger power usage compare to Table 5.3. This condition is caused by the difference of the hydrostatic pressure in different depth which is higher in deeper position.

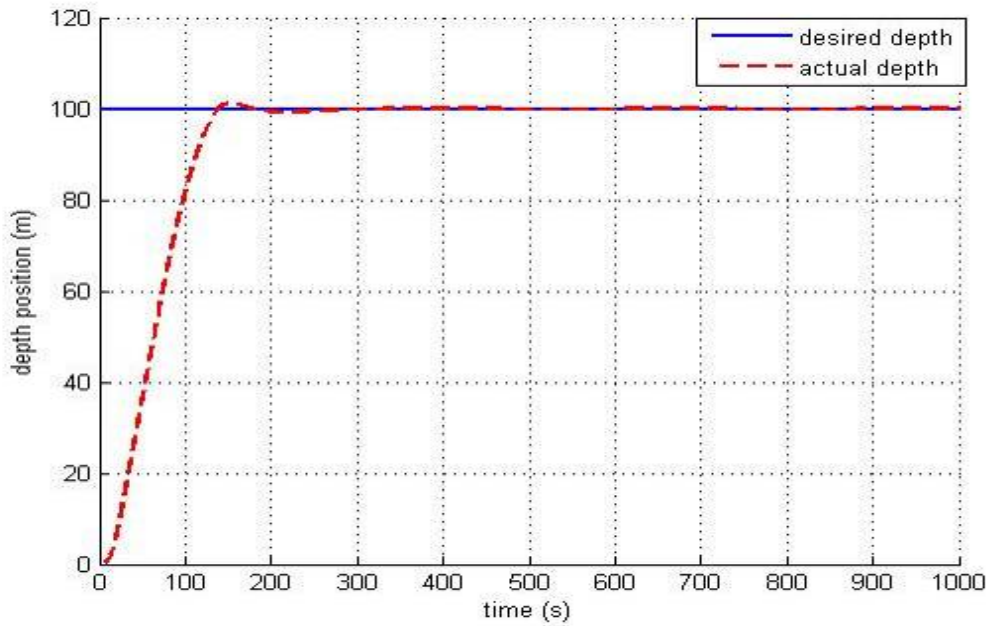


Figure 5.28 Response of the state-space feedback linearization strategy for single step model of input reference.

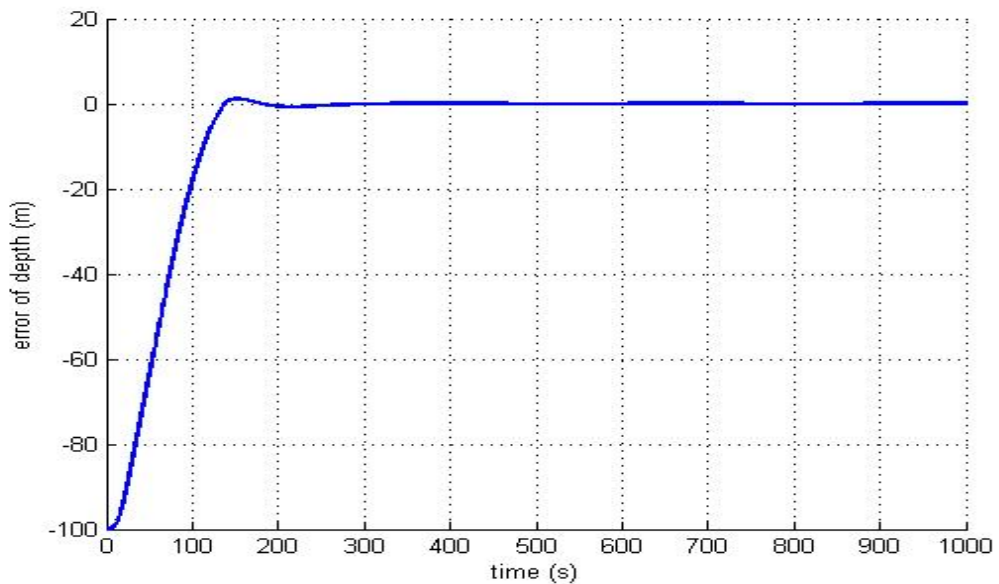


Figure 5.29 Error of the state-space feedback linearization strategy for single step model of input reference.

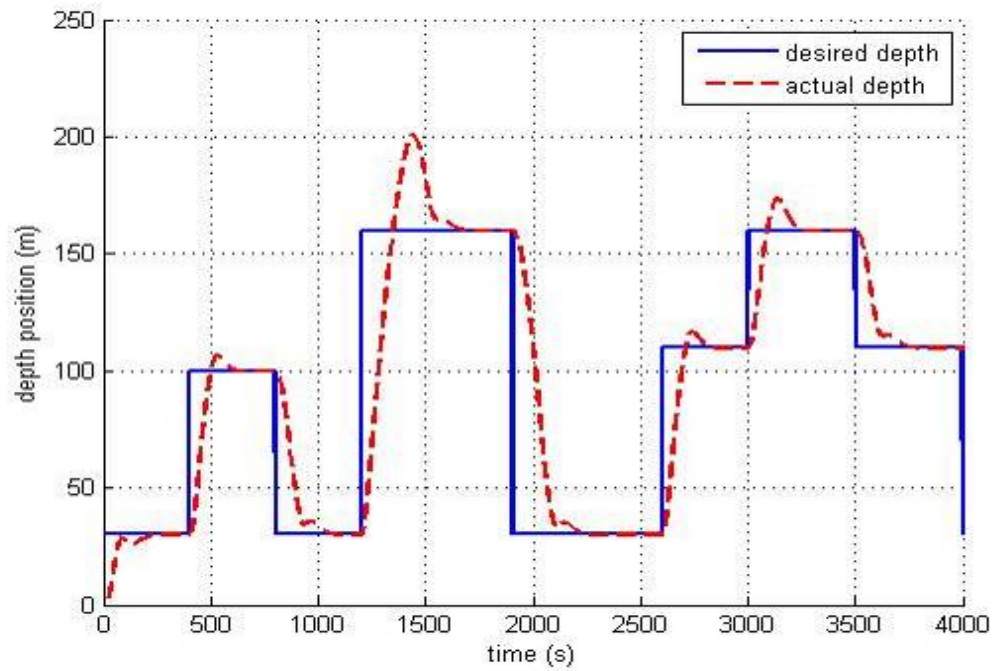


Figure 5.30 Response of the state-space feedback linearization strategy for multi step model of input reference.

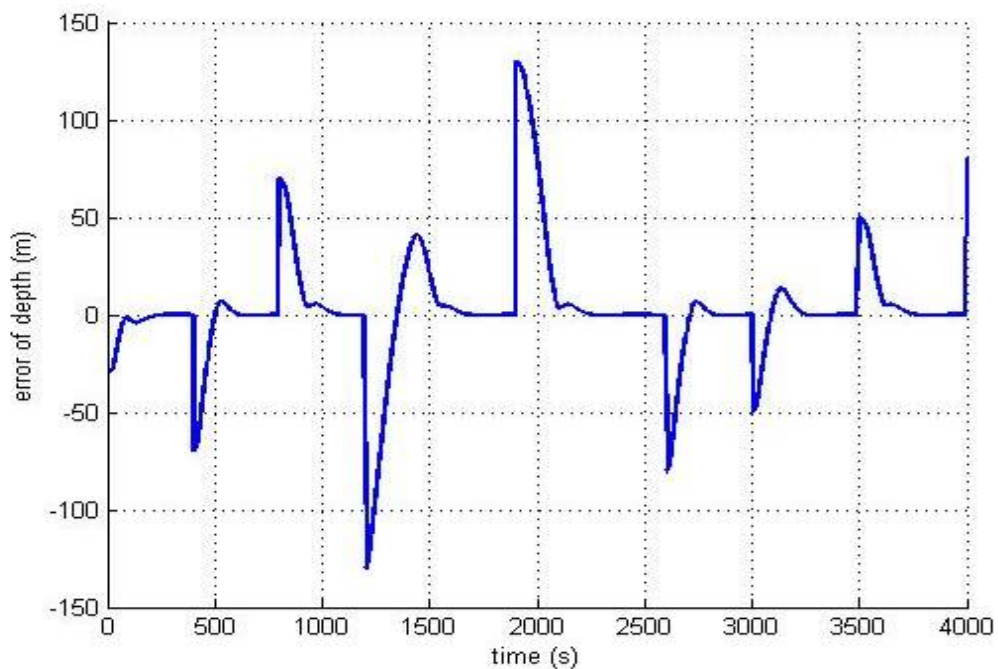


Figure 5.31 Error of the state-space feedback linearization strategy for multi step model of input reference.

Table 5.4 Performances of state-space feedback linearization strategy in multi step input reference of depth position.

Step change (Depth position) (m)	T_r (s)	T_s (s)	Overshoot (%)	$e_{ss}/RMSE$ (m)	Power usage (Watt second)
0-30	25.6	224	0.234	0.069	1028.794
30-100	65.2	194.2	6.775	0.213	9477.242
100-30	87	267.3	0.322	0.085	6743.544
30-160	106.7	432.8	25.537	0.357	24934.511
160-30	127.1	342.2	0.307	0.051	14410.108
110-160	57.1	223.8	8.507	0.293	13030.645
160-110	87.1	224.8	0.077	0.219	7664.011

By testing step input model, it is seen that the control strategy can asymptotically stabilizes the system, for $t \rightarrow \infty$, $e \rightarrow 0$. Therefore, the control strategy can be expected to be used in tracking a trajectory. If ramp input with saturation value is applied, the response of the system is shown in Figure 5.32 and the error is shown in Figure 5.33.

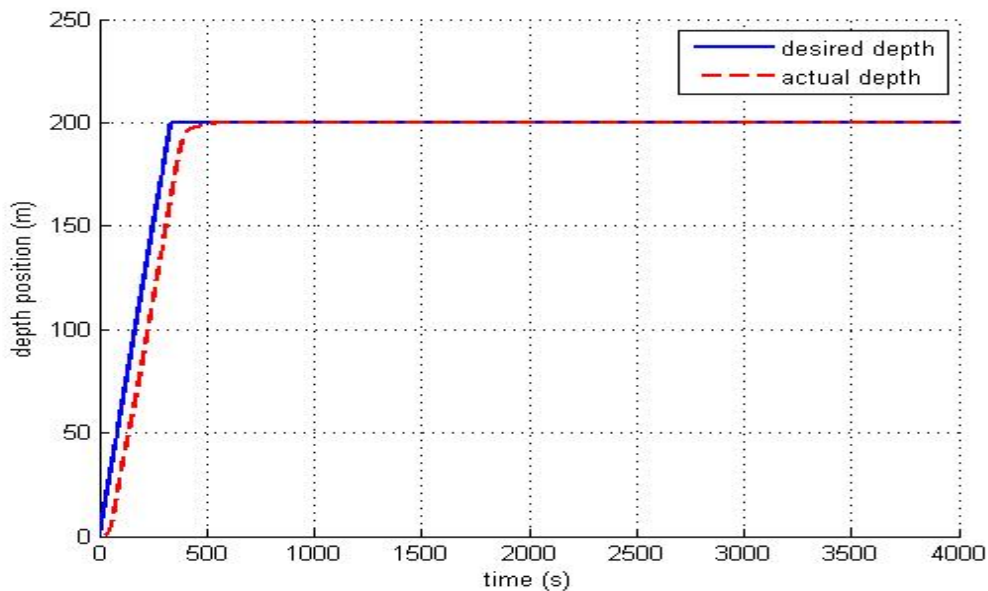


Figure 5.32 Response of state-space feedback linearization strategy for ramp model of input reference.

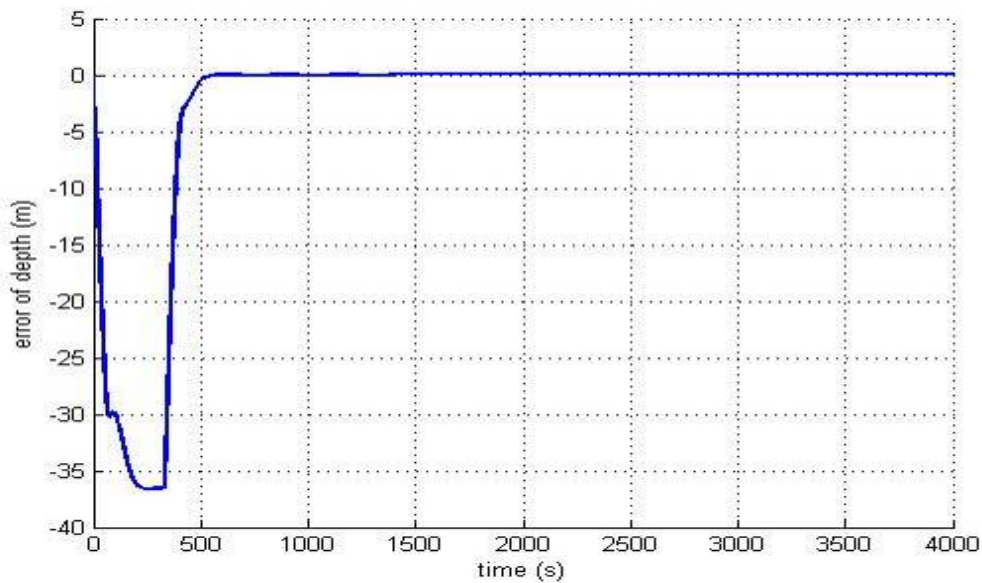


Figure 5.33 Error of state-space feedback linearization strategy for ramp model of input reference.

From Figure 5.32, it is clearly seen that by changing the model of input reference from step input into ramp input with saturation value, the controller can be used for out of the range of the depth position in which the feedback gain is tuned. The steady time is 553.3 second, overshoot is 0.017 %, RMSE in steady state is 0.004, and the energy consumed is 6743.027 Watt second. These performances are better compared to step input model. If step input reference with the same magnitude is given, the steady time is 595.3 second, overshoot is 35.925 %, RMSE in steady state is 0.135, and the energy consumed is 37604.955 Watt second. The response can be seen in Figure 5.34.

If the trajectory is given as sinus model and triangle model, the response is shown in Figure 5.35 and Figure 5.37 respectively. For sinus model, RMSE in tracking this trajectory is 6.741 m and the energy usage is 1944.425 Watt second. For triangle model, RMSE is 9.213 m and the energy usage is 3936.512 Watt second. From these simulations, it is seen that if the input is given as trajectory, the response of the controller is lagging. If the change of trajectory is linear, the error will converge to a constant, as shown in Figure 5.38. From simulation, if the change of input trajectory

is 0.1ms^{-1} then absolute error converge to 6.082m and if the change of input is 0.2ms^{-1} then absolute error converge to 12.163m

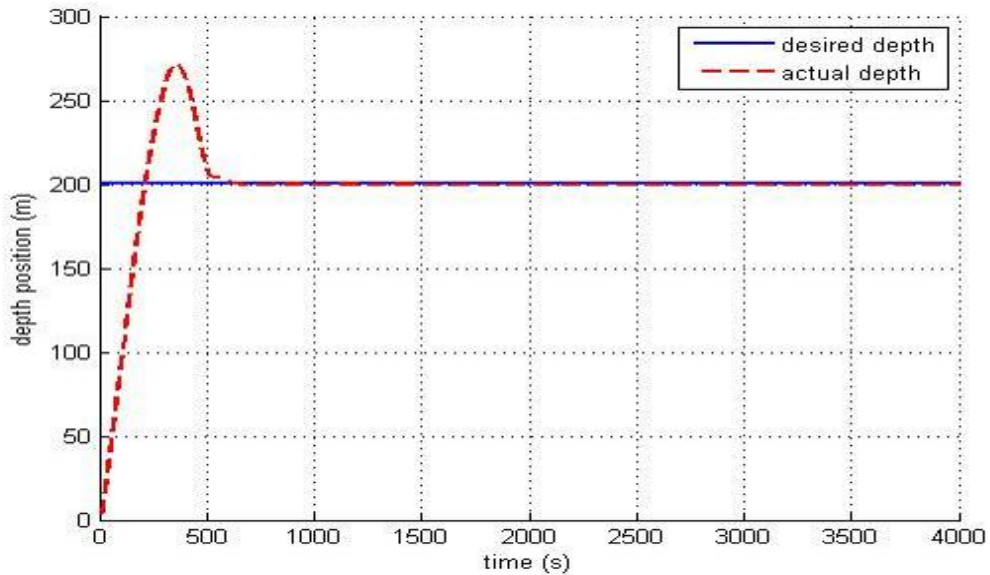


Figure 5.34 Response of state-space feedback linearization strategy for step input reference which is bigger than range of depth operation.

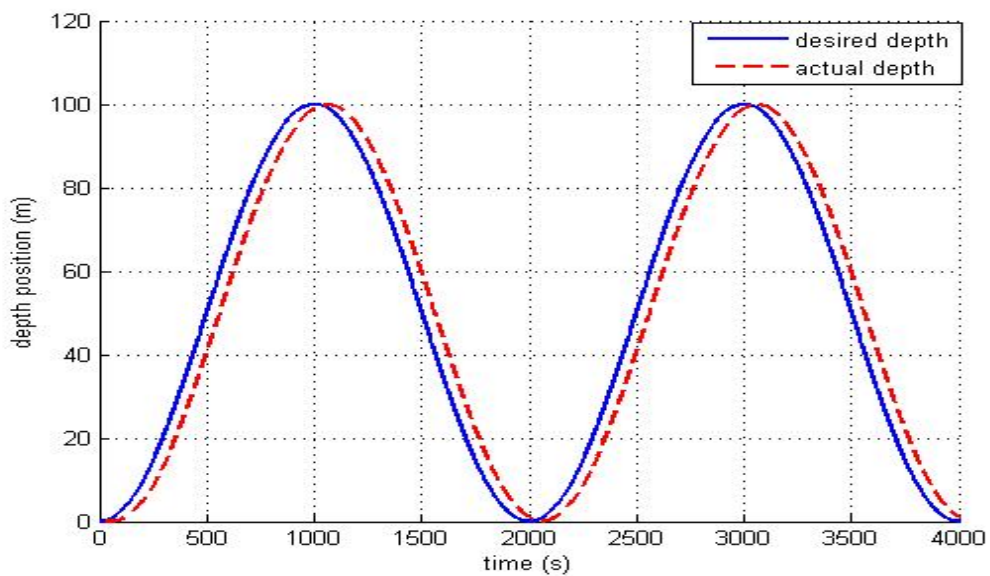


Figure 5.35 Response of state-space feedback linearization strategy for sinus model of input reference.

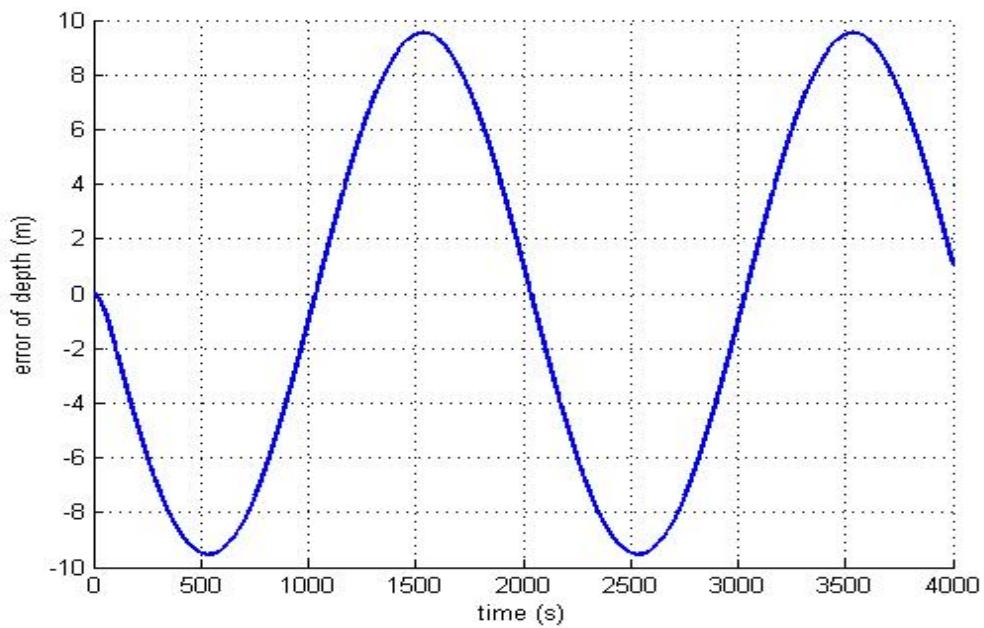


Figure 5.36 Error of state-space feedback linearization strategy for sinus model of input reference.

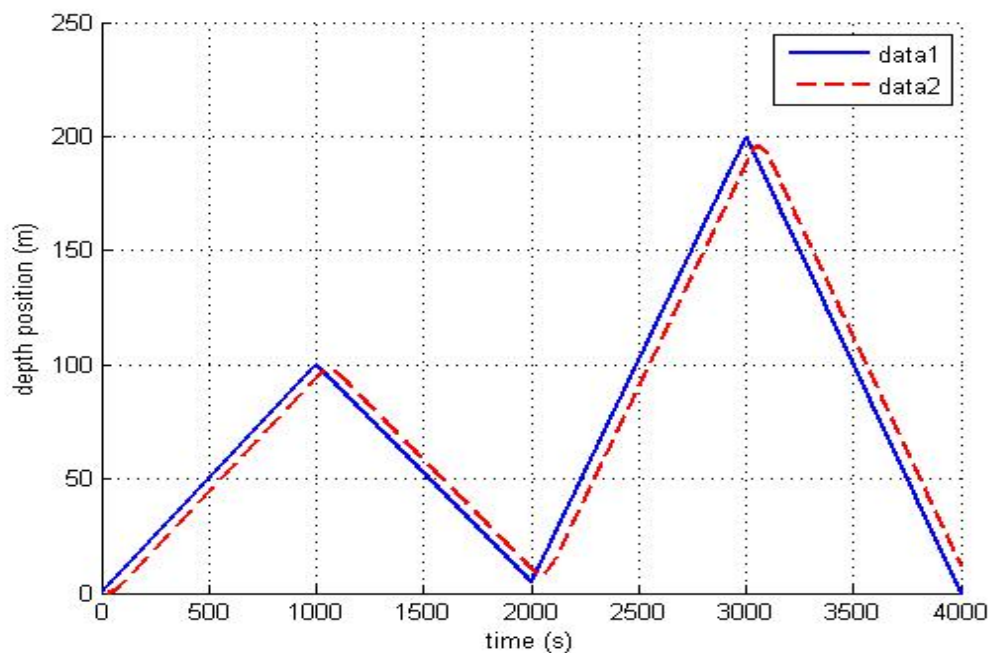


Figure 5.37 Response of state-space feedback linearization strategy for triangle model of input reference.

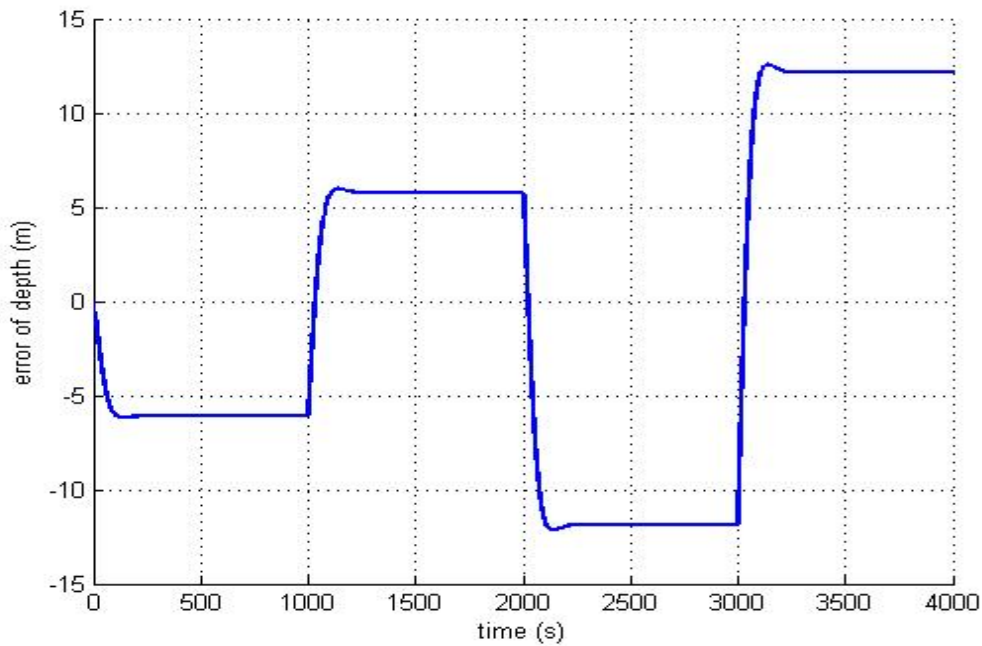


Figure 5.38 Error of state-space feedback linearization strategy for triangle model of input reference.

5.3.2 Input-Output Linearization

The simulation of input-output feedback linearization strategy is performed by the following schematic diagram given in Figure 5.39.

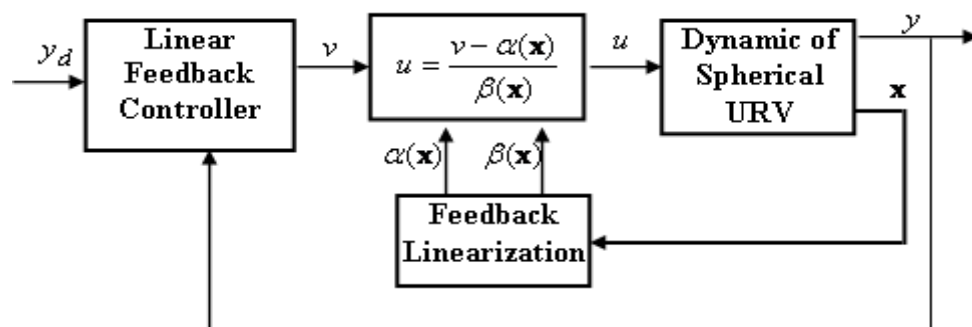


Figure 5.39 Schematic diagram of input-output feedback linearization control design.

The Simulink model for the control system is built block by block based on the mathematical model. Simulink model of the synthetic input obtained at Eq. 4.68 and

Eq. 4.69 is shown in Figure 5.40, and the Simulink model of the original input u written at Eq. 4.63 is shown in Figure 5.41.

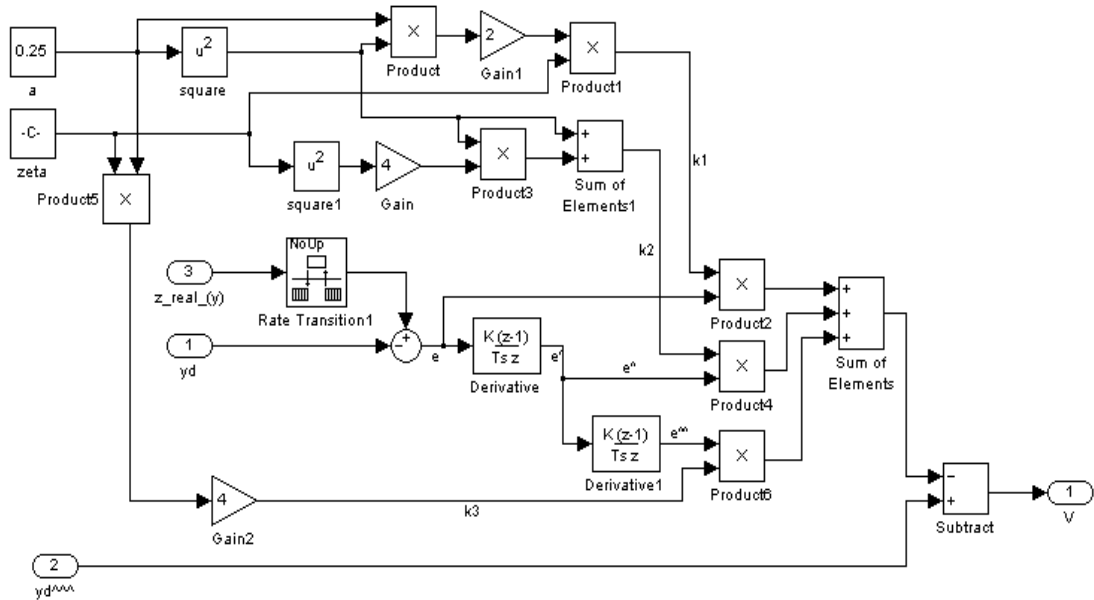


Figure 5.40 Simulink model of the synthetic input in input-output feedback linearization control design.

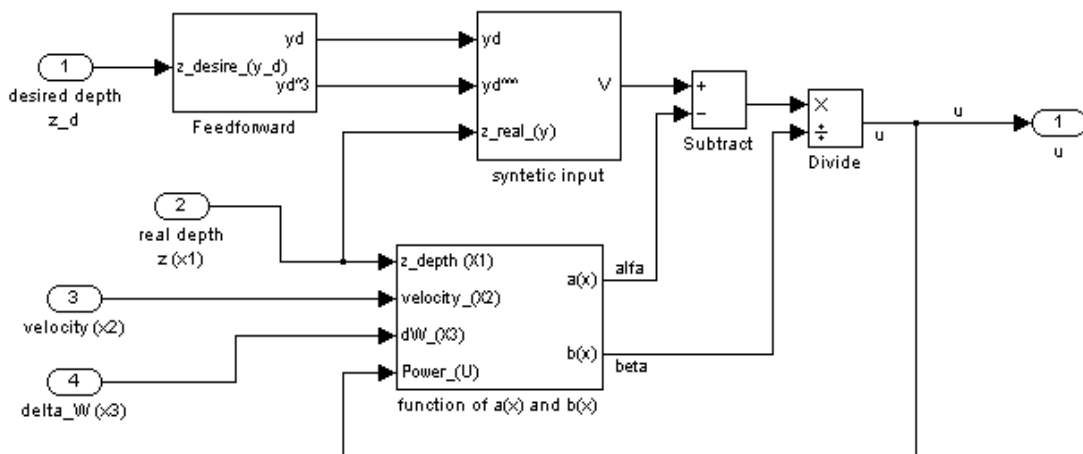


Figure 5.41 Simulink model of the original input in input-output feedback linearization control design.

And the Simulink models of $\alpha(\mathbf{x})$ and $\beta(\mathbf{x})$ are shown in Figure 5.42 and Figure 5.43 respectively.

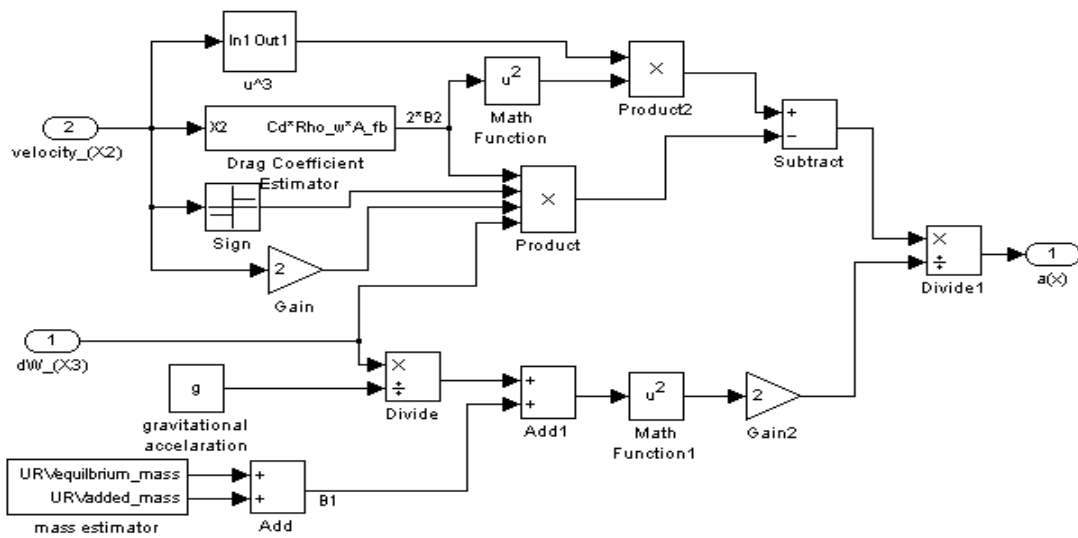


Figure 5.42 Simulink model of $\alpha(x)$

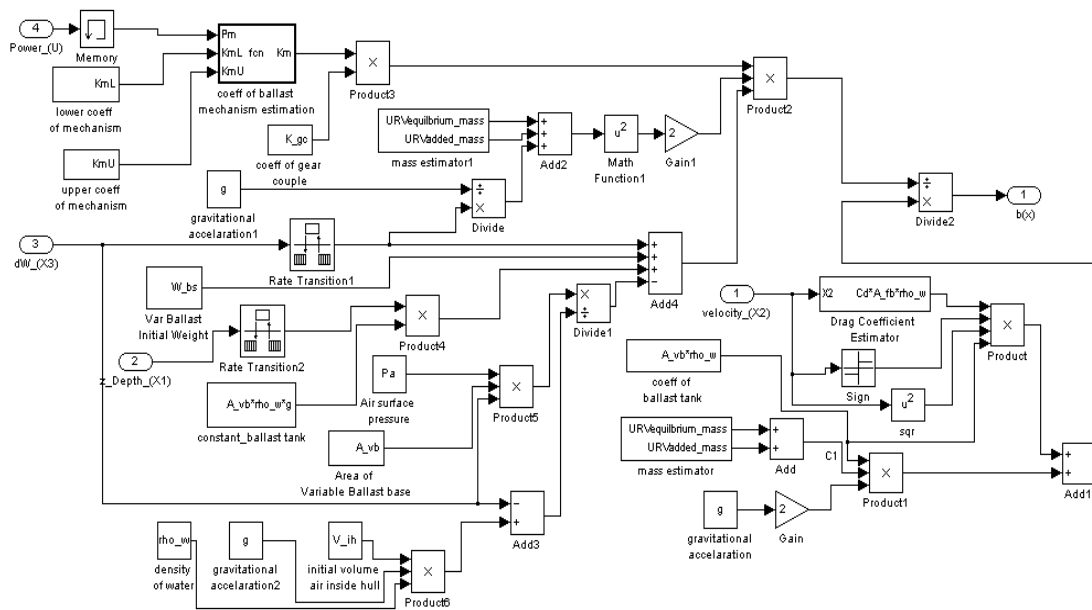


Figure 5.43 Simulink model of $\beta(x)$

In order to stabilize this system, the eigenvalues at Eq. 4.66 must be located at the left half of complex plane by choosing a proper value of a and ξ thus the system is asymptotically stable. By giving step input in different range of depth operation, the value of a and ξ are obtained as presented at Table 5.5. These values are obtained by tuning in order to get an optimum response. The duration of the simulation is 1000 second and the time sampling is 0.1 second.

Table 5.5 Some Parameters and performances of input-output feedback linearization strategy in different range of depth operation

Range operation (Depth) (m)	ξ	a	T_r (s)	T_s (s)	Overshoot (%)	$e_{ss}/RMSE$ (m)	% error	Energy usage (Watt second)
0-50	0.762	0.071	45.9	73.3	0.829	0.058	0.116	4122
0-100	0.762	0.036	89.4	132.8	0.77	0.244	0.244	7832
0-150	0.835	0.026	133.4	192.3	0.555	0.297	0.198	11450
0-200	0.85	0.02	177.1	250	0.932	0.498	0.249	15140

In order to know the characteristic of the control system, further, some models of input reference are applied in this depth positioning system. Models of the input reference are same as models applied in previous control design. These input reference models are simulated for $a = 0.036$ and $\xi = 0.762$. If steps input are applied as single step input and multi step inputs, the responses are shown in Figure 5.44 and Figure 5.46 respectively. The error for each input model can be seen in Figure 5.45 and Figure 5.47.

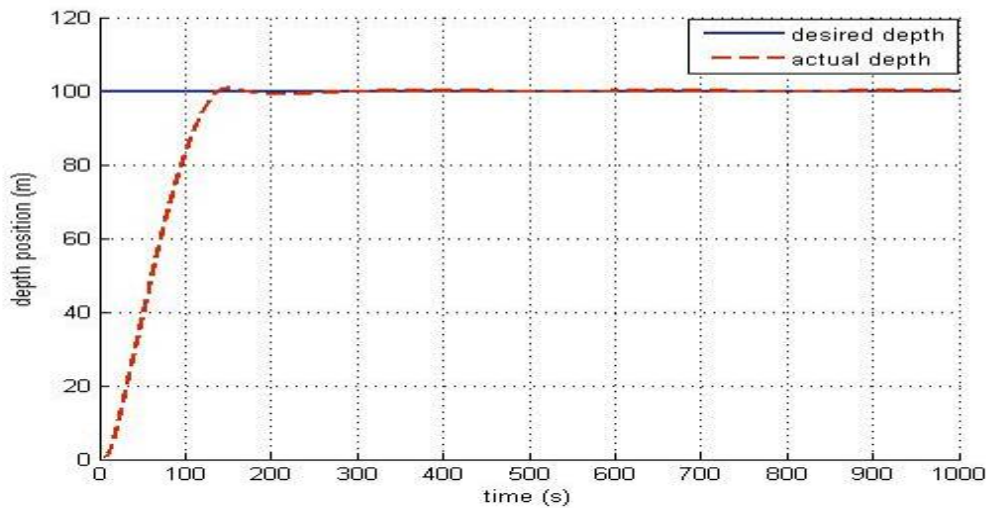


Figure 5.44 Response of input-output feedback linearization strategy for single step model of input reference.

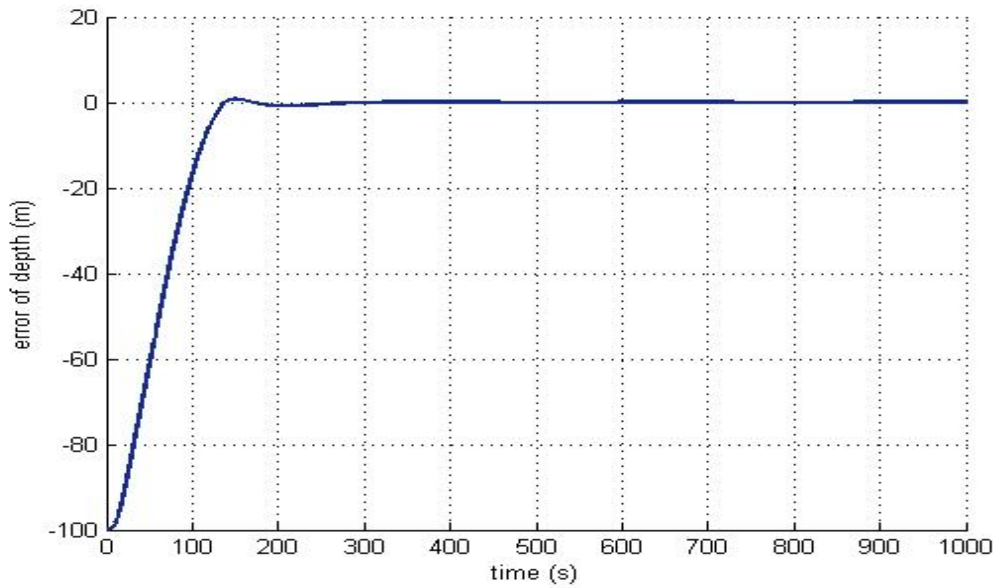


Figure 5.45 Error of input-output feedback linearization strategy for single step model of input reference

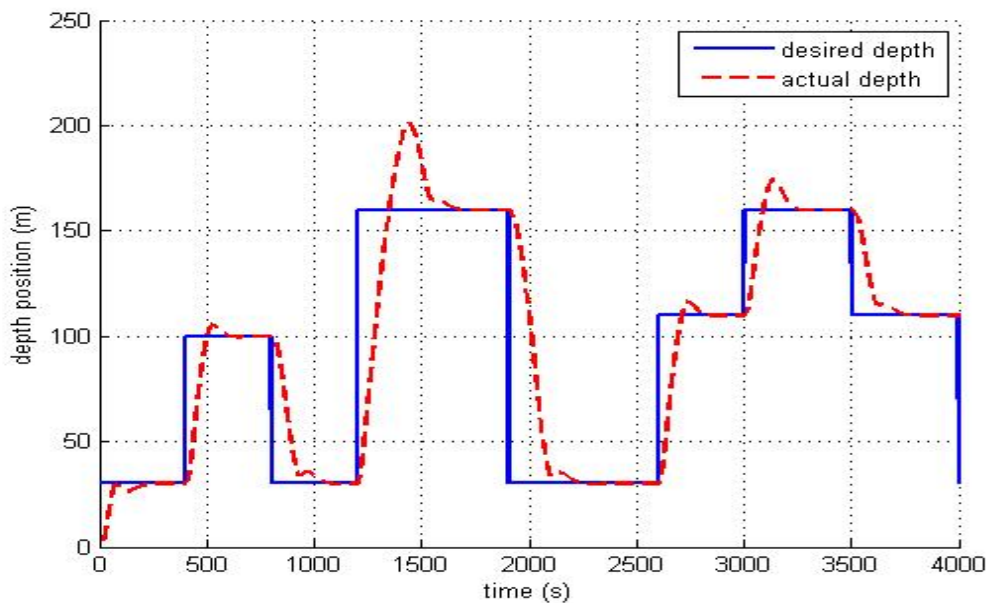


Figure 5.46 Response of input-output feedback linearization strategy for multi step model of input reference.

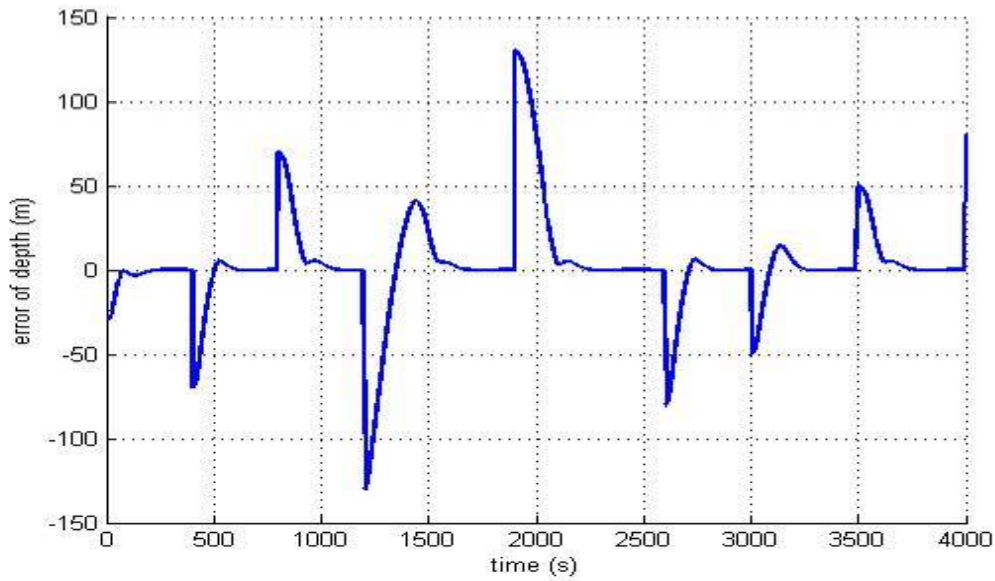


Figure 5.47 Error of input-output feedback linearization strategy for multi step model of input reference

The feedback gain \mathbf{K} is effective for certain range of depth operation, as shown in Figure 5.46. This gain must be tuned at maximum range of the depth operation and the control system is optimum if the operation is in this range. The performance of the control system when the URV is operated in different initial and final depth position is presented in Table 5.6. The gain used in this control system is obtained from tuning in the range of depth position at 100 m.

Table 5.6 Performances of input-output feedback linearization strategy in multi step input reference of depth position.

Step change (Depth position) (m)	T_r (s)	T_s (s)	Overshoot (%)	e_{ss} /RMSE (m)	% error	Energy usage (Watt second)
0-30	43.6	218.6	0.219	0.068	0.227	1254.617
30-100	65.8	183.4	5.394	0.212	0.212	9335.668
100-30	86.4	267.5	0.329	0.086	0.287	6773.23
30-160	106.5	433.4	25.666	0.357	0.223	25053.856
160-30	126.6	342.6	0.308	0.051	0.170	14423.567
110-160	56.7	225.8	8.994	0.291	0.182	13401.248
160-110	85.3	224.9	0.079	0.219	0.199	7712.397

Table 5.6 shows if the URV descends in the range of depth 0 – 100 m, it shows a good behavior with small overshoot. If the URV descends out of its range, the overshoot is increased and steady time is also increased. For ascent motion, the overshoot is small even the URV operates out of range of the depth position. The rise time is slower compare to descent motion. This condition is caused by the difference of hydrostatic pressure at different depth position. At the deeper position, the hydrostatic pressure is higher than shallower position. It causes the power needed to change the weight of URV, $x_3 = \Delta W$, is higher. Therefore with the same power, the rise time of descent motion is faster then ascent motion, because the rise time is proportional to the rate change of weight of URV, $\Delta \dot{W}$.

If a ramp model is given as input reference, response of the control system is shown in Figure 5.48 and the error is shown in Figure 5.49.

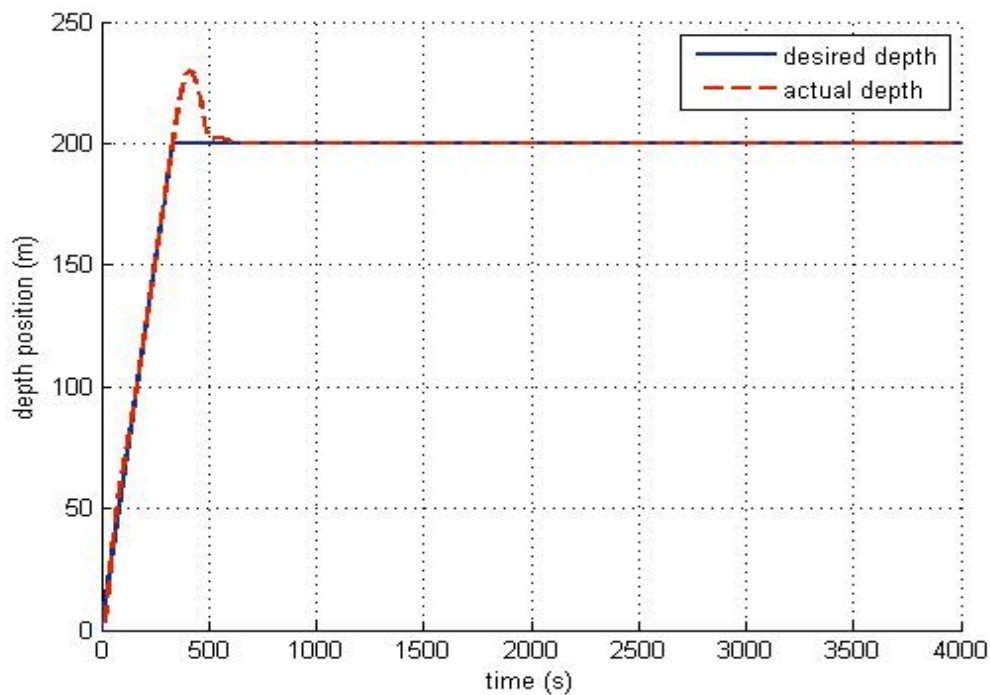


Figure 5.48 Response of input-output feedback linearization strategy for ramp model of input reference

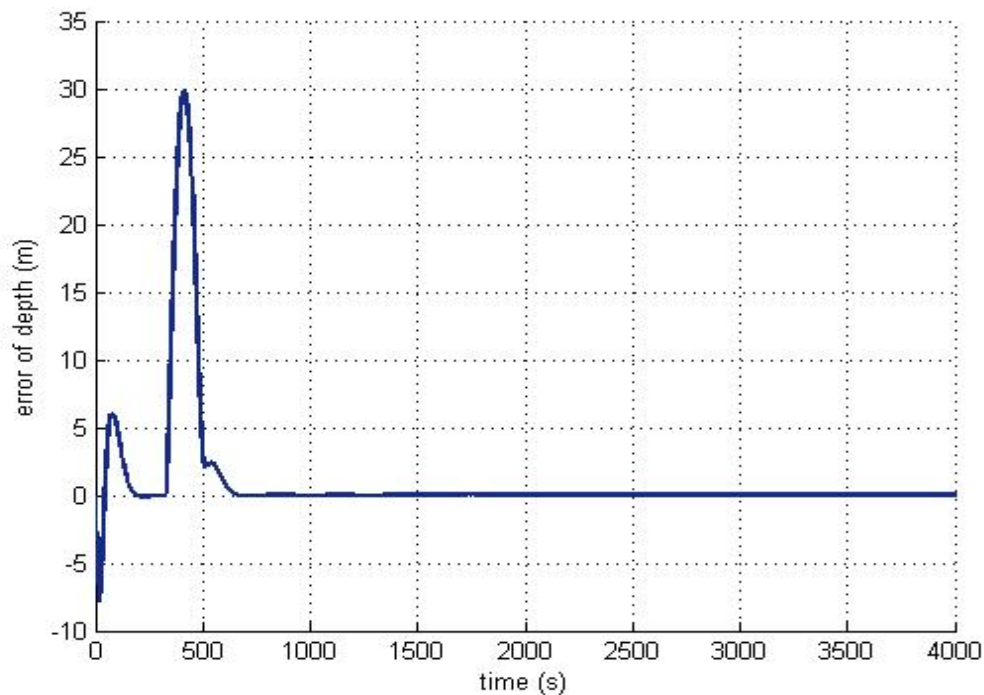


Figure 5.49 Error of input-output feedback linearization strategy for ramp model of input reference.

If desired depth position is deeper than maximum range of depth operation where feedback gain \mathbf{K} is tuned, the ramp model input reference with saturation value gives better response compare to step input. By giving ramp model input reference, shown in Figure 5.48, the steady time $T_s = 565.8$ s and steady state error $e_{ss} = 0.159$ m. This input model is faster to reach steady state compare to step input model, shown in Figure 5.50, which has steady time $T_s = 596.8$ s and steady state error $e_{ss} = 0.135$ m. If we consider to the energy used in this operation, for step input the energy usage is 37940 Watt second and for ramp input model the energy usage is 18410 Watt second. Therefore, by changing the input reference from step model into ramp model, the better response and optimal control will be obtained.

If we look again to the Figure 5.48 and Figure 5.49, before reach steady state, the error is minimized when the input reference keeps changing or dynamic. Therefore this controller can be expected to be applied for tracking a trajectory. If trajectory

input reference is given to the control system, the response can be seen in Figure 5.51 and Figure 5.53. The model of input reference is given as sinus and triangle.

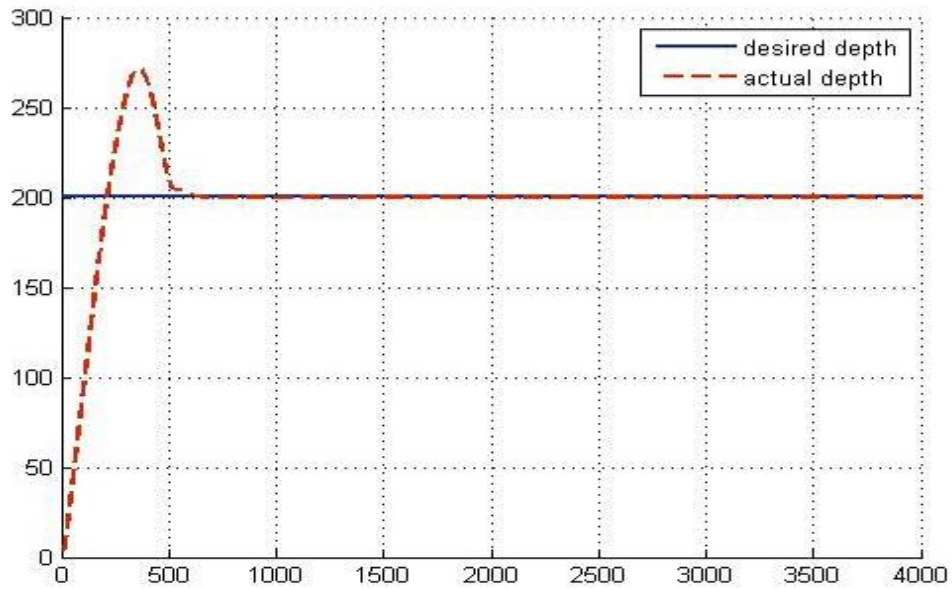


Figure 5.50 Response of input-output feedback linearization strategy for single step model of input reference bigger than range of depth operation.

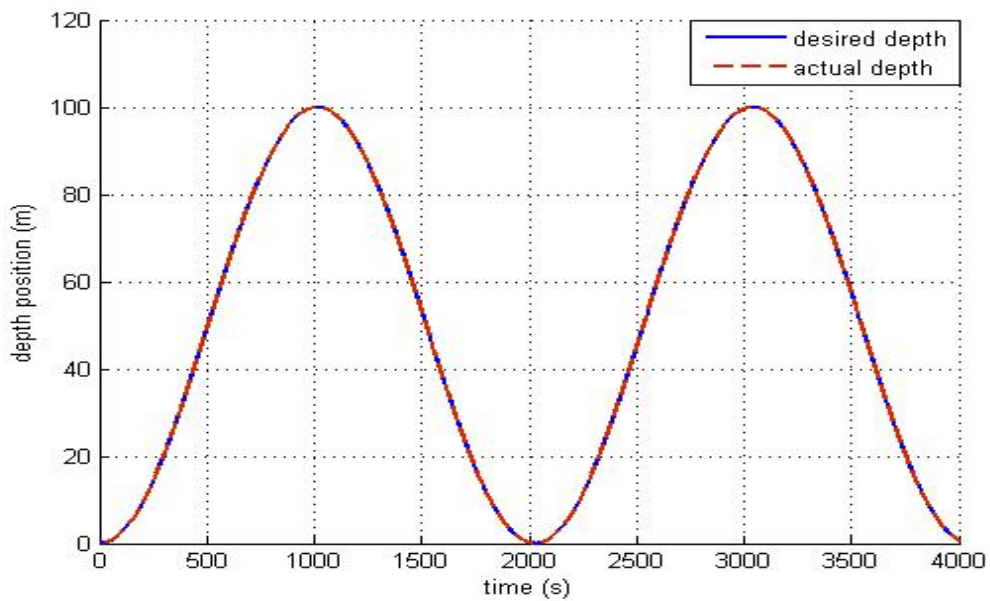


Figure 5.51 Response of input-output feedback linearization strategy for sinus model of input reference.

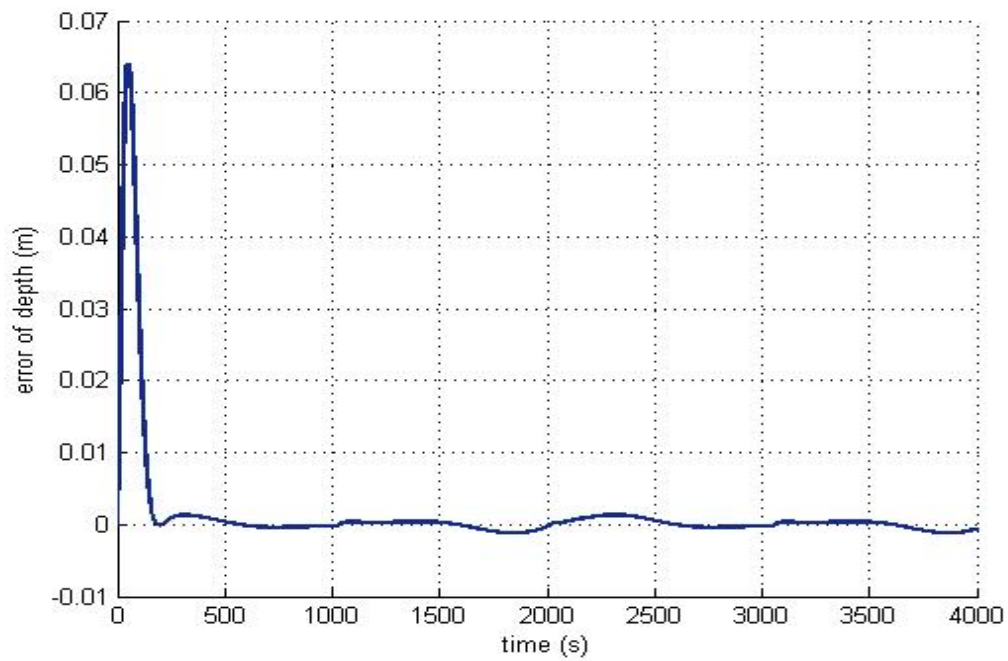


Figure 5.52 Error of input-output feedback linearization strategy for sinus model of input reference.

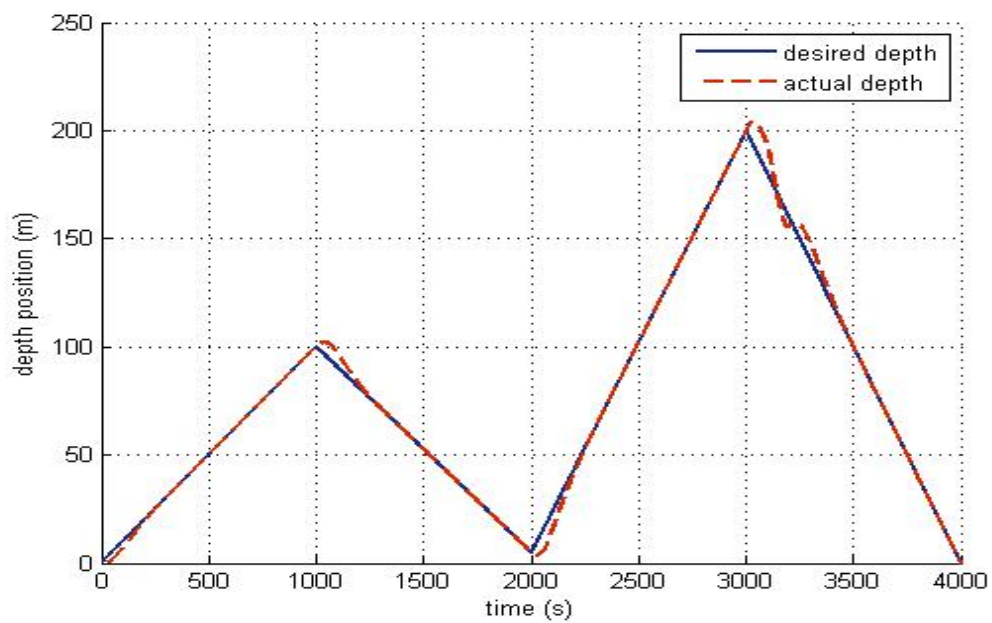


Figure 5.53 Response of input-output feedback linearization strategy for triangle model of input reference.

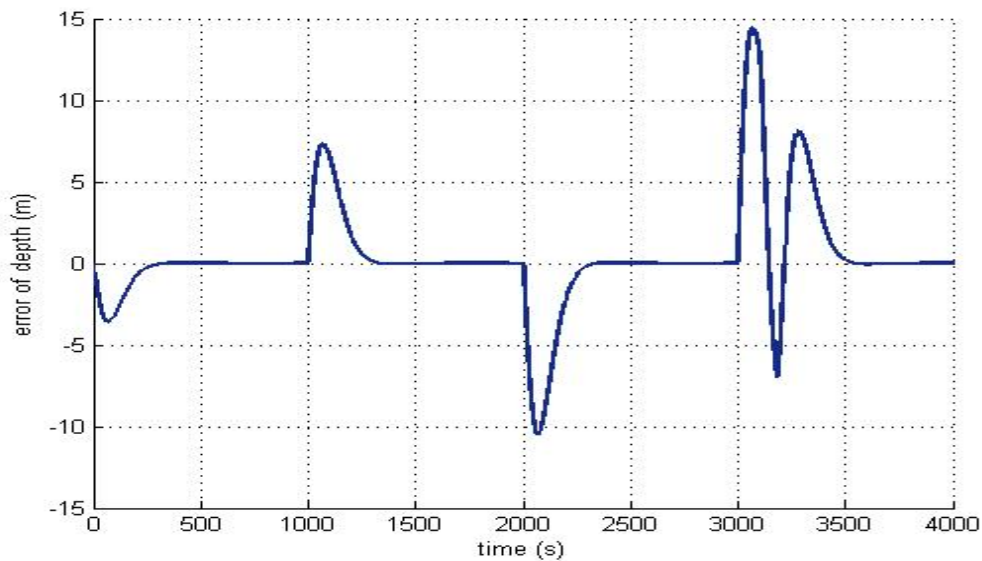


Figure 5.54 Error of input-output feedback linearization strategy for triangle model of input reference.

From Figure 5.51 and Figure 5.53, it is seen that the actual depth position of the URV keeps following the trajectory given as input reference. If the input reference is given as sinus model, the response is looked so smooth, error (RMSE) is 0.008 m. Figure 5.53 shows when the trajectory as input reference is extremely change, the resulting error position is increased, the error (RMSE) is 1.634 m. This condition is also shown in Figure 5.48 when input reference is given as a ramp model. The error is increased when the input reference is changed into constant value. From simulation, it is seen if the change of input trajectory is constant, then the error converges to zero.

If we consider to the energy needed in this operation, when the trajectory is given as sinus the energy usage is 1906 Watt second and if trajectory is given as triangular, the energy usage is 13560 Watt second.

5.4 Performances of The Controllers

Since the dynamic model for depth positioning of the spherical URV behaved as nonlinear system then two different approaches were designed in this thesis in order

to perform the depth positioning system, i.e. linearized approximation and feedback linearization. In feedback linearization approach, there are two methods, i.e. state-space linearization and input-output linearization. The performances for these approaches when step input was applied are shown in Table 5.7 and Table 5.8, and when trajectory input was applied, the performances are shown in Table 5.9. From Table 5.7, generally, it is seen that by using linearized approximation, the steady state is reached faster than both feedback linearization approaches. It also can be seen in Table A.1 (Appendix 3), when different multi step input is applied. If the URV is operated in the range in which the gain is tuned, the overshoot and steady state error of linearized approximation are also smaller than feedback linearization. But, if energy usage in operation is considered, feedback linearization strategy consumes less power than linearized approximation. It is seen in Table 5.8 and Table A.2 (Appendix 3). If performances of the state-space feedback linearization and input-output feedback linearization are compared when the step input reference is applied, it is seen that if the URV is operated within the range where the gain is tuned (0-100m), input-output feedback linearization give faster response in order to reach steady state. The overshoot and steady state error almost the same. But for the energy usage, state-space feedback linearization consumes less power.

Table 5.7 Rise time (T_r), steady time (T_s) and overshoot (OS) of the controllers.

Step change (Depth position) (m)	Linearized approximation			State-space feedback linearization			Input-output feedback linearization		
	T_r (s)	T_s (s)	OS (%)	T_r (s)	T_s (s)	OS (%)	T_r (s)	T_s (s)	OS (%)
0-30	59.2	108.8	0.005	25.6	224	0.234	43.6	218.6	0.219
30-100	68.9	102.7	0.061	65.2	194.2	6.775	65.8	183.4	5.394
100-30	84.2	170.7	0.005	87	267.3	0.322	86.4	267.5	0.329
30-160	105.2	387.1	31.601	106.7	432.8	25.537	106.5	433.4	25.67
160-30	128.4	248.1	0.005	127.1	342.2	0.307	126.6	342.6	0.308
110-160	52.9	227.4	14.221	57.1	223.8	8.507	56.7	225.8	8.994
160-110	77.8	141.6	0.001	87.1	224.8	0.077	85.3	224.9	0.079

Table 5.8 Steady state error (RMSE) and power usage for step input.

Step change (Depth position) (m)	Linearized approximation		State-space feedback linearization		Input-output feedback linearization	
	RMSE (m)	Power usage (Watt second)	RMSE (m)	Power usage (Watt second)	RMSE (m)	Power usage (Watt second)
0-30	0.04	1859.034	0.069	1028.794	0.068	1254.617
30-100	0.088	10642.417	0.213	9477.242	0.212	9335.668
100-30	0.044	7741.709	0.085	6743.544	0.086	6773.23
30-160	0.253	34967.527	0.357	24934.511	0.357	25053.856
160-30	0.032	15154.273	0.051	14410.108	0.051	14423.567
110-160	0.273	19204.848	0.293	13030.645	0.291	13401.248
160-110	0.155	8914.826	0.219	7664.011	0.219	7712.397

Table 5.9 Steady state error (RMSE) and power usage for trajectory input.

Input reference/ trajectory	Linearized approximation		State-space feedback linearization		Input-output feedback linearization	
	RMSE (m)	Power usage (Watt second)	RMSE (m)	Power usage (Watt second)	RMSE (m)	Power usage (Watt second)
Triangle	4.58	4215	9.213	1944.425	1.634	13560
Sinus	2.956	1935.541	6.741	3936.512	0.008	1906

If input reference is given as trajectory, different performances are obtained in simulation. Input-output feedback linearization approach results smallest steady state error compared to the others approaches. This condition is seen clearly if the trajectory is given in sinus model, as presented in Table 5.9 and Table A.3 (Appendix 3). If the energy usage is considered, the input-output feedback linearization approach consumes more energy compared to the others approaches. But, if we look to the sinus model reference the difference of energy usage between input-output feedback linearization approach and linearized approximation approach is not so big, but steady state error resulted by input-output feedback linearization is very small compared to linearized approach or state-space feedback linearization.

5.5 Summary

Simulation of dynamic model and controller design are simulated in this chapter by using Simulink/MATLAB. By simulating the dynamic model in open loop system, the characteristic of the system can be analyzed. In order to control depth position of the spherical URV by using a variable ballast mechanism, a proper controller is needed. Since the system behaves as nonlinear system, then the controllers are designed by using linearized approach and nonlinear approach. In nonlinear approach, feedback linearization which consist of state-space feedback linearization and input-output feedback linearization are applied. Performances of these controllers are discussed and compared each others in this chapter. Some input model such as step input, ramp and trajectory are tested to system in order to know the responses and performances of the controller.

CHAPTER 6

CONCLUSION AND FUTURE WORKS

6.1 Conclusion

This thesis presented depth positioning of a spherical underwater robot vehicle by using a variable ballast mechanism as motion actuator. A spherical shape has advantage that is having axially symmetry along its surface, so that it provides uniform drag force in any direction of its motion. Hence, it will be easier to design control strategy for its motion.

Since the depth positioning system was designed, then this thesis just interested in one degree of freedom from six in full degree of freedom, i.e. heave or vertical motion. A variable ballast mechanism which works based on Archimedes principle is utilized as motion actuator. By assuming there are no external disturbances and parameters of ambient such as water density, atmospheric pressure at surface, gravitational acceleration are constant, then the dynamic model of this depth positioning system was derived in this thesis. Since the dynamic model behaved as nonlinear system, then in order to control the depth position of the URV, two different approaches of the controllers were investigated, i.e. linearized approximation approach and nonlinear approach.

Some properties of these approaches, such as controllability, stability and observability, were analyzed. In linearized approximation approach, it was concluded that the linearized model is controllable and observable therefore the actual nonlinear model is also controllable and observable. Hence, the linear controller strategy can be designed based on the linearized model. In order to analyze the stability of the system about equilibrium point based on the linearized model, Lyapunov provided method that is known as Lyapunov linearization method. Since all of eigenvalues of the

linearized model presented in this thesis is zero, $\lambda = 0$, then Lyapunov linearization method cannot conclude whether the actual nonlinear model is stable or unstable.

In nonlinear approach, these properties were analyzed from the actual nonlinear model. In analyzing the controllability and observability of the system, Lie algebra was involved to construct the controllability and observability matrix. Based on these matrices, it can be concluded that the actual nonlinear model is controllable and observable. Considering the stability of the system based on the actual nonlinear model, Lyapunov also provided a method which is known as Lyapunov direct method. In this method, first, the possible Lyapunov function must be constructed. In this thesis, variable gradient method was utilized to construct the possible Lyapunov function. Then from this possible Lyapunov function, the Lyapunov direct method concluded that the actual nonlinear model is unstable. Hence, in order to stabilize the actual nonlinear model, the feedback linearization strategy was used. Since the actual nonlinear model is SISO system, then there are two kinds of feedback linearization methods possible to be applied, i.e. state-space feedback linearization and input-output feedback linearization. These two approaches of feedback linearization can perform the stabilization in order to control the depth position of the URV.

By the given parameters used in the design of variable ballast system which is utilized for vertical motion actuator of a spherical URV, then the VBS can change the weight of URV body, ΔW , in range $\pm 9.96\text{N}$ in order to make URV in positive buoyancy, neutral buoyancy or negative buoyancy. The buoyancy of URV is considered as a constant value. By using this mechanism, then the URV can move in vertical plane in the range of velocity $\pm 1.019\text{ms}^{-1}$.

From simulation of the controllers, can be concluded if the input reference of desired depth position is given as step input, the linearized approach can stabilize the system faster than both feedback linearization. If we consider to energy usage in the operation, then it is shown that state-space feedback linearization consume less energy compare to input-output feedback linearization and linearized approach. If the input reference is given as trajectory then input-output feedback linearization results the

smallest error. Since the change of input reference is constant, error of input-output feedback linearization is converge to zero, and the other two controller are converge to a constant value.

6.2 Thesis Contribution

In this thesis, a mechanism of variable ballast system was designed. This variable ballast mechanism utilized a variable tank as the chamber of amount of the water to be controlled. In this mechanism, water always fill all space in the tank but can be different in term of volume. Therefore, internal dynamic that is caused by movement of water in the tank when variable ballast utilizing fixed volume tank and amount of water is not maximum, will not occur. This variable ballast mechanism is suitable for small-scale URV, because this mechanism is compatible for small tank.

The dynamic model of the variable ballast mechanism was presented in this thesis. This mathematical model was derived based on the physical laws involved in this system. The dynamic model for vertical motion of a spherical underwater vehicle was also presented in this thesis. This vertical motion is caused by the change of weight force of the URV's body, which is from the variable ballast mechanism. By having the mathematical model of vertical motion of spherical URV which utilizing variable ballast mechanism as actuator, the simulation can be designed. Any controller strategy can be designed and tested in computer simulation in order to get an optimal controller.

Controller for depth positioning of a spherical URV by using variable ballast mechanism as actuator was designed in this thesis. As a nonlinear system, then to design the controller, some conditions must be considered. A controller can be designed based on linearized approximation approach if the linearized model is controllable otherwise this approach cannot be used. The linearized model of the actual dynamic of this system is controllable then linear feedback control strategy was designed based on the linearized model. A nonlinear approach was also performed to design the controller for this depth positioning system, i.e. feedback linearization. As

SISO system, there are two approaches of feedback linearization, i.e. state-space feedback linearization and input-output feedback linearization. In stabilizing the equilibrium point, the linearized approximation approach is faster to reach steady state compared to the feedback linearization approach, but it needs more power. In tracking the trajectory, input-output feedback linearization approach results smaller error compared to linearization approximation approach and state-space feedback linearization approach, but it needs more power. Therefore these approaches have weaknesses and advantages.

6.3 Future Work

In this thesis, the design and model of variable ballast mechanism was presented. The simulations are performed in ideal and constant parameters of ambient. Next, the model and the control design should be tested in varying parameters of ambient. Therefore, the performance of the controller can be analyzed. The robustness of the controller also should be tested by involving some external disturbances. An optimal controller also must be designed in order to optimal the usage of energy.

The availability of external disturbances could cause rolling or twisting on the spherical URV, therefore in the future works, the influence of this motion should be considered in the model.

The implementation of this design is needed so that it can be tested in the real condition. Furthermore, any controller design can be tested in the real system.

PUBLICATIONS

1. Bambang Sumantri, M. N. Karsiti, and H. Agustiawan, "Depth Positioning of a Spherical URV: Modeling and Simulation," in *National Postgraduate Conference on Engineering, Science and Technology (NPC)*, Tronoh, Malaysia, March 31, 2008.
2. Bambang Sumantri, M. N. Karsiti, and H. Agustiawan, "Development of Variable Ballast Mechanism for Depth Positioning of Spherical URV," in *International Symposium on Information Technology 2008*, vol. IV, *Engineering and Systems*. Kuala Lumpur-Malaysia, 2008, pp. 2473-2478.
3. Bambang Sumantri, M. N. Karsiti, and Salman Ahmed, "Input-Output Exact Feedback Linearization for Depth Positioning of Spherical URV," in *International Conference on Advanced Computer Control (ICACC 2009)*, Singapore, January 22 – 24, 2009.

REFERENCES

- [1] Y. Ito, N. Kato, J. Kojima, S. Takagi, K. Asakawa, and Y. Shirasaki, "Cable tracking for autonomous underwater vehicle," presented at Symposium on Autonomous Underwater Vehicle Technology, 1994.
- [2] J. Evans, Y. Petillot, P. Redmond, M. Wilson, and D. Lane, "AUTOTRACKER: AUV embedded control architecture for autonomous pipeline and cable tracking," presented at Oceans '03-IEEE, 2003.
- [3] Y. R. Petillot, S. R. Reed, and J. M. Bell, "Real time AUV pipeline detection and tracking using side scan sonar and multi-beam echo-sounder," presented at Oceans '02 MTS/IEEE, 2002.
- [4] M. Dunbabin, P. Corke, I. Vasilescu, and D. Rus, "Data Muling Over Underwater Wireless Sensor Networks Using an Autonomous Underwater Vehicle," presented at IEEE International Conference on Robotics and Automation (ICRA), Orlando, Florida, 2006.
- [5] J. C. Kinsey, D. A. Smallwood, and L. L. Whitcomb, "A New Hydrodynamics Test Facility for UUV Dynamics and Control Research," presented at Oceans '03-IEEE, 2003.
- [6] S. K. Choi, J. Yuh, and N. Keevil, "Design of Omni-Directional Underwater Robotic Vehicle," presented at Oceans '93-'Engineering in Harmony with Ocean', 1993.
- [7] C. Watts, E. McGookin, and M. Macauley, "Modelling and Control of a Biomimetic Underwater Vehicle with a Tendon Drive Propulsion System," presented at Oceans 2007, Europe, 2007.
- [8] J. G. Graver, "Underwater Gliders: Dynamics, Control and Design," in Mechanical and Aerospace Engineering, vol. Phd. Dissertation Princeton University 2005, pp. 292.
- [9] J.-M. Tung, M.-F. Guo, J. Guo, F.-C. Chiu, and S.-W. Cheng, "Design of an Underwater Glider with Fore and Aft Buoyancy Engines," presented at Symposium on Underwater Technology and Workshop on Scientific Use of Submarine Cables and Related Technologies, 2007.

-
- [10] K. Shibuya, Y. Kado, S. Honda, T. Iwamoto, and K. Tsutsumi, "Underwater Robot with a Buoyancy Control System Based on the Spermaceti Oil Hypothesis," presented at the IEEE/RSJ International Conference on Intelligent Robots and Systems, Beijing, China, 2006.
- [11] K. S. Wasserman, J. L. Mathieu, M. I. Wolf, A. Hathi, S. E. Fried, and A. K. Baker, "Dynamic Buoyancy Control of an ROV Using a Variable Ballast Tank," presented at Oceans, 2003.
- [12] M. Xu and S. M. Smith, "Adaptive Fuzzy Logic Depth Controller for Variable Buoyancy System of Autonomous Underwater Vehicles," presented at the Third IEEE Conference on IEEE World Congress on Computational Intelligence, Orlando, Fl, USA, 1994.
- [13] J. S. Riedel, A. J. Healey, D. B. Marco, Beyazay, and Bahadir, "Design and Development of Low Cost Variable Buoyancy System for the Soft Grounding of Autonomous Underwater Vehicles," presented at 11th International Symposium on Unmanned Untethered Submersible Technology (UUST'99), 1999.
- [14] M. Worall, A. J. Jamieson, A. Holford, R. D. Neilson, M. Player, and P. M. Bagley, "A Variable Buoyancy System for Deep Ocean Vehicles," presented at IEEE Oceans, Europe, 2007.
- [15] C. L. Nickell, "Modular Modification of a Buoyant AUV for Low-Speed Operation," in *Aerospace Engineering*, vol. Master of Science. Blacksburg, Virginia: Virginia Polytechnic Institute and State University, 2005, pp. 72.
- [16] R. E. Davis, D. C. Webb, L. A. Regier, and J. Dufour, "The Autonomous Lagrangian Circulation Explorer (ALACE)," *Journal of Atmospheric and Oceanic Technology*, vol. 9, pp. 264-285, 1991.
- [17] C. C. Eriksen, T. J. Osse, R. D. Light, T. Wen, T. W. Lehman, P. L. Sabin, J. W. Ballard, and A. M. Chiodi, "Seaglider: A Long-Range Autonomous Underwater Vehicle for Oceanographic Research," *IEEE Journal of Oceanic Engineering*, vol. 26, No. 4, pp. 424-436, 2001.
- [18] C. Waldmann, "Performance Data Of A Buoyancy Driven Deep Sea YOYO-Profiler For Long Term Moored Deployment," presented at OCEANS'99 MTS/IEEE. Riding the Crest into the 21st Century, Seattle, WA, USA, 1999.

- [19] M. Listak and M. Kruusmaa, "Buoyancy Control of a Semiautonomous Underwater Vehicle for Environmental Monitoring in Baltic Sea," presented at The International IEEE Conference Mechatronics and Robotics (MechRob'04), Aachen, 2004.
- [20] S. Tangirala and J. Dzielski, "A Variable Buoyancy Control System for a Large AUV," *IEEE Journal of Oceanic Engineering*, vol. 32, No. 4, pp. 762-771, 2007.
- [21] K. H. Low, "Locomotion Consideration and Implementation of Robotic Fish with Modular Undulating Fins: Analysis and Experimental Study," presented at 2006 IEEE/RSJ International Conference on Intelligent Robots and Systems, Beijing, China, 2006.
- [22] M. Brown, M. Kelley, and P. McGill, "MBARI Vertical Profiler," presented at OCEANS, 2001. MTS/IEEE Conference and Exhibition, Honolulu, HI, USA, 2001.
- [23] G. Antonelli, F. Caccavale, S. Chiaverini, and L. Villani, "An Output Feedback Algorithm for Position and Attitude Tracking Control of Underwater Vehicles," presented at The 37th IEEE Conference on Decision and Control, Tampa, FL, USA, 1998.
- [24] K. Y. Pettersen and O. Egeland, "Position and Attitude Control of an Underactuated Autonomous Underwater Vehicle," presented at The 35th IEEE Conference on Decision and Control, Kobe, Japan, 1996.
- [25] P. A. DeBitetto, "Fuzzy Logic for Depth Control of Unmanned Undersea Vehicles," *IEEE Journal of Oceanic Engineering*, vol. 20, pp. 242-248, 1995.
- [26] E. S. Ammeen and G. O. Beale, "Fuzzy depth control for a submersible vehicle," presented at IEEE International Symposium on Industrial Electronics, Guimaraes, Portugal, 1997.
- [27] T. Chatchanayuenyong and M. Parnichkun, "Neural network based-time optimal sliding mode control for an autonomous underwater robot," *Elsevier Journal of Mechatronics*, vol. 16, pp. 471-478, 2006.
- [28] K. D. Do, Z. P. Jiang, J. Pan, and H. Nijmeijer, "A Global Output-Feedback Controller for Stabilization and Tracking of Underactuated ODIN: A Spherical Underwater Vehicle," *Elsevier Journal of Automatica*, vol. 40, pp. 117-124, 2004.

- [29] S. Liu, D. Wang, E. K. Poh, and C. S. Chia, "Nonlinear output feedback controller design for tracking control of ODIN in wave disturbance condition," presented at Proceedings of MTS/IEEE-OCEANS, 2005.
- [30] N. S. Nise, Control Systems Engineering, 4th ed: John Wiley & Sons, Inc., 2004.
- [31] N. E. Leonard and J. G. Graver, "Model-Based Feedback Control of Autonomous Underwater Gliders," IEEE Journal of Oceanic Engineering, vol. 26, pp. 633-645, 2001.
- [32] I. Schjøllberg and T. I. Fossen, "Modelling and Control of Underwater Vehicle-Manipulator Systems," presented at the 3rd Conference on Marine Craft Maneuvering and Control (MCMC'94), Southampton, UK, 1994.
- [33] A. Chellabi and M. Nahon, "Feedback Linearization Control of Undersea Vehicles," presented at Oceans '93. 'Engineering in Harmony with Ocean', 1993.
- [34] R. K. Rajput, A Textbook of Fluid Mechanics and Hydraulics Machines in SI Units. New Delhi: S. Chand and Company, 2003.
- [35] M. Drtil, "Electronics and Sensor Design of an Autonomous Underwater Vehicle," in School of Electrical, Electronic and Computer Engineering, vol. Diplom-Ingenieur. Perth: The University of Western Australia, 2006, pp. 204.
- [36] "http://www.roymech.co.uk/Useful_Tables/Cams_Springs/Power_Screws_1.html."
- [37] "[http://www-mdp.eng.cam.ac.uk/resources/2.007/Lead Screws, Gears, and Power Budgets.pdf](http://www-mdp.eng.cam.ac.uk/resources/2.007/Lead_Screws,_Gears,_and_Power_Budgets.pdf)."
- [38] J. A. Collins, Mechanical Design of Machine Elements and Machines: a Failure Prevention Perspective. New York: John Wiley & Sons Inc, 2003.
- [39] M. J. Moran and H. N. Shapiro, Fundamentals of Engineering Thermodynamics, 3rd ed. Chichester-England: John Wiley & Sons Inc, 1998.
- [40] M. Kawski, "The Combinatorics of Nonlinear Controllability and Noncommuting Flows," in Lecture Notes. Arizona, USA.: Department of Mathematics, Arizona State University, 2001.
- [41] J.-J. E. Slotin and W. Li, Applied Nonlinear Control: Prentice-Hall, 1991.
- [42] M. S. Santina, A. R. Stubberud, and G. H. Hostetter, Digital Control System Design. USA: Saunders College Publishing, 1998.

-
- [43] F. J. D. III and M. A. Henson, "Chapter 3: Nonlinear Systems Theory," in *Nonlinear Process Control*. New Jersey: Prentice-Hall.
 - [44] Z. Vukic, L. Kuljaca, D. Donlagic, and S. Tesnjak, *Nonlinear Control System*. New York: Marcel Dekker, 2003.
 - [45] K. A. Morgansen, "Observability," in *Geometric Methods for Nonlinear Control Systems Lecture Notes*. Washington: Department of Aeronautics and Astronautics, University of Washington, April 26, 2004.
 - [46] J. K. Hedrick and A. Girard, *Lecture Notes for Control of Nonlinear Dynamic Systems: Theory and Applications*. Berkeley: University of California, 2005.
 - [47] M. A. Henson and D. E. Seborg, "Chapter 4: Feedback Linearizing Control," in *Nonlinear Process Control*. New Jersey: Prentice-Hall.
 - [48] H. K. Khalil, *Nonlinear System*. New Jersey: Prentice-Hall, 2002.

APPENDIX 1: M file in linearized approximation analysis.

```
%linearized.m
%programmed by Bambang S

syms x1 x2 x3 C1 C2 k1 k2 k3;
%OPEN-LOOP LINEARIZED SYSTEM
A=[0 1 0;0 0 C1;0 0 0];
B=[0;0;C2];
C=[1 0 0];

%constructing the controllability matrix
Cm=[B A*B A*A*B];

%testing the rank of controllability matrix
n_Cm=rank(Cm);

%constructing the observability matrix
Mo=[C;C*A;C*A*A];

%testing the rank of observability matrix
n_Mo=rank(Mo);

%CLOSED-LOOP LINEARIZED SYSTEM
K=[k1 k2 k3];

%coefficient matrix of closed-loop system
Acl=[A-B*K];

%scaling factor
F=inv(C*(-inv(Acl))*B);
```

APPENDIX 2: M file in feedback linearization analysis.

```

%feedback.m
%programmed by Bambang S

syms x1 x2 x3 b1 b2 b3 b4 b5 b6 w_bs g;
%OPEN-LOOP NONLINEAR SYSTEM

f=[x2;(x3-b2*abs(x2)*x2)/(b1+x3/g);0];
g=[0;0;b3/(w_bs+x3+b4*x1-(b5*x3/(b6-x3)))]];
h=x1;

%=====
%Lie bracket
dg=[diff(g,x1) diff(g,x2) diff(g,x3)];
df=[diff(f,x1) diff(f,x2) diff(f,x3)];

adfg=dg*f-df*g;
dadfg=[diff(adfg,x1) diff(adfg,x2) diff(adfg,x3)];
ad2fg=dadfg*f-df*adfg;
%=====

%constructing the controllability matrix of nonlinear system
C=[g adfg ad2fg];

%testing the rank of controllability matrix of nonlinear system
n_C=rank(C);

%=====
%observability analysis
Lfh=[diff(h,x1) diff(h,x2) diff(h,x3)]*f;
Lflh=[diff(Lfh,x1) diff(Lfh,x2) diff(Lfh,x3)]*f;

%constructing the observability map of nonlinear system
phi=[h;Lfh;Lflh];

%Jacobian of observability map = observability matrix
%d_phi=[diff(phi,x1) diff(phi,x2) diff(phi,x3)]
d_phi=jacobian([h;Lfh;Lflh],[x1 x2 x3]);

%testing the rank of obseravability matrix of nonlinear system
n_d_phi=rank(d_phi);
%=====

%STATE-SPACE LINEARIZABLE ANALISYS

%constructing involutivity vector field of nonlinear system
X2=adfg;
dX2=[diff(X2,x1) diff(X2,x2) diff(X2,x3)];
adgX2=dX2*g-dg*X2;

```

```
%involutivity analysis
v_f=[g adfg adgX2];
n_vf=rank(v_f);

%state transformation
z1=x1;
z2=jacobian(z1,[x1 x2 x3])*f;
z3=jacobian(z2,[x1 x2 x3])*f;

lfz1=jacobian(z1,[x1 x2 x3])*f;
lf2z1=jacobian(lfz1,[x1 x2 x3])*f;
lf3z1=jacobian(lf2z1,[x1 x2 x3])*f;
lglf2z1=jacobian(lf2z1,[x1 x2 x3])*g;

psi=-1*lf3z1/lglf2z1;
gamma=1/lglf2z1;
```

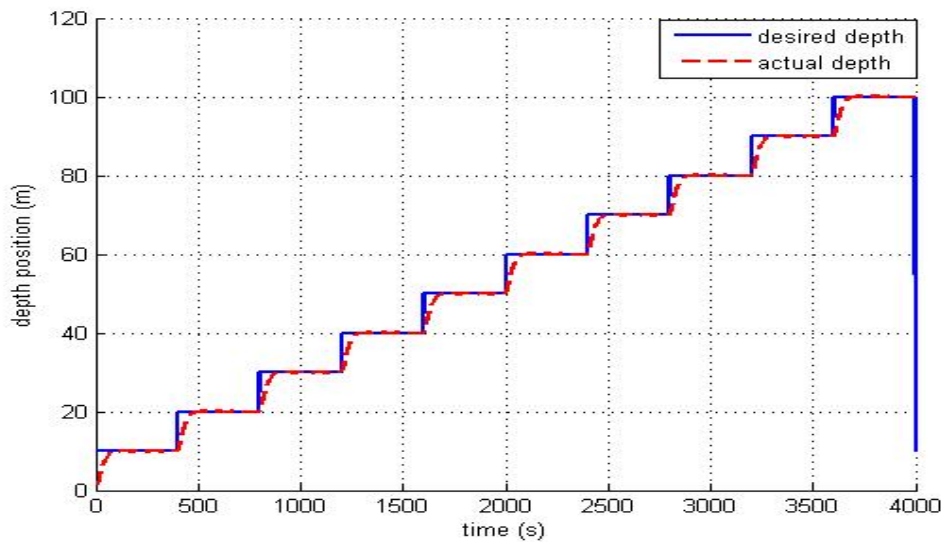
APPENDIX 3: Simulation result for different input reference models.

Figure A.1 Response of linearized approximation controller with multi step input reference in fixed increment.

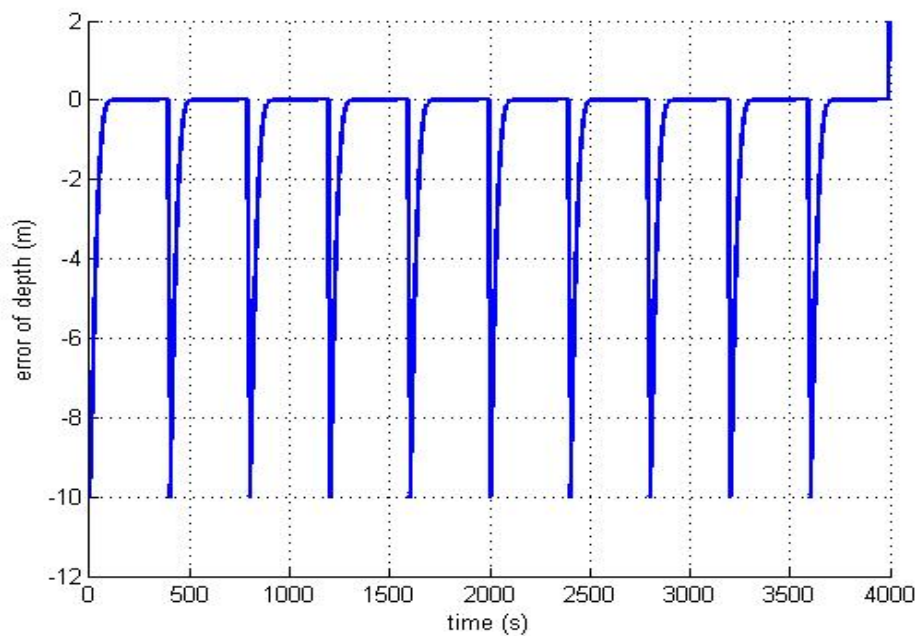


Figure A.2 Error of depth position for linearized approximation controller with multi step input reference in fixed increment.

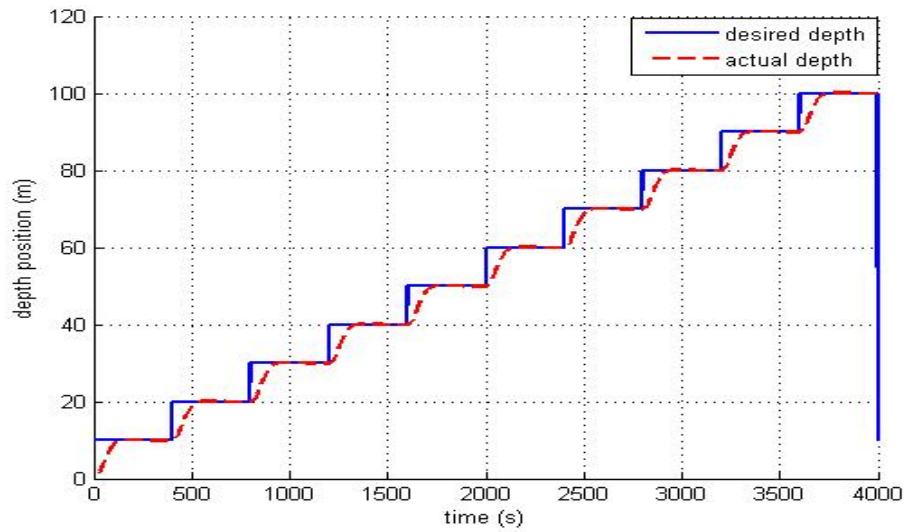


Figure A.3 Response of state-space feedback linearization controller with multi step input reference in fixed increment.

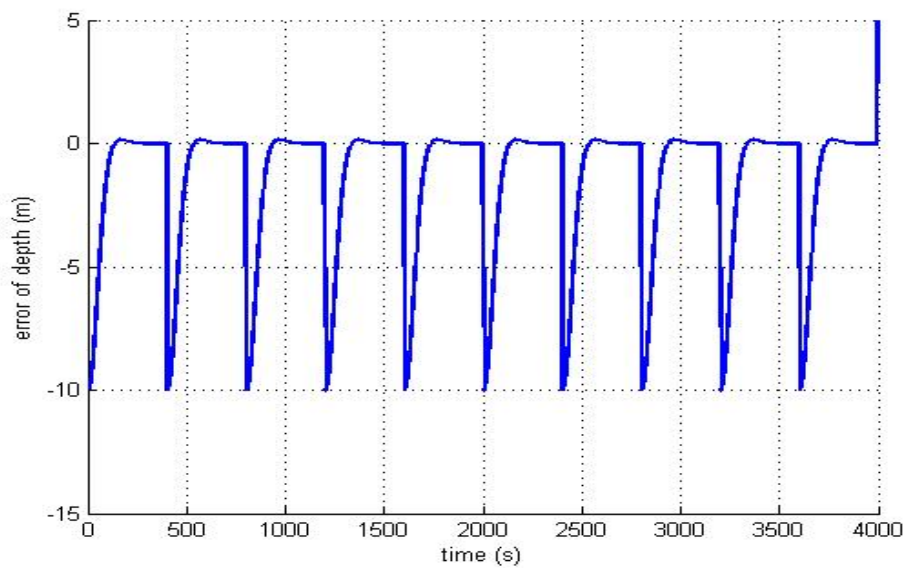


Figure A.4 Error of depth position for state-space feedback linearization controller with multi step input reference in fixed increment.

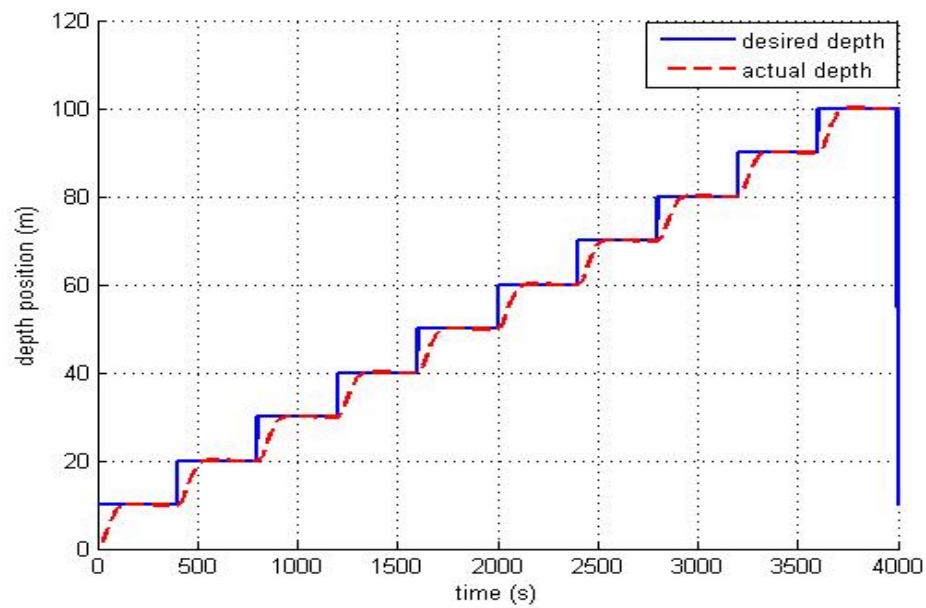


Figure A. 5 Response of input-output feedback linearization controller with multi step input reference in fixed increment.

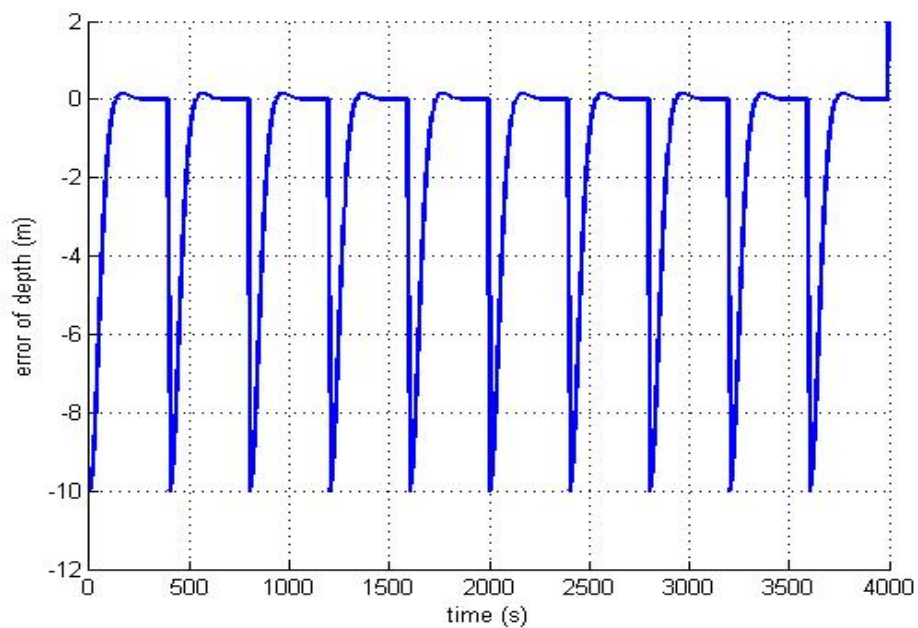


Figure A. 6 Error of depth position for input-output feedback linearization controller with multi step input reference in fixed increment.

Performances for each the controller with multi step input are presented in Table A.1 and Table A.2.

Table A.1 Rise time (T_r), steady time (T_s) and overshoot (OS) of the controllers with multi step input in fixed increment.

Step change (Depth position) (m)	Linearized approximation			State-space feedback linearization			Input-output feedback linearization		
	T_r (s)	T_s (s)	OS (%)	T_r (s)	T_s (s)	OS (%)	T_r (s)	T_s (s)	OS (%)
0-10	51.6	87.8	0.014	77.4	197.7	1.498	75.9	142.5	1.587
10-20	51.0	80.0	0.007	77.5	125.7	0.749	76.9	123.1	0.782
20-30	50.8	75.5	0.005	77.5	121.6	0.499	76.9	119.1	0.523
30-40	50.8	72.0	0.004	77.5	118.1	0.374	76.9	115.1	0.393
40-50	50.7	69.1	0.003	77.5	115.1	0.300	76.8	111.7	0.315
50-60	50.5	66.7	0.002	77.5	112.3	0.250	76.8	108.7	0.263
60-70	50.6	64.7	0.002	77.4	109.7	0.214	76.8	106.4	0.225
70-80	50.7	63.1	0.002	77.5	107.4	0.187	76.9	104.6	0.197

Table A.2 Steady state error (RMSE) and power usage for multi step input in fixed increment.

Step change (Depth position) (m)	Linearized approximation		State-space feedback linearization		Input-output feedback linearization	
	RMSE (m)	Power usage (Watt second)	RMSE (m)	Power usage (Watt second)	RMSE (m)	Power usage (Watt second)
0-10	0.011	288.342	0.028	29.065	0.067	60.181
10-20	0.024	552.503	0.067	86.331	0.069	115.699
20-30	0.037	834.563	0.073	143.597	0.075	171.830
30-40	0.051	1072.580	0.082	200.864	0.084	227.042
40-50	0.066	1294.861	0.094	258.131	0.095	281.966
50-60	0.081	1509.595	0.108	315.397	0.109	336.922
60-70	0.096	1732.926	0.124	372.664	0.124	392.853
70-80	0.111	1964.222	0.141	429.930	0.140	450.129

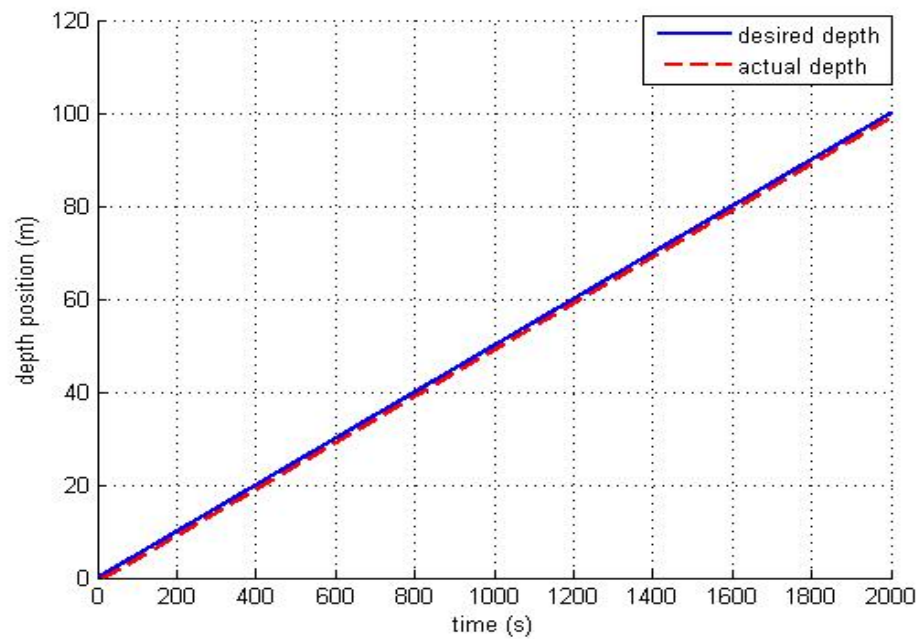


Figure A.7 Response of linearized approximation controller in ramp input reference with gradient 0.05.

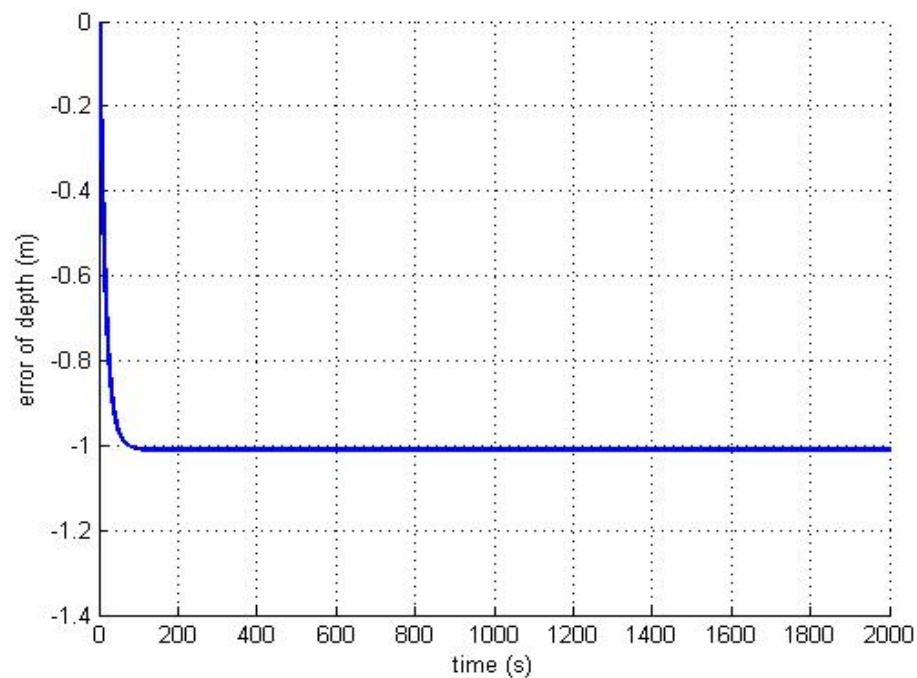


Figure A.8 Error depth position of linearized approximation controller in ramp input reference with gradient 0.05.

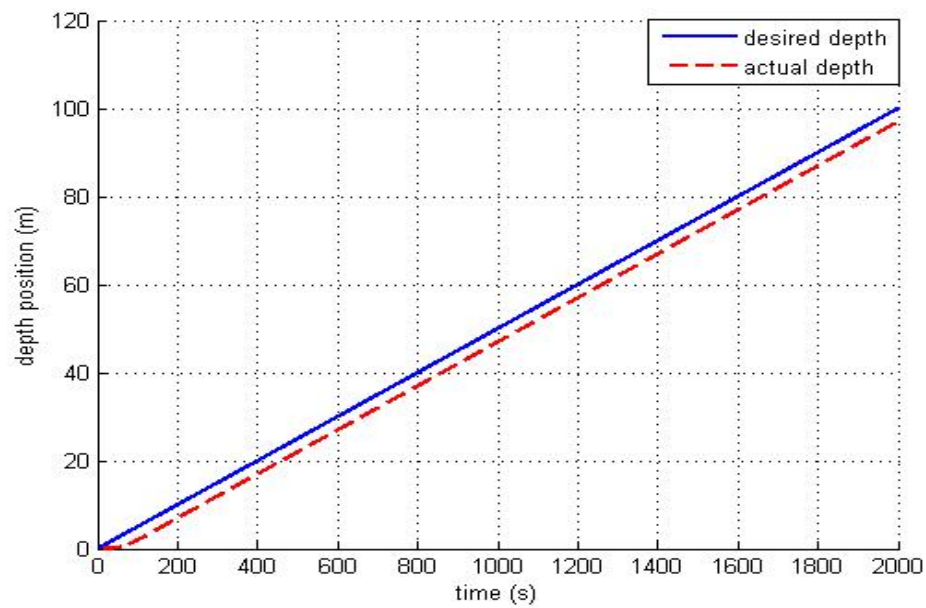


Figure A.9 Response of state-space feedback linearization controller in ramp input reference with gradient 0.05.

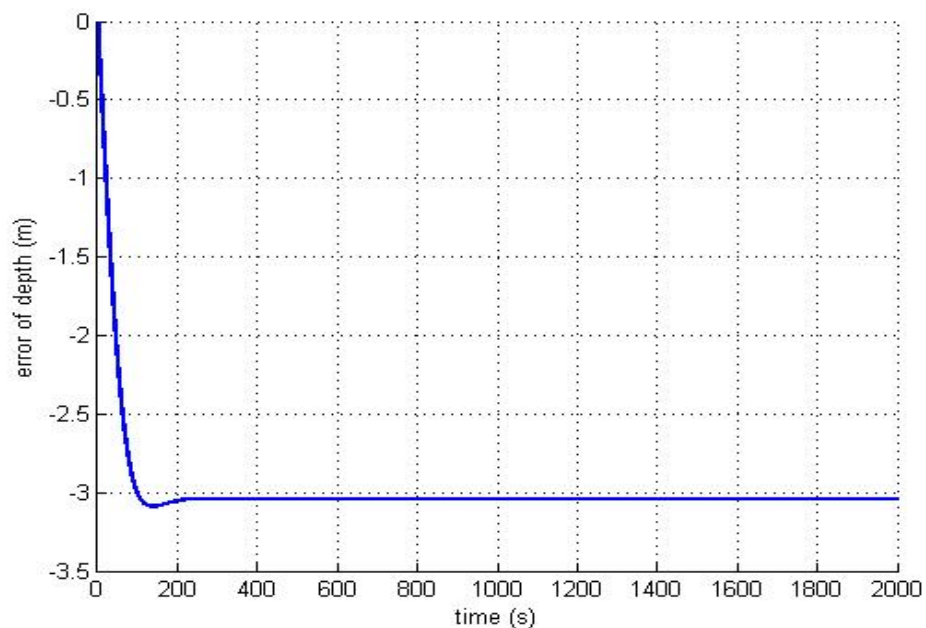


Figure A.10 Error depth position of state-space feedback linearization controller in ramp input reference with gradient 0.05.

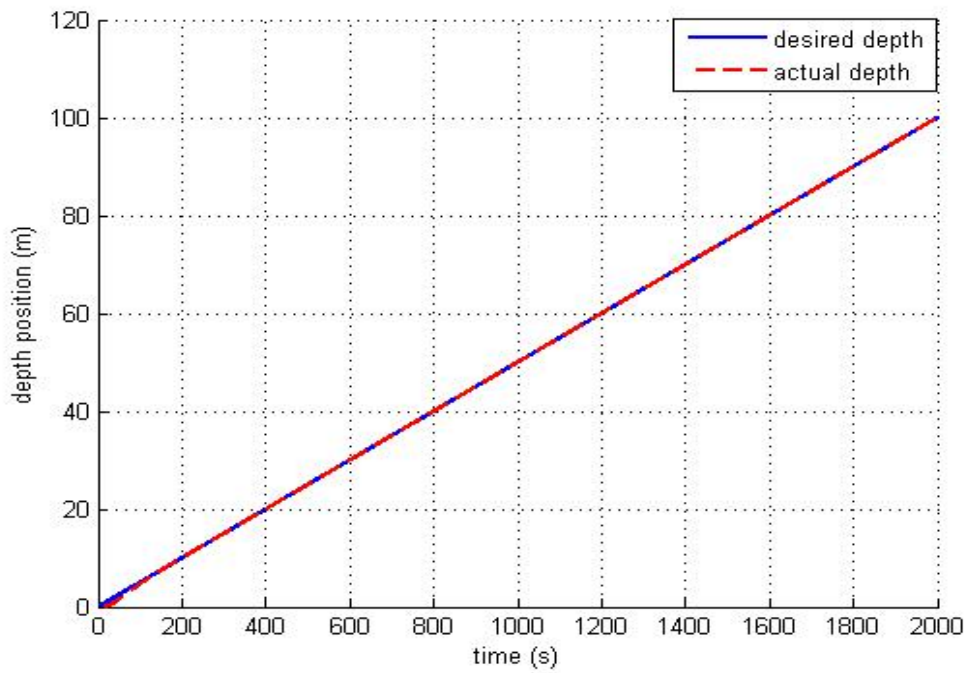


Figure A.11 Response of input-output feedback linearization controller in ramp input reference with gradient 0.05.

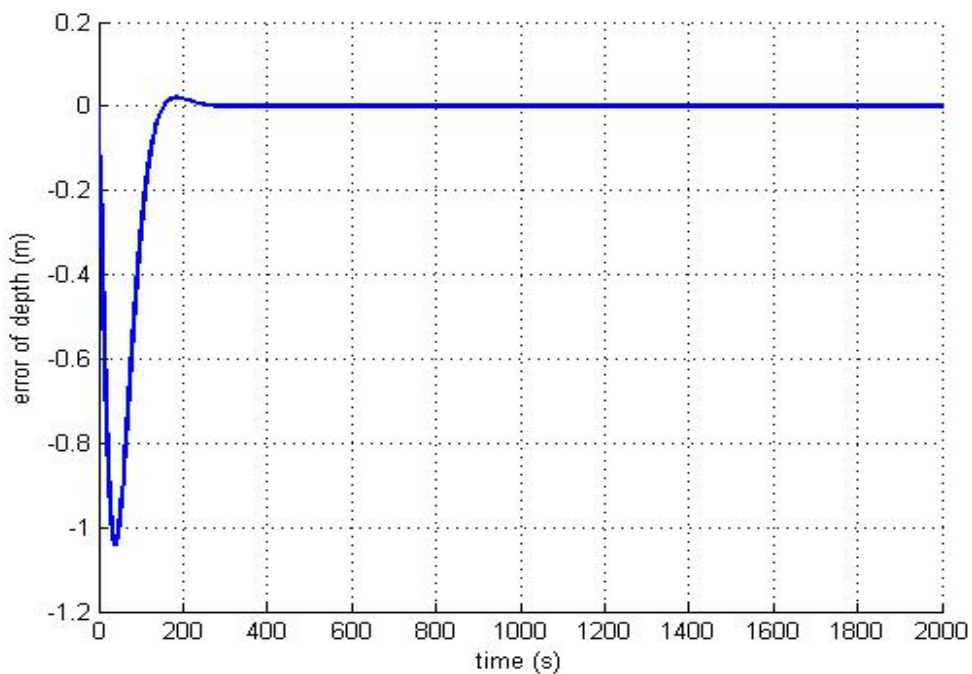


Figure A.12 Error depth position of input-output feedback linearization controller in ramp input reference with gradient 0.05.

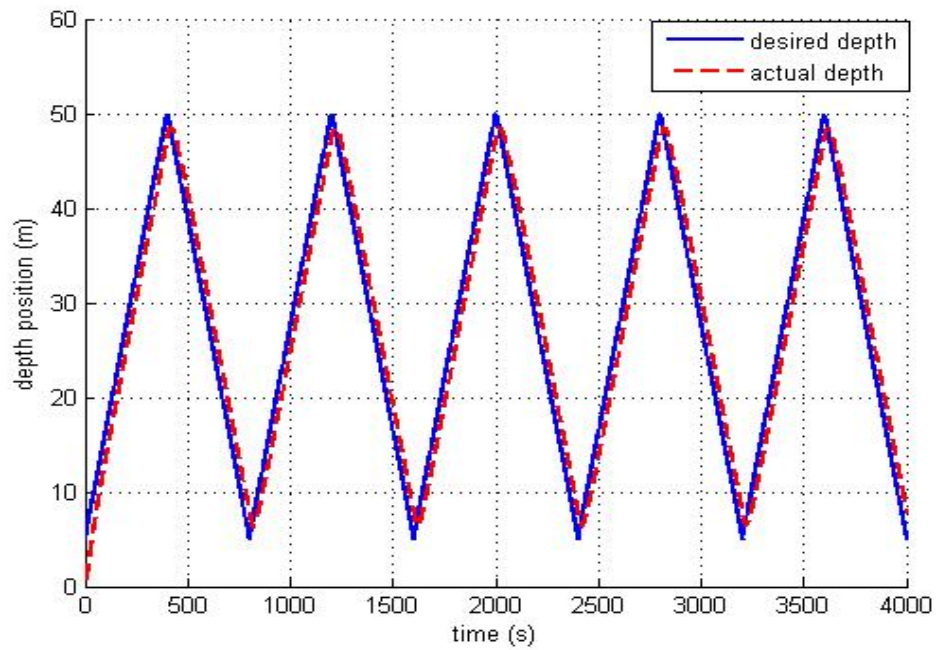


Figure A.13 Response of linearized approximation controller in triangle input reference (range operation 5-50 m).

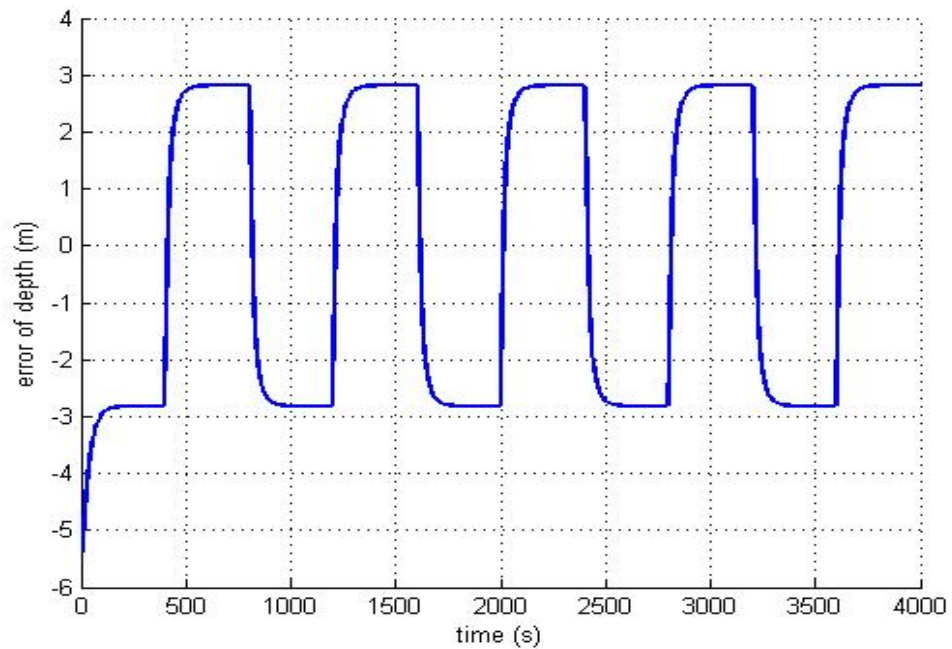


Figure A.14 Error depth position of linearized approximation controller in triangle input reference (range operation 5-50 m).

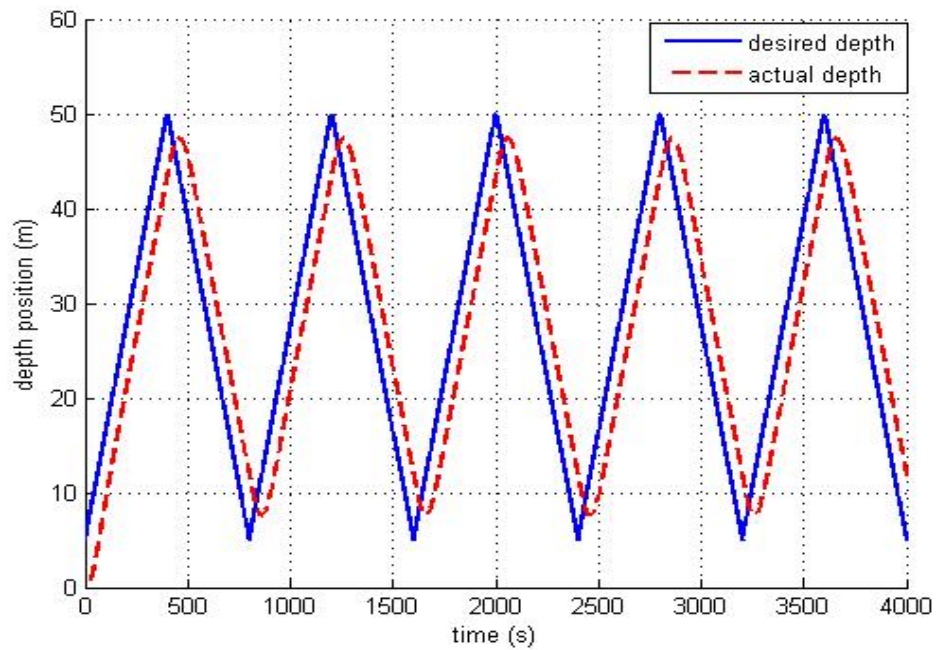


Figure A.15 Response of state-space feedback linearization controller in triangle input reference (range operation 5-50 m).

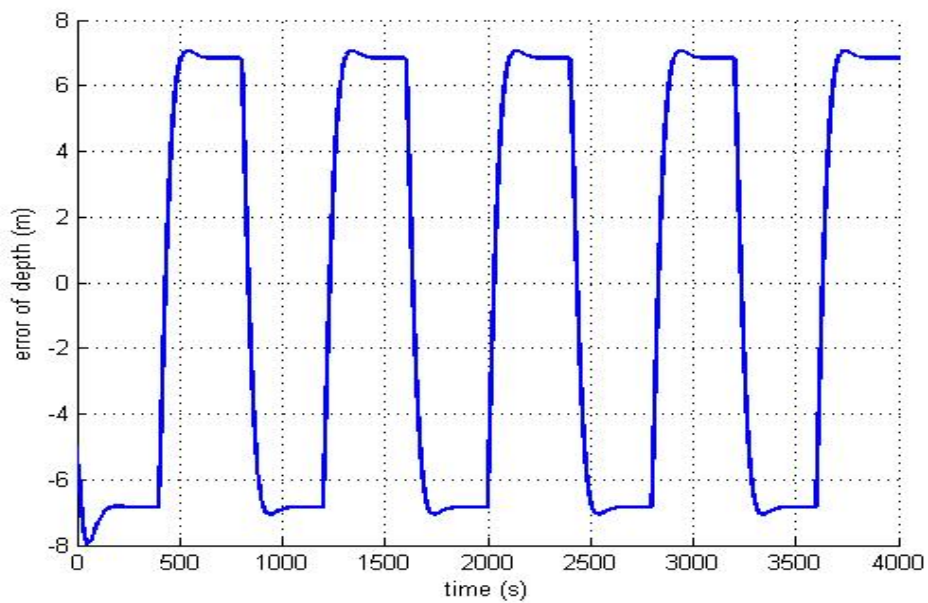


Figure A.16 Error depth position of state-space feedback linearization controller in triangle input reference (range operation 5-50 m).

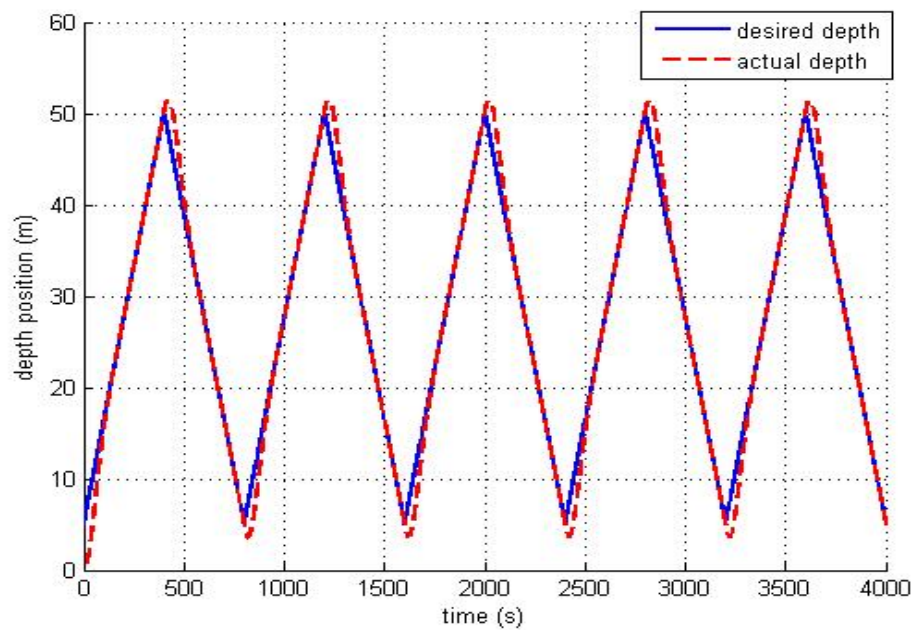


Figure A.17 Response of input-output feedback linearization controller in triangle input reference (range operation 5-50 m).

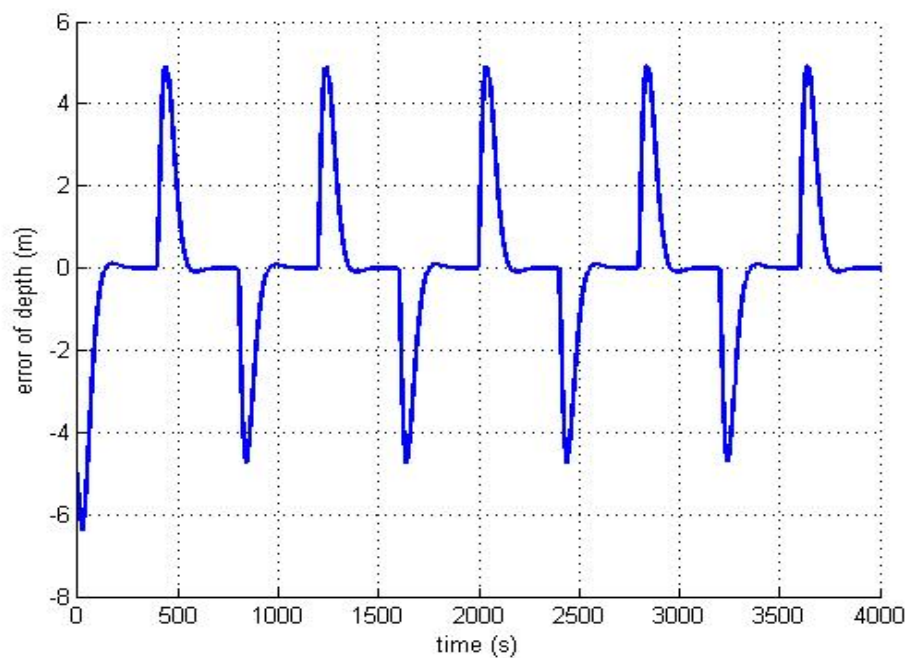


Figure A.18 Error depth position of input-output feedback linearization controller in triangle input reference (range operation 5-50 m).

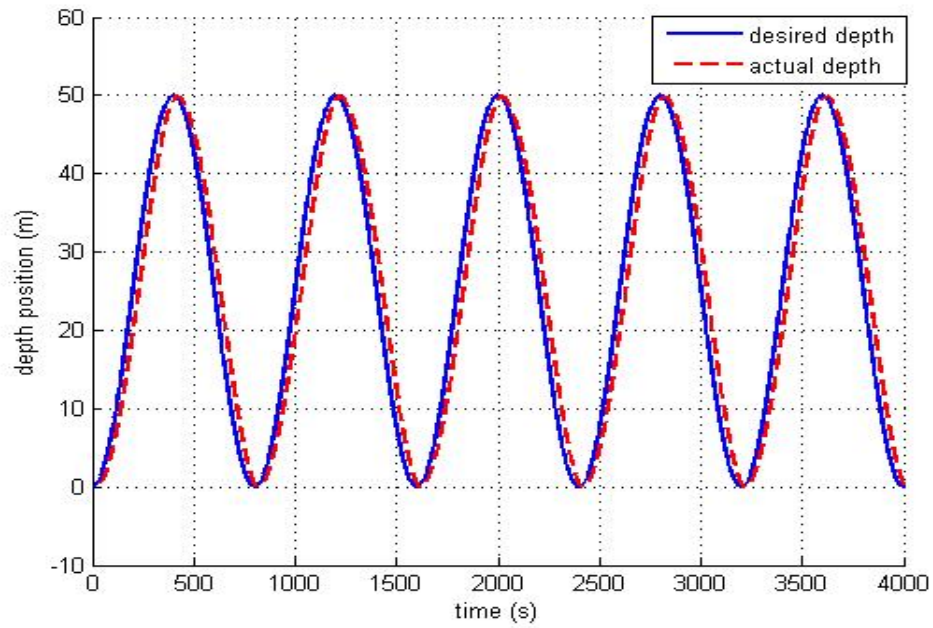


Figure A.19 Response of linearized approximation controller in sinus input reference (range operation 0-50 m).

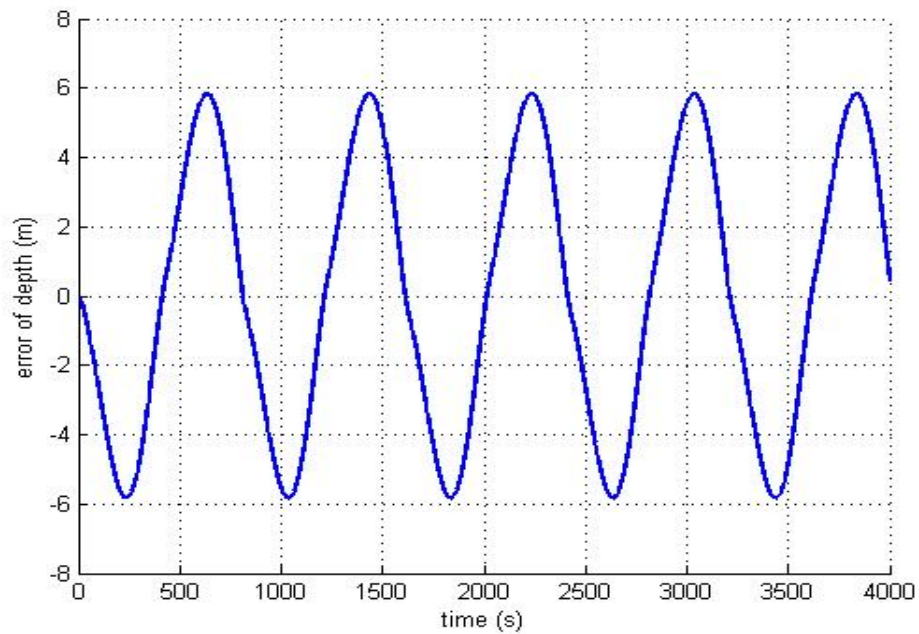


Figure A.20 Error depth position of linearized approximation controller in sinus input reference (range operation 0-50 m).

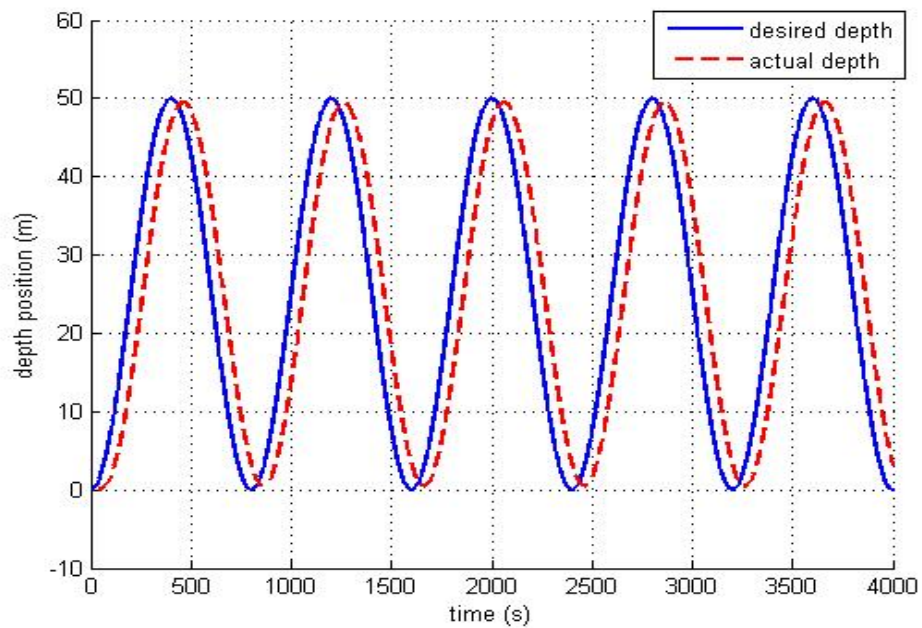


Figure A.21 Response of state-space feedback linearization controller in sinus input reference (range operation 0-50 m).

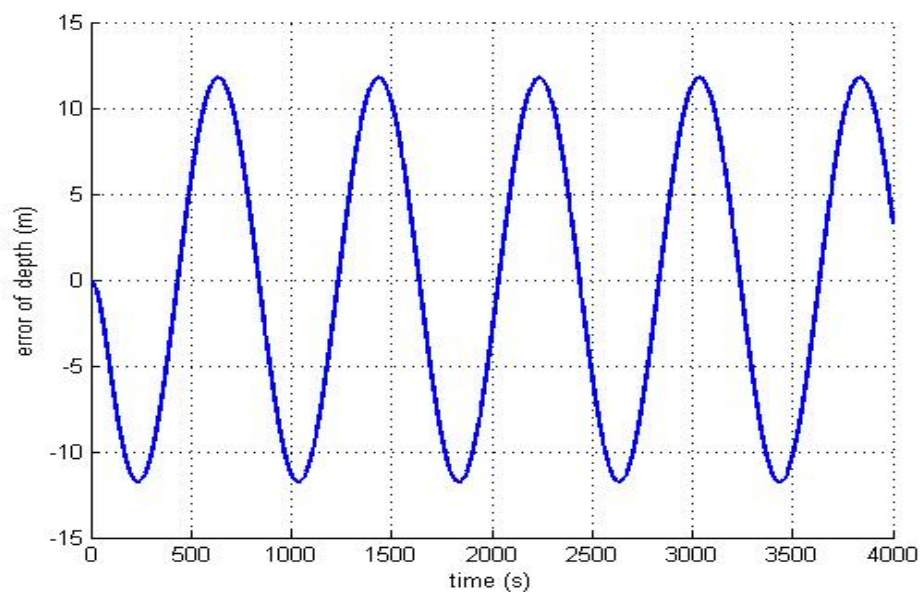


Figure A.22 Error of state-space feedback linearization controller in sinus input reference (range operation 0-50 m).

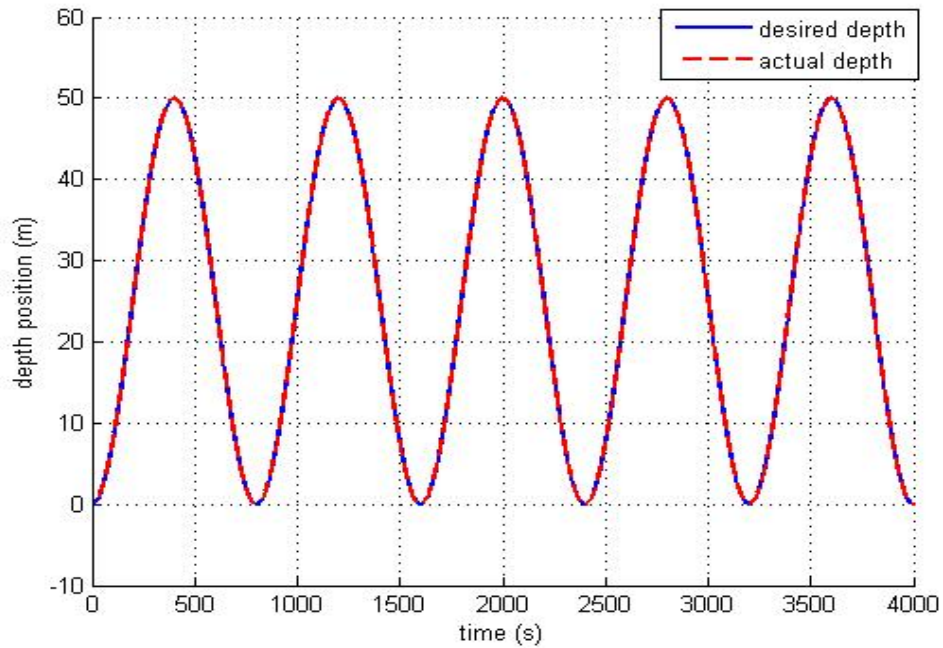


Figure A.23 Response of input-output feedback linearization controller in sinus input reference (range operation 0-50 m).

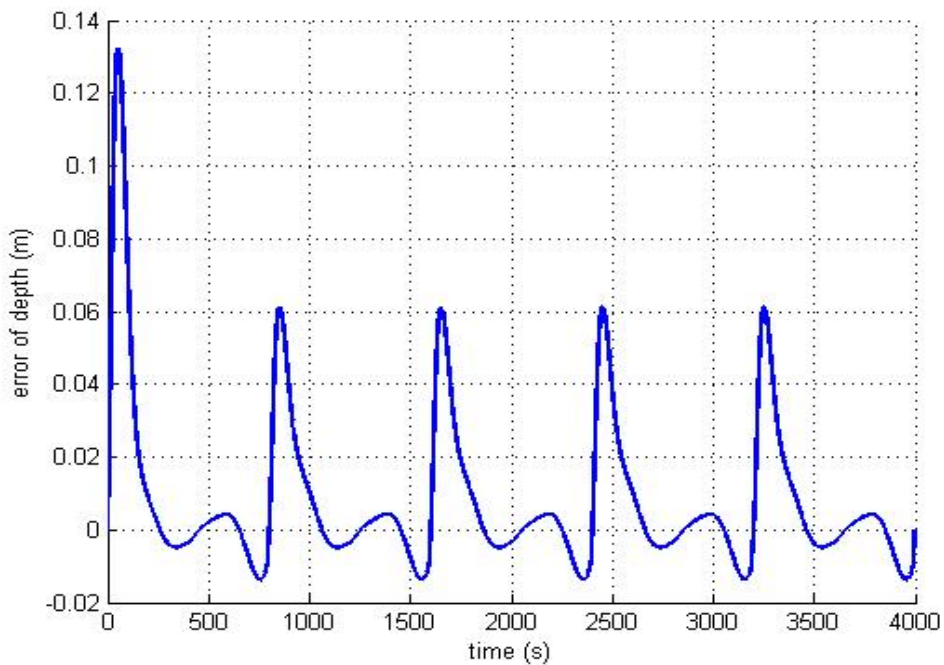


Figure A.24 Error depth position of input-output feedback linearization controller in sinus input reference (range operation 0-50 m).

Table A.3 Steady state error and power usage for trajectory input.

Input reference/ trajectory	Linearized approximation		State-space feedback linearization		Input-output feedback linearization	
	RMSE (m)	Power usage (Watt second)	RMSE (m)	Power usage (Watt second)	RMSE (m)	Power usage (Watt second)
Ramp	1.005	0.081	3.004	0.312	0.172	11.032
Triangle	2.711	1661.95	6.436	1447.597	1.853	3739.012
Sinus	3.935	3545.082	8.326	3663.743	0.024	3825.309